Synthesis, Structure and Physicochemical Properties of Ethanolamine-Based Lipids

A Thesis
Submitted for the Degree of
DOCTOR OF PHILOSOPHY

By

PRADIP K. TARAFDAR

School of Chemistry
University of Hyderabad
Hyderabad – 500 046
INDIA

October 2009

Synthesis, Structure and Physicochemical Properties of Ethanolamine-Based Lipids

A Thesis
Submitted for the Degree of
DOCTOR OF PHILOSOPHY

By

PRADIP K. TARAFDAR

School of Chemistry
University of Hyderabad
Hyderabad – 500 046
INDIA

October 2009

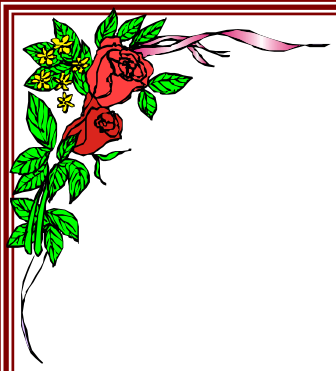

Dedicated to
my beloved
family & friends

যতদিন দেশে অজ্ঞানতা ও অনধ্কার থাকিবে ততদিন যাহারা শিক্ষালাভ করিয়াও ইহার প্রতিকারে ততপর নহেন, তাহাদিগকে দেশদ্রোহী এবং সমাজদ্রোহী বলিব।

বিবেকানন্দ

School of Chemistry
University of Hyderabad
Hyderabad – 500 046

STATEMENT

I hereby declare that the matter embodied in this thesis is the result of investigations carried out by me in the School of Chemistry, University of Hyderabad, Hyderabad, under the supervision of **Prof. Musti J. Swamy**.

In keeping with the general practice of reporting scientific observations, due acknowledgements have been made whenever the work described is based on the finding of other investigators. Any omission which might have occurred by oversight or error is regretted.

Hyderabad

October 2009 **Pradip K. Tarafdar**

School of Chemistry
University of Hyderabad
Hyderabad – 500 046

CERTIFICATE

Certified that the work embodied in this thesis entitled **"Synthesis, Structure and Physicochemical Properties of Ethanolamine-Based Lipids"** has been carried out by **Mr. Pradip K. Tarafdar**, under my supervision and the same has not been submitted elsewhere for any degree.

Hyderabad

October 2009

Prof. Musti J. Swamy
(Thesis Supervisor)

Dean
School of Chemistry

ACKNOWLEDGEMENTS

First, I am grateful to Almighty Bhagaban for giving me an opportunity, physical and mental strength, to pursue research work.

I sincerely thank and express my deep gratitude to my mentor Prof. Musti J. Swamy, for his guidance, constant encouragement, mental support, freedom and valuable suggestions given throughout the Ph.D program. I appreciate his patience, kindness and humanistic approach. I am fortunate that I have pursued my PhD work under the guidance of an honest man.

My sincere thanks to Prof. D. Basavaiah, Dean, School of Chemistry as well as past Deans of the School for providing the infrastructure for carrying out the research work and all the faculty members for the help and encouragement at different times.

I sincerely thank to my teachers, Dr. Chandan Saha, Dr. Atanu Bhattacharya, Dr. Pinaki Choudhuri, Dr. Debasish Jana and Dr. S. S. Jana, Dr. Suprakash Acharya, Kalipada Sarkar, Rantonda, Bhaskarda, Amitava Das, Sunil Kumar Das, Pijush Kanti Basak, Swapanda and Luchiapa for building interest towards higher study.

A special word of thanks to Prof. D. Basavaiah, Prof. A. Samanta and Dr. Tushar Jana to help in various ways. I thank all the research scholars of School of Chemistry and specially members of the COSIST lab for providing a cheerful atmosphere around me. I thank Chandrasekharji, Veerendarji, Rajuji, Utpalda, Rameshda, Suparna, Sekhar, Satpal and Mallikarjuna Reddy for their invaluable support on initial days and afterwards at COSIST building and Gurbakhsh Singh Building.

I am grateful to Prof. Amitabha Chattopadhyay, Prof. Appa Rao Podile, Dr. Vasudev, Anil and Pushpendra for their help in carrying out collaborative projects, to Prof. Samudranil Pal for advice in X-ray data analysis and to Dr. B. Gopalakrishnan (Tata Consultancy Services, Hyderabad) for helpful suggestions and for critically reading some of my manuscripts. I thank Prof. Anunay Samanta for help in carrying out time-revolved fluorescence measurements and Dr. Arabinda Chaudhuri (IICT, Hyderabad) for DLS measurements.

I would like to record my thanks to all my labmates Rajeshwer, Kishore, Thirupathi, Pavan and Dr. Krishnaprasad for providing a good working atmosphere in the lab. I would like to thank my seniors Dr. Anbu, Dr. Ravikanth, Dr. Roopa, Dr. Rajani, Dr. Kavitha and Dr. Narahari for the fruitful discussions and suggestions. My special thanks to my senior K. Ravikanth and A. Narahari for their help and suggestions throughout my Ph.D.

I thank all non-teaching staff of the School of Chemistry and CIL for their help and cooperation and would like to specially thank Dr. P. Raghavaiah, Mr. Satyanarayana, Mr. Suresh and Ms. Asia Pervej for their kind cooperation.

I would also like to express my sincere thanks to all my Dadas with whom I have some wonderful memories and they are the people who take the care for me throughout their stay. The senior Dadas who still matter are Dinuda, Rahulda, Binoyda, Sandipda, Abhikda, Sunirbanda, Archanda, Bishuda, Manabda, Subhasda, Moloyda, Saikatda, Aniruddhada, Prasantda, Utpalda, Saumyada, Dipankarda, Tejender and Abhijitda.

I cherished the close association of Bhaswatidi, Arindam, Pati, Tapta, Tanmoy, Ghata, Sandip, Vasudhara, Rumpa, Sanjib, Ranjit, Naba, Dinesh, Susruta, Rishi, Palash, Tulika, Sudhangshu, Anup, Mehboob, Tanmoy, Sandip, Tridib, Sanghamitra, Paromita, Monima, Chandrani, Debdityo, Raja, Satyajit,.

My special thanks to my ex-roommate Aniruddhada for various discussions on various topics, my local guardian Abhikda, and my local teacher Archanda. I also thank Sunirbanda, Dinuda, Abhikda, Prasantda, Dadu and Ranjit for their help to learn X-ray crystallography. I Thank Rishi, Dinesh and Rajeshwer for critically reading the Thesis.

I thank my 04 friends Tanmoy, Bipul, Suparna, Anindita, Satish, Sekhar, Phani, Rajesh, Kishore, Ramkumar, Ramu, Vikram and Srinivas for their help in various ways.

The Thesis would be incomplete without my family members who have stood beside me at various stages of this journey. I am very grateful to my parents, Prafulla and Prabhabati and my brother, Prabir. I am fortunate that I get parents and brother like them. I wholeheartedly thank my other family members: Masi (Pankojdar Ma), Kalyan & Soma, Nagenda & Anitadi & Pritam, Anjana, Jhutan & Rumpa, Mamara & Mamira, Masi & Mesu, Kakura and Kakimara, Pishira & Pishamahashoyra, Dadura & Didimara, Swapanda & Boudi, Rupalidi & Prabirda, Arotimasi & Dineshmesu.

My sincere gratitude to Arabinda Maharaj and Palash Maharaj for spiritual knowledge at RKMV, Belur. I thank all my childhood and existing friends: Raju, Bappaditya, Nabakumar, Kausick (Bag), Subhendu, Manas, Mrinal, Chanchal, Kausick (ketluda), Asim, Nirbhik, Soumitra, Jango,

Krishnendu, Sailen, Nilu, Samir, Rabi, Sobhan, Mukulesh, Mahabir, Piplu, Tapan, Pradosh, Mihir, Raja.

When people lose some of his childhood friends during PhD, they may get some new friends. I thank my new friends: Nagenda, Anitadi, Pranatidi, Monica, Subhra, Ramadi, Santoshda, Sujit, Jaya, Boudira (Saraswati, Ganga, Suchandra), Paranda, Litonda, Bipulda, Subratada, Vijoy, Pintuda, Subratada, Ushadi, Sunilda, Nepalmama, Gautom, Uttam, Pankajda & Boudi, Raju (Prabir's friend).

I thank my Hyderabadi friends, Dipankar, Sanjoy, Krishnendu, Jayanta, Santanu, Sayantani, Rajarshi, Jaya and Ausmita for their valuable company on weekends.

I feel very much proud that I am (was) in touch with some supernaturally honest man; Nagenda, Priotosh, Nirbhik, Dipankar, Sanjoy, Mriganko (Paira) and Prabir.

I thank CSIR for the fellowship and at last I thank all the people who have helped me during this marathon journey.

Pradip K. Tarafdar

LIST OF ABBREVIATIONS

General

DCC	Dicyclohexylcarbodiimide
EDTA	Ethylenediamine tetra acetic acid
DMAP	4-Dimethylaminopyridine
Sn	Stereo specific numbering
TLC, tlc	Thin layer chromatography
Tris	Tris (hydroxymethyl) aminomethane
CSD	Cambridge Structural Database
PLA_2	Phospholipase A_2

Lipids

5-SASL	Stearic acid spin labeled on the 5^{th} C-atom
DAE	*N*-, *O*-Diacylethanolamine
DSPC	1,2-Distearoyl-*sn*-glycero-3-phosphocholine
DMPC	1,2-Dimyristoyl-*sn*-glycero-3-phosphocholine
NAE	*N*-Acylethanolamine
NAPE	*N*-Acylphosphatidylethanolamine
PAF	Platelet activating factor
OAE	*O*-Acylethanolamine
OAC	*O*-Acylcholine
NMEA	*N*-Myristoylethanolamine
NPEA	*N*-Palmitoylethanolamine
NSEA	*N*-Steroylethanolamine
LPC	Lysophosphatidylcholine
ELPC	Egg lysophosphatidylcholine

NPOO	*N*-Palmitoyl, *O*-octanoylethanolamine
NPON	*N*-Palmitoyl, *O*-nonanoylethanolamine
NPOD	*N*-Palmitoyl, *O*-decanoylethanolamine
NPOU	*N*-Palmitoyl, *O*-undecanoylethanolamine
OLEA.HCl	*O*-Lauroylethanolamine hydrochloride
OMEA.HCl	*O*-Myristoylethanolamine hydrochloride
OPEA.HCl	*O*-Palmitoylethanolamine hydrochloride
OSEA.HCl	*O*-Stearoylethanolamine hydrochloride
OSEA	*O*-Stearoylethanolamine hydrochloride
OLEA.HI	*O*-Lauroylethanolamine hydroiodide
OMEA.HI	*O*-Myristoylethanolamine hydroiodide
OMEA.HBr	*O*-Myristoylethanolamine hydrobromide
OLEA.TFA	*O*-Lauroylethanolamine trifluoroacetate
OMEA.TFA	*O*-Myristoylethanolamine trifluoroacetate
OPEA.TFA	*O*-Palmitoylethanolamine trifluoroacetate
OSEA.TFA	*O*-Stearoylethanolamine trifluoroacetate
OLC	*O*-Lauroylcholine
OMC	*O*-Myristoylcholine
OPC	*O*-Palmitoylcholine
OSC	*O*-Stearoylcholine
OArC	*O*-Arachidylcholine
SDS	Sodium dodecyl sulfate
SDBS	Sodium dodecylbenzene sulfonate
OLEA-DS	*O*-Lauroylethanolamine dodecanoyl sulfate complex

Techniques

ΔH_t	Transition enthalpy

ΔS_t	Transition entropy
$2A_{max}$	Outer hyper fine splitting
^{31}P-NMR	Phosphorus-31 nuclear magnetic resonance
^{1}H-NMR	Proton nuclear magnetic resonance
CMC	Critical micellar concentration
DSC	Differential scanning calorimetry
ESR	Electron magnetic resonance
H_I	Hexagonal phase I
H_{II}	Hexagonal phase II
NMR	Nuclear magnetic resonance
ppm	Parts per million
T_t	Transition temperature
$\Delta T_{½}$	The width of the phase transition at half-height
ORTEP	Oak Ridge Thermal Ellipsoid Plot
FTIR	Fourier transform infrared spectroscopy
GooF	Goodness of fit
ΔH_o	End contribution of transition enthalpy
ΔS_o	End contribution of transition entropy
ΔG_b	Gibbs free energy of binding
ΔH_b	Enthalpy of binding
ΔS_b	Entropy of binding
S_b	Binding constant
*a*o	Optimal surface area
P	Packing parameter
v	Volume of the hydrophobic portion
l_c	Chain length of the hydrophobic portion
I_1/I_3	Polarity ratio

AFM	Atomic force microscopy
DLS	Dynamic light scattering

CONTENTS

Chapter 1

Introduction

The living matter is made up of four major classes of small organic molecules: sugar, amino acid, nucleotide and lipid. These small elementary building blocks combine to form macromolecules or macromolecular assemblies like polysaccharides, proteins, nucleic acids and lipid membranes. Among these four basic classes of entities present in living systems, lipids are endowed with rather unusual properties and may be considered as one of the greatest inventions of nature. Lipids are simple amphiphilic molecules, not so complex (structure wise) like proteins and nucleic acids, but in the presence of excess water they will form a variety of aggregates depending upon their structure and the bilayer assembly is used by nature to make cell and organelle membrane. Therefore lipid molecules give the boundary and identity to cells and intracellular organelles and are as important for life as proteins, sugars, and nucleic acids. Unfortunately, for long they have been considered to be dull molecules compared to other biomolecules such as proteins that catalyze biochemical reactions and genes that contain the information required to produce proteins.

The traditional view of lipids as dull molecules has changed significantly over the last decade, and their role as second messengers in cell signaling, cell function and health have been emphasized (Mouritsen, 2005; Hilgemann, 2003). For example, it is now widely accepted that the lipid rafts (Anderson & Jacobson, 2002), presumed submicroscopic domains of certain high-abundance cell lipids, likely organize and regulate signaling processes in cells. In membrane fusion, there is wide agreement that a lipidic pore forms and expands at some point during the fusion of two membranes. From model studies and from theory, it seems likely that specific phospholipid species, with different physical properties, will strongly affect this process and therefore may regulate it (Chanturia et al., 1997; Markin & Albanesi, 2002; Weinreb & Lentz, 2007). The third example is the discovery of

phosphatidylinositol-tris-phosphate (PIP_3), which serves as a key regulator of cell proliferation, apoptosis, and some forms of membrane trafficking (Cantley, 2002). However, the largest fraction of lipids in most cells is used to form membranes.

1.1. The molecular constituents of biomembranes

Membranes contain primarily lipids and proteins. In addition, carbohydrates, which are covalently attached to the membrane proteins and lipids, are also present on the surface. In general, membrane protein content varies between 25 and 75% by weight, whereas lipids comprise the rest. Carbohydrates, which are covalently attached to proteins and lipids, typically make up less than 10% of the membrane by weight. By employing different fractionating procedures the membrane components can be separated. The relative proportion of protein and lipid differ in different membranes (Table 1.1), reflecting the diversity of biological roles associated with different membranes (Lehninger et al., 1993).

Table 1.1: Major components of plasma membranes of different species*.

	Protein (%)	Phospho-lipid (%)	Other lipids	Sterol (%)	Sterol type
Mouse liver	45	27	-	25	Cholesterol
Corn leaf	47	26	Galactolipids	7	Sitosterol
Yeast	52	7	Triacylglycerols Steryl esters	4	Ergosterol
Paramecium	56	40	-	4	Stigmasterol
E. coli	75	25	-	0	-

Taken from Lehninger et al. (1993). *Values are given as weight percentages.

1.2. Membrane lipids and derivatized ethanolamine lipids

Lipids are the major structural elements of biomembranes. The universal description of a lipid is that it is an amphiphilic organic compound of biological

origin, which is water insoluble or slightly soluble in water. Lipids encompass a diverse range of compounds including waxes, fatty acids, fatty-acid derived phospholipids, sphingolipids, glycolipids, and terpenoids such as retinoids and steroids. In one of the recent classifications, lipids have been divided into eight categories depending on their structure, i.e., fatty acids, glycerolipids, glycerophospholipids, sphingolipids, sterol lipids, prenol lipids, saccharolipids, and polyketides containing distinct classes and subclasses of molecules (Fahy et al., 2005).

Ethanolamine is a central building block in a number of important membrane phospholipids and other amphiphiles. Diacyl phosphatidylethanolamine, dialkyl phosphatidylethanolamine and phosphatidylethanolamine plasmalogen are some of the membrane lipids that contain ethanolamine. In addition, choline – which is partly derived by the progressive methylation of ethanolamine in certain tissues such as liver and brain (Stetten, 1941; Kewitz & Pleul; 1976) – is present in phosphatidylcholine, sphingomyelin and platelet activating factor (PAF). Besides these well-known membrane phospholipids, ethanolamine is also a structural component of *N*-acylethanolamines (NAEs), *N*-acylphosphatidylethanolamines (NAPEs), *N*-, *O*-diacylethanolamines (DAEs), *O*-acylethanolamines (OAEs) and *O*-acylcholines (OACs), which are likely to be present in wide variety of organisms (see, for structures, Fig. 1.1 and Fig. 1.2).

1.3. *N*-Acylethanolamines and *N*-acylphosphatidylethanolamines

The content of long-chain NAEs and NAPEs increases quite dramatically in the parent organisms under conditions of stress (Schmid et al., 1990, 1996). For example, both NAEs and NAPEs accumulate in animal tissues during stress conditions such as post-decapitative ischemia in rat brain (Natarajan et al., 1986;

Moesgaard et al., 1999), traumatic brain injury (Hansen et al., 2001a, b) and their content rises to very high levels when extensive membrane degradation occurs, such as in myocardial infarction (Epps et al., 1979, 1980; Schmid et al., 1990, 1996; Marsh & Swamy, 2000; Chapman, 2000). They also accumulate in a variety of human tumors and surrounding normal tissues. Since NAEs have been shown to inhibit the growth of different cell lines *in vitro*, this suggests that their accumulation in the tumor tissue may be due to the production of NAEs by the adjacent tissues to fight the cancerous growth (Schmid et al., 2002). These observations have led to the postulate that increase in the levels of NAEs and NAPEs is probably due to a stress- or disease-fighting response of the parent organisms. In addition to their putative role in combating stress, NAEs also exhibit interesting biological and medicinal properties. It has been shown that *N*-arachidonylethanolamine (anandamide) acts as an endogenous ligand of type-1 cannabinoid receptors, inhibits gap-junction conductance and reduces the fertilizing capacity of sperm (Devane et al., 1992; Schuel et al., 1994; Venance et al., 1995), whereas *N*-palmitoylethanolamine acts as an agonist for the type-2 cannabinoid receptor (Facci et al., 1995). *N*-Myristoylethanolamine (NMEA) and *N*-lauroylethanolamine are secreted into the culture medium of tobacco cells when challenged by the fungal elicitor, xylanase (Chapman et al., 1998). NAEs also exhibit anti-inflammatory, antibacterial and antiviral properties, which are of considerable application potential (Ganley et al., 1958; Schmid et al., 1990). Besides their interesting biological and medicinal properties mentioned above, NAEs and NAPEs have also been reported to exhibit membrane stabilizing property. Some studies suggest that *N*-acyl egg PE and *N*-palmitoyl dipalmitoylphosphatidylethanolamine (*N*-16 DPPE) stabilize liposomes against leakage (Domingo et al., 1993; Mercadal et al., 1995). Especially, *N*-16 DPPE has been shown to stabilize liposomes even in the presence of human serum. NAEs

have been shown to stabilize the bilayer structure in the sense of inhibiting the formation of inverted hexagonal phase (Ambrosini et al., 1993). Because of the diverse biological activities exhibited by them and in view of their putative roles in combating stress and signaling events in animals and plants, several groups including ours have been investigating the biophysical properties of NAPEs and NAEs and characterized their interaction with other membrane lipids (Akoka et al., 1988; LaFrance et al., 1990; Swamy et al., 1997, 2000; Li et al., 2002; Kamlekar et al., 2007; Ramakrishnan et al., 2002, 2007).

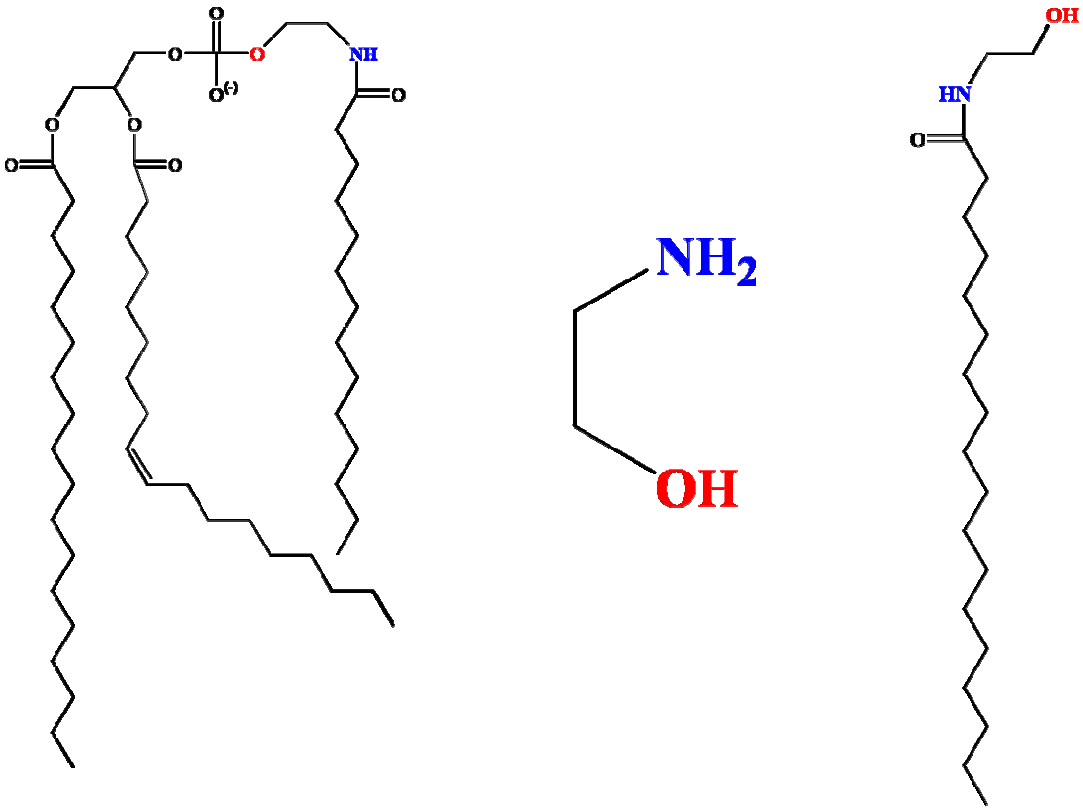

Fig. 1.1: Structures of *N*-acylphosphatidylethanolamine (left), ethanolamine (middle) and *N*-acylethanolamine (right). Both lipids contain ethanolamine moiety.

1.4. *N*-, *O*-Diacylethanolamines (DAEs)

NAEs can be further derivatized via the hydroxy group and a recent study reported the occurrence of phosphorylcholine derivatives of NAEs *in vivo* (Mulder & Cravatt, 2006). Also, *O*-aryloxyacetyl derivatives of NAEs have shown better plant growth stimulating effect than NAEs (Han et al., 2007). It has also been reported that rat heart cell-free preparations can catalyze *O*-acylation of NAEs in the presence of fatty acid and acyl-CoA-generating cofactors to produce *N*-, *O*-

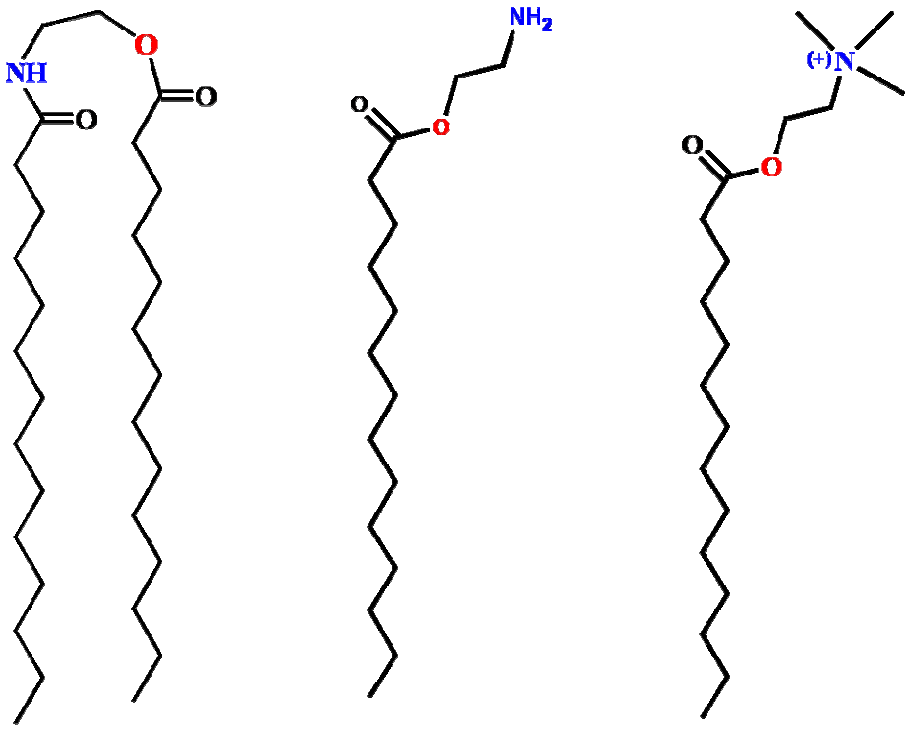

Fig. 1.2: Structures of *N*-, *O*-diacylethanolamine (left), *O*-acylethanolamine (middle) and *O*-acylcholine (right). All three lipids contain ethanolamine or derivatized ethanolamine moiety.

diacylethanolamines (DAEs) (Schmid et al., 1990). In another study it was shown that lipases can catalyze *O*-acylation of *N*-acylethanolamines to yield DAEs (Furutani et al., 1997). All these observations suggest that DAEs may be present in

biological membranes as minor constituents, which may play some biological role in the parent organisms. In order to understand the possible role played by DAEs, it is essential to investigate the properties of these molecules in a systematic manner. Particularly, studies aimed at understanding the phase behavior and structures formed by them in the solid state as well as in the fully hydrated state will be of great value in understanding their biological implications in the parent organism. Recently, studies from our laboratory reported the synthesis of a homologous series of DAEs with matched acyl chains and characterization of their thermotropic phase transitions in the dry state by differential scanning calorimetry (DSC) (Kamlekar et al., 2009).

1.5. *O*-Acylethanolamines (OAEs)

Besides *N*-acylation of ethanolamine to produce NAEs, amphiphiles can also be produced by the *O*-acylation of ethanolamine with a long acyl chain to form an ester derivative of ethanolamine, namely *O*-acylethanolamine (OAE). Recently it has been shown that *O*-acylethanolamines are converted to *N*-acylethanolamines in a facile manner under mildly basic conditions, whereas the reverse reaction – formation of *O*-acylethanolamines from *N*-acylethanolamines – is catalyzed by acid (Markey et al., 2000). These observations suggested the possible presence of OAEs as minor constituents in membranes which are in acidic environment e.g., endosomes and ischemic tissues (Murphy et al., 1984; Rybak & Murphy, 1998; Boomer & Thompson, 1999). It is likely that these minor constituents of membranes might have escaped detection for a long time due to their conversion to NAEs under conditions employed in the extraction, purification or detection (e.g., **tlc** using solvents containing ammonia). Interestingly, subsequent studies have led to the detection and identification of *O*-arachidonylethanolamine (virodhamine) – a

structural isomer of anandamide – in mammalian brain, which exhibits partial agonist/antagonist activity to the type-1 cannabinoid receptor and agonist activity to the type-2 cannabinoid receptor (Porter et al., 2002). These observations indicate that OAEs containing other fatty acyl moieties may also be present in biological membranes, with potentially interesting biological properties. In this regard it is of considerable interest to investigate the phase behavior and membrane interactions of OAEs and to identify their possible biological role.

1.6. *O*-Acylcholines (OACs)

O-Acylcholines (OACs) are fatty acid esters of choline, which are true cationic lipids due to the presence of the quaternary ammonium functionality in the head group. OACs with different fatty acyl chains have been shown to exhibit hemolytic activity and it was observed that their potential as hemolytic agents is comparable to that of acylcarnitines and lysolecithins (Cho & Proulx, 1969, 1971). Another choline ester, *O*-palmitoylcholine has been isolated from the skin secretions of the smooth trunk fish, *Lactophrus triqueter* Linn (Goldberg et al., 1982). This compound had been shown to exhibit toxicity against mosquitofish at low concentration (2 ppm). OACs can also act as inhibitors of enzymes, e.g., it was observed that wheat embryo Ca^{2+}-dependent protein kinase (CDPK) is inhibited by a variety of long-chain acylcholines (Jinsart et al., 1991). Beside the biological properties, OACs attract interest due to their medicinal properties. It was reported long ago that OACs with various fatty acyl chains can modulate the blood pressure (Schneider & Timms, 1957). OACs with different acyl chains (from lauroyl to stearoyl) were evaluated as skin penetration enhancers by testing their effects on the penetration of drugs like acyclovir, 17β-estradiol, hydrocortisone, nitroglycerin etc. (Loftsson et al., 1989). *O*-acylcholines also show rapid antimicrobial activity against a wide range of microorganisms (Ahlström et al., 1995). As the OACs are

enzymatically hydrolyzable to eco-friendly components, these substances are projected to have a good potential to replace the more toxic, stable quaternary ammonium compounds (Ahlström et al., 1995). Although, as indicated above, a considerable amount of knowledge exists on the biological and pharmacological properties of OACs, very little is known regarding their supramolecular structure in solution, thermotropic and chaotropic denaturation and interaction with other lipids.

1.7. Physicochemical properties of lipids

This section will give a brief outline of several physicochemical properties of lipids, e.g., polymorphism (hydrated state and dry state), phase transitions and denaturation of lipids.

1.7.1. Polymorphism in lipids (hydrated state)

Upon dispersion in water, lipid molecules can self-assemble in a variety of different aggregated structures and exhibit polymorphism. This aspect of polymorphism in biophysics deals with the behavior of lipids that influences their long-range order, i.e. how they aggregate. This can be in the form of spheres of lipid molecules (micelles), pairs of layers that face one another (lamellar phase, observed in biological system as a lipid bilayer) and aggregates with lipid cylinders arranged in a hexagonal symmetry (hexagonal and inverted hexagonal phases) (Fig. 1.3). Various parameters such as the lipid concentration, temperature, pressure, ionic strength, and pH and the molecular shape and charge of lipid affect the formation of different polymorphic structures by lipids.

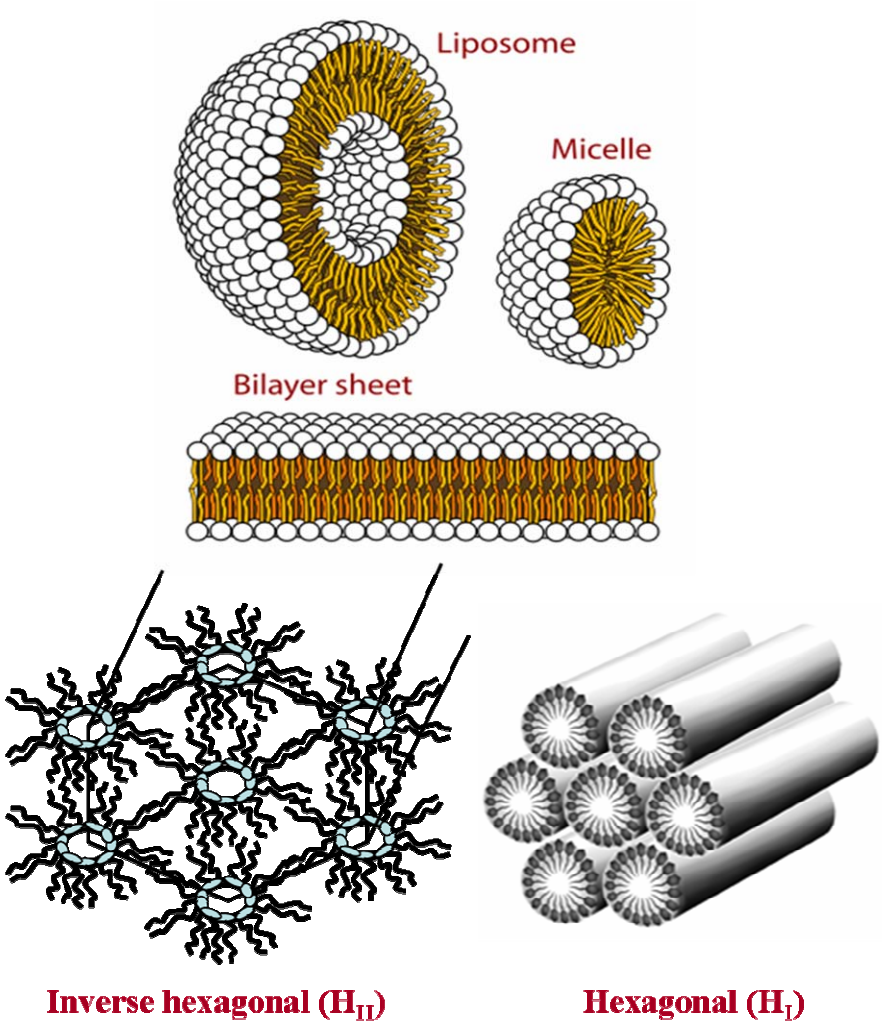

Fig. 1.3: Schematic illustration of different lipid aggregates in hydrated state.

1.7.2. Polymorphism in lipids (solid state)

Polymorphism of lipids in the solid state is familiar to researchers for several decades. Although structural polymorphism of lipids in the solid state has been discussed for more than fifty years, it is still a matter of uncertainty and

incompleteness compared to the polymorphism in hydrated state due to the similarity of different polymorphic forms and the difficulty of obtaining isolated forms. Physical properties such as melting point, softness, flexibility and stability of fats and lipids might be different in different polymorphic forms. Thus structure determination of different polymorphic forms at the atomic level has critical implications for the understanding of structure-function relationships of lipids and a knowledge of their polymorphism may help in better understanding the phase transition mechanisms. Understanding phase transition mechanisms is useful to control crystallization behavior of lipids, which is an important factor that determines the quality of lipids that are used as food products and cosmetics. However, only a few single-crystal structures of lipid polymorphs are found in Cambridge Structural Database (CSD), which may be due to the difficulty of growing high quality-single crystals for X-ray diffraction. In addition, the diffraction patterns of lipids are dominated by strong subcell reflections arising from the regular hydrocarbon chain matrix, which complicate or sometimes hinder the structure solution (Pascher et al., 1992)

Beside single-crystal X-ray diffraction, spectroscopic and calorimetric methods such as X-ray powder diffraction, differential scanning calorimetry (DSC), Fourier transform infrared spectroscopy (FTIR) and Fourier transform Raman spectroscopy have been widely used to investigate polymorphism in fatty acids (Moreno et al., 2007; Arutyunova, 1961), monoacylglycerols (Chapman, 1962), diacylglycerols (Hom & Malkin, 1951; Kodali et al., 1990), triacylglycerols (Chapman, 1962; Lutton & Fehl, 1970), NAEs (Ramakrishnan et al., 1997; Wouters et al., 2002), ceramides (Raudenkolb et al., 2003, 2005) and other lipids. Now the questions that arise are the following. Is it possible to predict if any class of lipid can show polymorphism and if so is it possible to predict how many polymorphs can exist in

a specific class of lipids? What is the role of molecular structure in determining polymorphism in lipids? Generally different packing arrangement with similar lattice energy can increase the possibility of polymorphism. In one study it was shown that difficulty in packing increases the number of polymorphs in 1-stearoyl, 2-oleoylglycerol (Di & Small, 1993). However, there have been no detailed studies aimed at predicting the number of polymorphs and the molecular packing in the different polymorphs at an atomic level.

1.7.3. Phase transition of lipids

Phase transitions of lipids in dry state as well as in the hydrated state have been investigated in detail. While the solid state phase transitions are mainly governed by temperature, polymorphic transition between two phases in hydrated state can be modulated by concentration, pH, ionic strength and temperature. For example, some lamellar lipid phases can undergo a transition to a hexagonal (H_I) phase by increasing water content and to an inverted hexagonal (H_{II}) phase by decreasing the water content. Such transitions are referred to as lyotropic transitions. Besides lyotropic phase transitions, thermotropic phase transitions between lamellar gel to liquid crystalline phase and lamellar liquid crystalline phase to inverted hexagonal phase have been widely studied (Marsh, 1991a; Lewis et al., 1987). The thermodynamic characterization of these phase transitions are important since non-bilayer lipid phases have been postulated to play a significant role in several biological process (Chernomordik, 1996; Chapman, 1993). For example, lysophosphatidylcholine adopts an interdigitated lamellar gel phase at low temperature, whereas it forms micelles near body temperature and acts as a membrane destabilizer (Weltzien, 1979).

1.7.4. Denaturation of lipids

The three major macromolecular assemblies of living systems are proteins, nucleic acids and lipids. Among them proteins and nucleic acids have secondary and tertiary structure and they are biologically active when the well-defined secondary and tertiary structure is retained. This state is referred to as 'native' state and they will be inactive when the secondary and tertiary structures are partially or fully-compromised. The state in which the secondary and tertiary structures are completely disturbed is referred to as 'denatured' state. The transition from a native state to a denatured state is termed as denaturation and it was shown that the process of denaturation in proteins and nucleic acids can be triggered by various stimuli, like heat, addition of chaotropes etc. While heat breaks the specific interactions, chaotropic ions interfere with stabilizing intra-molecular interactions mediated by non-covalent forces such as hydrogen bonds and hydrophobic interactions. The third major class are lipids, which are a diverse group of compounds that perform many key biological functions, such as structural components of cell membranes, energy storage sources and intermediates in signaling pathways. Many lipid molecules, which consist of a hydrophobic tail and a hydrophilic head group also possess surface activity and are also referred to as surfactants. Surfactants self-associate and give rise to well developed supramolecular assemblies, which are among the most versatile materials appearing in diverse products such as motor oils, pharmaceuticals, detergents and as flotation agents for beneficiation of ores (Rosen, 2004). Among various surfactants one class is cationic surfactants and they have been used as anti-bacterials (Davis & Jordan, 1990; Stephenson, 1990), liquid crystals (Sudholter, 1982), gene transfection agents (Ronsin et al., 2001; Karmali & Chaudhuri, 2007) etc.

In lipids and surfactants although the concept of denaturation is uncommon, the tendency of lipids to form precipitate may be likened to denaturation (on the basis of loss of activity). The precipitation occurs below a characteristic temperature and when the concentration exceeds the saturation concentration of monomeric dispersion. Below this temperature lipids will be separated form the bulk medium and it is expected that they will lose some of the biological activity and surfactants will lose some of its surface activities such as dispersing, emulsifing, and micelle-forming properties (Tsujii & Mino, 1978, Rodriguez et al., 2001). This characteristic temperature is known as Krafft temperature and is recognized as the temperature above which the solubility of a surfactant increases dramatically in aqueous systems, and is interpreted as the melting temperature of a hydrated solid surfactant (Shinoda, 1963; Tsujii & Mino, 1978). Since below the Krafft temperature lipids/surfactants behave as though in a denatured state, to keep the lipids/surfactants in their native form, it is desirable to lower the Krafft temperature for a given lipid/surfactant. So, unlike proteins where denaturation occurs due to increase in temperature, for lipids denaturation seems to appear at low temperature. Now, if the concept of denaturation can also be applied to the third major kingdom of life (lipids), is there any existence of Hofmeister series in lipids?

The Hofmeister series, first reported in 1880-1890s (Kunz et al., 2004), ranks the relative influence of ions on the physical behavior of a diverse variety of processes that takes place in aqueous media ranging from colloidal assembly to protein folding (Zhang & Cremer, 2006). Although Hofmeister effects for macromolecules in aqueous solution are ubiquitous, the precise origin of action of the ions in the series has not yet been understood and no generally accepted explanation exists at the molecular level (Collins & Washabaugh, 1985; Cacace et al., 1997; Zhang & Cremer, 2006; Kunz et al., 2004). Originally, it was thought

that an ion's influence on macromolecular properties is caused due to its ability to make and break hydrogen bonds (known as kosmotropic *vs* chaotropic behavior) (Zou et al., 2002; Vanzi et al., 1998; Washabaugh & Collins, 1986), but recent experiments indicate that the ions have little effect on the overall hydrogen bonding of water in the bulk solution (Omta et al., 2003; Batchelor et al., 2004). An entirely different approach suggests that unusually neglected dispersion forces play a role in the order of the Hofmeister series (Ninham & Yaminsky, 1997; Boström et al., 2001), although this hypothesis has been largely examined only theoretically rather than experimentally (Gurau et al., 2004).

The influence of chaotropic and kosmotropic ions on the phase behavior of lipids has been studied extensively (Aroti et al., 2004; Leontidis & Aroti, 2009; Jendrasiak, 1972; Loshchilova & Karvaly, 1978; Epand & Bryszewska, 1988; Cunningham & Lis, 1986; Rydall & Macdonald, 1992, Clarke & Lüpfert, 1999, Gurau et al., 2004; Sachs & Woolf, 2003; Aroti et al., 2007; Sanderson et al., 1991). ^{1}H-NMR and Raman spectroscopic studies have shown that the interaction of anions with zwitterionic lipids follow the Hofmeister series (Jendrasiak, 1972; Loshchilova & Karvaly, 1978). It was observed that chaotropic anions affect conformational fluctuations of the headgroups of phosphatidylcholine bilayers, with the magnitude of this effect paralleling the Hofmeister series (Rydall & Macdonald, 1992). The influence of the same series of anions on the dipole potential of dimyristoylphosphatidylcholine vesicles was studied using voltage sensitive dyes (Clarke & Lüpfert, 1999). This study as well as other studies suggests that the chaotropic anions may penetrate more deeply into the bilayer interior than do the non-chaotropic anions (Gurau et al., 2004; Sachs & Woolf, 2003). The chaotropic ions have pronounced effects on the thermotropic phase transition of lipids (Epand & Bryszewska, 1988; Cunningham & Lis, 1986) and it was shown that chaotropic

ions increase the bilayer-hexagonal phase transition temperature of 1-palmitoyl, 2-oleoyl phosphatidylethanolamine (Sanderson et al., 1991). In alkyltrimethylammonium surfactants the counterion ability to induce the sphere-to-rod transition follows the Hofmeister sequence (Nguyen & Bertrand, 1992; Leontidis, 2002) and in dodecyltrimethylammonium micelles, the aggregation numbers have been shown to increase with the Hofmeister sequence of the counterion (Anacker & Ghose, 1963). It was also observed that the swelling effect of dipalmitoylphosphatidylcholine bilayers follow the Hofmeister series and on the salt concentration (Aroti et al., 2007). The major aim of those studies was to investigate the origin of the Hofmeister effect by studying the interaction of ions with model systems rather than to understand the role of ions on the modulation of Krafft temperature.

The Krafft temperature of lipids and surfactants sometime depend upon the counterion and ions present in the solution (Shinoda et al., 1972; Tsujii & Mino, 1978). Thus ions will have a definite role on the denaturation of lipids or surfactants as below the Krafft temperature the system may behave as denatured state. The effect of ions on the modulation of Krafft temperature or the denaturation of lipid can be compared with denaturation of proteins with various chaotropic ions. It was reported earlier that chaotropic ions make insoluble ion pairs with cationic surfactants (Anacker & Ghose, 1963, 1968; Leontidis, 2002; Underwood & Anacker, 1987). Although these studies mentioned about the influence of ions on precipitation, they did not correlate the observed fact with the role of the ions on the modulation of Krafft temperature and chaotropic denaturation. In the studies reported in this thesis counterion-induced modulation of Krafft temperature and precipitation of cationic amphiphiles has been referred to as chaotropic denaturation of lipids.

1.8. Lipids in targeted drug delivery

One of the key problems in the treatment of serious diseases like cancer is that many potent drugs have serious side effects due to their action not only on diseased cells but also on healthy ones. Therefore, targeting a drug to a specific site may reduce the side effects and dose level. Liposomes have been used by scientists for targeted drug delivery. A review in 2003 reported that there are over 18,000 papers (listed in PubMed), 600 patents (USPTO Web Patent Database), six approved liposomal drug formulations, and numerous clinical trials of liposome-encapsulated agents (Guo & Szoka, 2003, presently PubMed hits 36,000 papers on liposomes). Despite tremendous efforts made by many researchers to devise lipid-based drug delivery systems, it is only recently that some success has been achieved. Ideally, a drug-loaded liposome should remain stable until it reaches the target site. Upon accumulation of the liposome at the target, the drug must be released at a high enough concentration level to mediate an effective therapeutic response. For the above reasons, drug release in response to a specific stimulus at the target site, i.e., triggered release, is an essential feature of effective targeted delivery systems (Drummond et al., 1999). Recently, triggerable liposomal systems have been designed, which unload the drug at different stimuli, e.g., acid, radiation, heat and redox-potential (Huang et al., 2006; Shum et al., 2001; Needham & Dewhirst, 2001; Ong et al., 2008). The lipids in these liposomes generally contain a triggerable subunit that is responsible for gating the stability and/or permeability of the lipid bilayer. Various physiological environments such as low endosomal pH and elevated enzymatic activity (Davidsen et al., 2003; Meers, 2001) and external sources, including radiation and hyperthermia, supply the necessary stimuli that induce the unloading of the liposomal cargo; this occurs either by perturbing the

permeability or by completely disrupting the noncovalent stability of the bilayer assembly (Fig. 4).

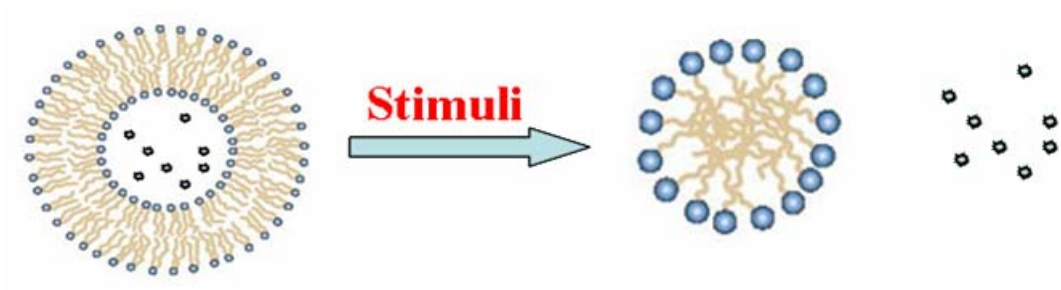

Fig. 1.4: Stimuli sensitive drug release of liposome (schematic depiction).

Although various acid, redox, heat and light triggerable liposomal system have been designed, there are no reports on lipid-based, base-triggerable systems for the delivery of drugs and pharmaceuticals. Base-triggerable drug delivery systems may be useful to target colon in Chron's disease, ulcerative colitis, colorectal cancer etc. (McConnel et al., 2008). Targeting drugs to the colon is challenging and involves the exploitation of site-specific triggers; the two main strategies involve the use of the colonic microbiota and its high metabolic and fermentative capacity, or utilisation of the pH changes along the gastrointestinal tract (McConnel et al., 2008). The pH-responsive colon-specific systems are based on the reported luminal pH increase gradually along the small intestine (from 6.63±0.53 in the jejunum) reaching a peak at the ileocaecal junction (7.49±0.46) (Evans et al., 1988). Polymer coating of Eudragit S, which was designed in 1982 to dissolve above pH 7 have been a most widely used system for colon targeted pH-responsive dosage and is still used for site-specific delivery of the anti-inflammatory drug mesalazine to the large intestine for the treatment of ulcerative colitis (Dew et al., 1982; McConnell et al., 2008).

1.9. Objectives

As NAPEs, NAEs, DAEs, OAEs and OACs have been reported to exhibit various interesting biological and medicinal properties, it is important to carry out systematic investigations on the above lipids directed at understanding their metabolism, physicochemical properties (e.g., phase transitions and supramolecular structure) as well as their interaction with other membrane lipids and proteins. In earlier studies from this laboratory, NAPEs and NAEs have been investigated in considerable detail. Therefore the present thesis deals with DAEs, OAEs and OACs to understand their structure and physicochemical properties with the following specific objectives.

- To synthesize and characterize a homologous series of *N*-, *O*-diacylethanolamines (DAEs) with fixed *N*-acyl (palmitoyl) and varying *O*-acyl chains (*n*=6-16) and to investigate their thermotropic phase transitions.
- To synthesize OAEs with various counterions and to investigate the role of counterions on the molecular packing and intermolecular interactions.
- To understand the phase behavior of OAEs in water and in the presence of salt.
- To investigate the polymorphism, molecular packing, and physicochemical properties of *O*-acylcholines.
- To investigate the interaction of NAEs and *O*-stearoylethanolamine with lysophosphatidylcholine by ^{31}P-NMR spectroscopy, turbidimetry, DSC and atomic force microscopy.
- To design base labile catanionic mixed lipid system from mixtures of *O*-lauroylethanolamine with anionic surfactants.

Chapter 2

Synthesis, Polymorphism and Calorimetric Studies on *N*-, *O*-Diacylethanolamines with Mixed Acyl Chains (*n* = 6-16)

2.1. Summary

Recent studies show that *N*-, *O*-diacylethanolamines (DAEs) can be derived by the *O*-acylation of *N*-acylethanolamines (NAEs) under physiological conditions. Since the content of NAEs in a variety of organisms increases in response to stress, it is likely that DAEs may also be present in biomembranes. In view of this, a homologous series of DAEs with fixed *N*-acyl chain (n=16) and varying *O*-acyl chains (n = 6 – 16) have been synthesized and characterized. Transition enthalpies (ΔH_t) and entropies (ΔS_t) of dry DAEs with even and odd acyl chains obtained from differential scanning calorimetry, independently exhibit linear dependence on the chainlength. Linear least squares analyses yielded incremental values contributed by each methylene group to the transition enthalpy and entropy and the corresponding end contributions. Results of single crystal X-ray diffraction studies show that DAEs adopt an 'L' shaped structure in the solid state and exhibit packing polymorphism, resulting in two structural forms. In the α form a mixed type chain packing have been observed whereas in the β form symmetric chain packing has been detected. It is proposed that similar polymorphic forms may exist in other bioactive 'L' shaped lipids such as 1,3-diacylglycerols and ceramides, where polymorphism has been detected earlier, but the 3-dimentioanal structures which can give precise information about the packing at atomic resolution, have not been reported. The results also suggest that at least two polymorphic forms can exist in an 'L' shaped lipids.

2.2. Introduction

From the introduction (Chapter 1) it is seen that recent observations point to look for possible biological role of *N*-, *O*-diacylethanolamines (DAEs) which may be present in biological membranes as minor constituents. Since the *N*- and *O*-acyl chains of DAEs can be identical or different, it would be important to investigate the structure and phase behavior of DAEs with matched acyl chains as well as with mixed acyl chains. Recently, the synthesis of a homologous series of DAEs with matched acyl chains and characterization of their thermotropic phase transitions in the dry state by differential scanning calorimetry (DSC) have been reported (Kamlekar et al., 2009). In the present study, a homologous series of DAEs of fixed *N*-acyl chain (n = 16) and varying *O*-acyl chains (n = 6-16) have been synthesized. The thermotropic phase transitions of these DAEs with mixed chains have been characterized by DSC. Some of the DAEs in this series exhibited a minor phase transition before the chain melting phase transition, suggesting the possibility of polymorphism in the solid state in DAEs. Single crystal X-ray diffraction studies revealed the existence of two polymorphic forms in DAEs with mixed chains. In both polymorphs the DAE molecules adopt a bent structure, resembling the letter 'L', with a mixed chain packing being seen in the α polymorph whereas in the β form a symmetric chain packing has been observed. It is proposed that similar polymorphic forms may exist in other 'L' shaped lipids such as 1,3-diacylglycerols (Larsson, 1963; Hybl & Dorset, 1971; Goto et al., 1995), *N*-tetracosanoylphytosphingosine (Dahlén & Pascher, 1972), which belongs to the class of compounds known as ceramides, where polymorphism has been identified earlier (Malkin et al., 1937; Baur et al., 1949; Raudenkolb et al., 2003, 2005) but 3-dimentional structures of the polymorphs were not established. Finally,

the odd-even alternation of the thermodynamic properties in DAEs with mixed chains has been rationalized from a structural point of view.

2.3. Materials and methods

2.3.1. Materials

Long chain fatty acids, CH_3-$(CH_2)_n$-COOH, of even and odd chain lengths (n = 4-14) were purchased from Aldrich (USA). Oxalyl chloride was obtained from Merck (Germany). Ethanolamine and other solvents were purchased locally.

2.3.2. Synthesis of N-, O-diacylethanolamines

N-Palmitoylethanolamine (NPEA) was prepared by the reaction of palmitoyl chloride with ethanolamine as reported earlier (Ramakrishnan et al., 1997). The fatty acids were converted to the corresponding acid chlorides by treating with 4 mole equivalents of oxalyl chloride at room temperature for 2 hours under nitrogen atmosphere (Akoka et al., 1988). After completion of the reaction, excess oxalyl chloride was removed under a stream of dry nitrogen gas. *N*-Palmitoyl, *O*-acyl (C_6 to C_{16}) ethanolamines were synthesized by the drop-wise addition of 1.2 mole equivalent of the acid chloride in dichloromethane to a solution of 1 mole equivalent NPEA in the same solvent, under constant stirring. After all the reagent was added, the reaction was allowed to continue overnight (Scheme 2.1). The reaction mixture was then washed successively with double distilled water and extracted with dichloromethane. The crude products were purified by silica-gel column chromatography using increasing concentration of ethyl acetate in *n*-hexane as the eluant. The products obtained were recrystallized from a mixture of dichloromethane and acetone. Overall yields ranged around 55-60%. The products were further characterized by IR and ^{1}H NMR spectroscopy. IR spectra of DAEs

with mixed acyl chains contained absorption bands due to the ester linkage at 1738 cm^{-1}, amide linkage at 1639 cm^{-1} (amide-I) and 1554 cm^{-1} (amide-II). The C-H stretching bands were observed at 2918 cm^{-1} and 2851 cm^{-1}. Methylene bending and rocking bands were observed near 1470 cm^{-1} and 721 cm^{-1}. The N-H and O-H stretching bands were observed above 3300 cm^{-1}. Since all the compounds are isostructural, their NMR spectra were almost identical except the value of integration in one peak. ^1H NMR spectra of the DAEs gave the following resonances: 0.88 δ (3H, t), 1.25δ (nH, s), 1.56δ (2H, m), 2.18δ (2H, t), 2.32δ (2H, t), 3.52δ (2H, q), 4.17δ (2H, t), 5.71δ (1H, bs). The resonances are consistent with the structure of *N*-, *O*-diacylethanolamines.

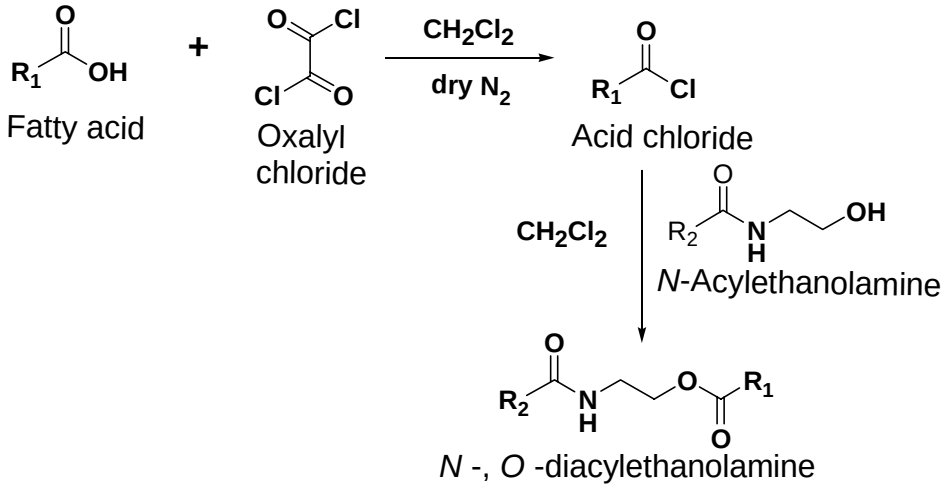

Scheme 2.1: Synthesis of *N*-, *O*-diacylethanolamines.

2.3.3 Crystallization, X-ray diffraction and structure solution

Thin colorless crystals of *N*-palmitoyl, *O*-octanoylethanolamine (NPOO) and *N*-palmitoyl, *O*-decanoylethanolamine (NPOD) were grown at room temperature from dichloromethane containing a trace of methanol. For both compounds, several of the crystals obtained were indexed and it was observed that in each case the crystals

obtained in a single crystallization experiment contained two different crystal forms, orthorhombic and monoclinic, suggesting the presence of two different polymorphs in the crystalline state. Therefore, both types of crystals were further analyzed by single-crystal X-ray diffraction. Thin colorless crystals of *N*-palmitoyl, *O*-nonanoylethanolamine (NPON) and *N*-palmitoyl, *O*-undecanoylethanolamine (NPOU) were also grown at room temperature from dichloromethane having a trace of methanol. Measurements were carried out at room temperature (ca. 25°C) with a Bruker SMART APEX CCD area detector system using a graphite monochromator and Mo-Kα (λ = 0.71073 Å) radiation obtained from a fine-focus sealed tube. Data reduction was done using Bruker SAINTPLUS program. Absorption correction was applied using SADABS program and refinement was done using SHELXTL program (Sheldrick, 1997). The crystal parameters of all crystals are presented in Tables 2.1 and 2.2.

2.3.4. Differential scanning calorimetry

DSC studies were carried out on a Perkin-Elmer Pyris Diamond differential scanning calorimeter. Samples of dry DAEs (1-3 mg) were weighed accurately into aluminium sample pans, covered with an aluminium lid and sealed by crimping. Reference pans were prepared similarly, but without any sample in them. Heating and cooling scans were performed from room temperature (ca. 25°C) to about 110°C at a scan rate of 1.0°/min or 2.0°/min and each sample was subjected to two heating scans and one cooling scan. Transition enthalpies were determined by integrating the peak area under the transition curve. Transition entropies were determined from the transition enthalpies assuming a first order transition according to the expression (Marsh, 1990):

$$\Delta H_t = T.\Delta S_t \qquad (2.1)$$

Table 2.1. Crystallographic data for *N*-, *O*-diacylethanolamines of even *N*- and *O*-chains at 298 K.

	NPOO α form (NPOOα)	NPOO β form (NPOOβ)	NPOD α form (NPODα)	NPOD β form (NPODβ)
Formula	C_{26} H_{51} N O_3	C_{26} H_{51} N O_3	C_{28} H_{55} N O_3	C_{28} H_{55} N O_3
Formula wt.	425.68	425.68	453.73	453.73
Crystal system	orthorhombic	monoclinic	orthorhombic	monoclinic
Space group	*Pca_{21}*	*P2(1)/c*	*Pbc_{21}*	*P2(1)/c*
a (Å)	9.0641(15)	61.416(11)	4.882(3)	65.695(13)
b (Å)	4.8824(8)	4.8659(8)	9.039(5)	4.8826(10)
c (Å)	61.645(11)	9.0232(16)	65.54(3)	9.0350(17)
α	90.00	90.00	90.00	90.00
β	90.00	93.324(3)	90.00	90.438(4)
γ	90.00	90.00	90.00	90.00
Z	4	4	4	4
V ($Å^3$)	2728.1(8)	2692.0(8)	2892(3)	2898.0(10)
D_{calc} (g cm^{-3})	1.036	1.050	1.042	1.040
R_1	0.0740	0.1077	0.0896	0.1179
wR_2	0.1920	0.3050	0.2655	0.2999
GooF	1.023	1.013	0.965	1.083

Table 2.2. Crystallographic data for *N*-, *O*-diacylethanolamines of even *N*-acyl and odd *O*-acyl chains at 298 K.

	NPON	NPOU
Formula	C_{27} H_{53} N O_3	C_{29} H_{57} N O_3
Formula wt.	439.70	467.76
Crystal system	monoclinic	monoclinic
Space group	*P2(1)/c*	*P2(1)/c*
a (Å)	64.921(7)	69.079(11)
b (Å)	4.8832(5)	4.8901(8)
c (Å)	9.0299(9)	8.9962(14)
α	90.00	90.00
β	90.679(2)	91.818(3)
γ	90.00	90.00
Z	4	4
V ($Å^3$)	2862.5(5)	3037.4(8)
D_{calc} (g cm^{-3})	1.020	1.023
R_1	0.0883	0.1141
wR_2	0.3016	0.3432
GooF	1.029	1.034

2.4. Results and discussion

2.4.1. Differential scanning calorimetry

Heating thermograms corresponding to dry DAEs of even, mixed acyl chains are shown in Fig. 2.1. This figure shows that each DAE exhibits a major transition and this transition was found to correspond to the capillary melting point of the compound. Some of the DAEs show minor transitions at lower temperatures and in

some cases the thermogram consists of two sharp endotherms that are closely spaced. It is unlikely that the two peaks arise due to the presence of a significant impurity, because in such a case the impurity will lead to broadening of the endotherm rather than yielding a second sharp peak in the thermogram. These observations indicate the possibility of polymorphism in DAEs with mixed chains.

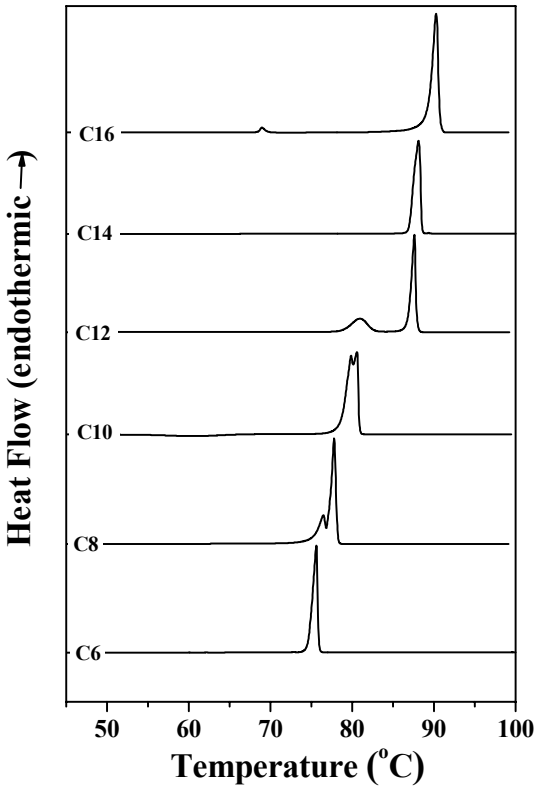

Fig. 2.1. DSC heating thermograms of *N*-, *O*-diacylethanolamines. The number of C-atoms in the *O*-acyl chain is indicated against each thermogram.

When the samples were subjected to a second heating scan, it was observed that the additional transitions disappear in some cases and small decreases have been noted in the transition enthalpies. This suggests that during cooling scan some of the DAEs do not come back to the structure of initial starting form. Therefore, in

all cases the first heating scan was considered for further analysis and the total area under the major and minor transitions was integrated to get the transition enthalpies. The transition temperatures (T_t), transition enthalpies (ΔH_t) and transition entropies (ΔS_t) obtained from the first heating thermograms are presented in Table 2.3.

Table 2.3: Chain-melting phase transition temperatures (T_t), enthalpies (ΔH_t) and entropies (ΔS_t) of DAEs. Data obtained from the DSC thermograms of dry samples of *N*-, *O*-diacylethanolamines of matched acyl chainlengths (n = 6-16) are shown.

O*-Acyl chainlength, *n	**T_t (°C) (°C)**	**ΔH_t (kcal.mol^{-1})**	**ΔS_t (cal.mol^{-1}.K^{-1})**
C_6	74.7	15.43	44.36
C_7	75.7	16.22	46.49
C_8	77.7	17.65	50.3
C_9	78.1	18.53	52.75
C_{10}	81.1	20.5	57.87
C_{11}	82.4	20.77	58.41
C_{12}	87.5	21.85	60.58
C_{13}	87.7	22.1	61.24
C_{14}	87.1	24.52	68.06
C_{15}	87.6	23.86	66.13
C_{16}	90.1	26.38	72.62

*For C_{16} the obtained value is close to the reported value (T_t=89.9, ΔH_t =26.4, ΔS_t =72.7)

When the DSC scans were run with *N*-, *O*-dipalmitoylethanolamine in the presence of excess water the thermograms obtained were essentially identical to those obtained with the dry samples, suggesting that the chain melting phase transitions of DAEs with long, matched acyl chains are not affected by the presence of water. As DAEs have no major polar groups, it is unlikely that water easily penetrates the crystalline lattice. The hydration of polar head group generally reduces the chain melting transition temperature. For example, it was observed that phosphatidylcholines, which contain a more polar head group than diacylglycerols,

have lower chain melting temperature in the hydrated state (Di & Small, 1995). Similarly, in *N*-acylethanolamines with long acyl chains, hydration results in a decrease in the phase transition temperatures (Ramakrishnan et al., 1997). The present results show that derivatization of the hydroxy group in NAEs by attaching a long acyl chain reduces the polarity of the head group region significantly, which completely eliminates interaction of the lipid with water. In view of this no further DSC studies were conducted with the DAEs in the presence of water.

2.4.2. Chainlength dependence of transition enthalpy and transition entropy

The chainlength dependence of transition enthalpy and transition entropy for the chain-melting phase transitions of DAEs of fixed *N*-acyl (palmitoyl) and varying *O*-acyl chains (C_6-C_{16}) are given in Fig. 2.2A and Fig. 2.2B, respectively. In both cases it is observed that the even and odd series independently exhibit linear dependence of the calorimetric parameters on the acyl chainlength. However, when the data obtained with the even and odd chainlength series are viewed together, a zig-zag pattern is seen with the values of enthalpy and entropy for the odd chainlength series being slightly lower than those of the even chainlength series. In other words, the calorimetric data exhibit even-odd alternation and this aspect will be discussed in more detail below.

The enthalpy and entropy data for DAEs of mixed, even and odd acyl chainlegths could be fit well to expressions 2.2 and 2.3 given below (Larsson, 1986), as observed earlier with NAEs with even and odd acyl chainlengths (Ramakrishnan et al., 1997; Ramakrishnan & Swamy, 1998):

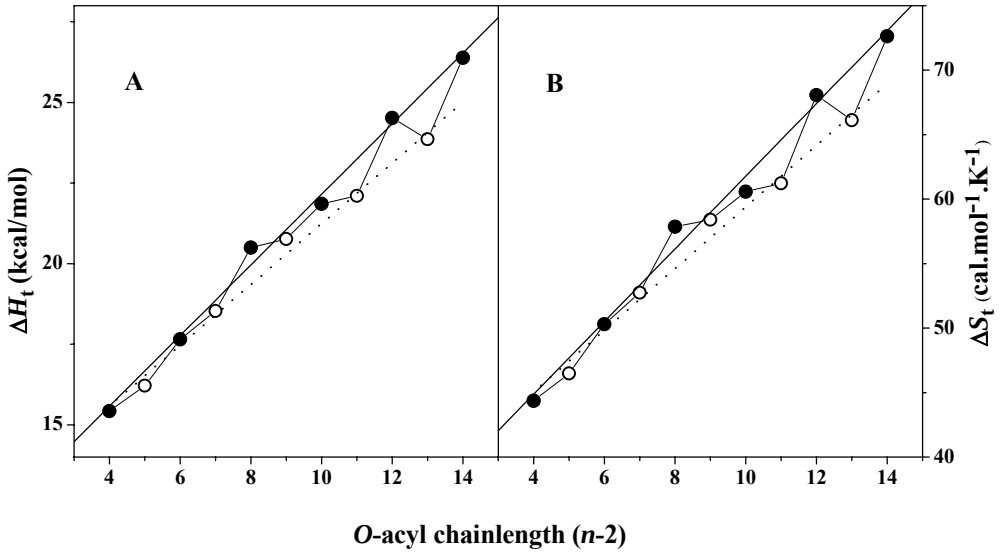

Fig. 2.2: Chainlength dependence of transition enthalpies (ΔH_t) and transition entropies (ΔS_t). Transition enthalpies (A) and transition entropies (B) obtained for the thermotropic phase transitions of *N*-, *O*-diacylethanolamines of mixed acyl chainlengths are plotted against the number of methylene units (*n*-2, where *n* is the number of C-atoms in the *O*-acyl chains) in each acyl chain. Data obtained from the heating scans are shown. The even-odd alternation is clearly seen in the plot.

$$\Delta H_t = \Delta H_o + (n\text{-}2)\Delta H_{inc} \quad (2.2)$$

$$\Delta S_t = \Delta S_o + (n\text{-}2)\Delta S_{inc} \quad (2.3)$$

where ΔH_o and ΔS_o are the end contributions to ΔH_t and ΔS_t, respectively, arising from the fixed *N*-acyl chain, the central polar region and methyl group of *O*-acyl chain. ΔH_{inc} and ΔS_{inc} are the incremental values of ΔH_t and ΔS_t contributed by each CH_2 group. Linear least squares analysis of the chainlength-dependent values of ΔH_t and ΔS_t for the even and odd series DAEs yielded the incremental values (ΔH_{inc} and ΔS_{inc}) and end contributions (ΔH_o and ΔS_o). These values are listed in Table 2.4.

The ΔH_{inc} and ΔS_{inc} values were obtained as 1.09 and 0.94 kcal.mol^{-1}, and 2.81 and 2.38 cal.mol^{-1}.K^{-1}, respectively for the DAEs with even and odd chainlengths, respectively. The corresponding per-chain ΔH_{inc} values for DAEs with matched chains were reported as 0.92 and 0.99 kcal.mol^{-1}, respectively, for the even and odd chainlength series (Kamlekar et al., 2009). A comparison of the values obtained from DAEs with mixed chains and matched chains with the corresponding values obtained previously for the NAEs (Ramakrishnan et al., 1997) show that the incremental enthalpy contributed by each CH_2 unit in the DAEs is higher than that observed with the NAEs. The ΔS_{inc} values obtained here for the DAEs with mixed acyl chainlengths are also considerably higher than the ΔS_{inc} values obtained for the NAEs (Table 2.4). These two factors, taken together, suggest that the change in the order resulting from the chain melting phase transition is higher for the DAEs than the NAEs and indicate that acyl chains in DAEs are packed more tightly.

Table 2.4. Incremental values (ΔH_{inc}, ΔS_{inc}) of chain length dependence and end contributions (ΔH_o, ΔS_o) to phase transition enthalpy and entropy of dry *N*-, *O*-diacylethanolamines with mixed acyl chains.

Lipid	ΔH_{inc}	ΔH_o	ΔS_{inc}	ΔS_o
DAEs Even chainlength	1.09±0.04	11.19±0.4	2.81±0.13	-33.60±1.32
DAEs Odd chainlength	0.94±0.05	11.81±0.53	2.38±0.17	-35.50±1.64
NAEs (even-chainlength)	0.82 ± 0.02	-.10 ± 0.26	2.01 ± 0.06	2.12 ±0.71

*For NAEs the values obtained from a similar analysis of the thermodynamic data available in the literature (Ramakrishnan et al., 1997).

2.4.3. Description of the structure

Initial cell indexing of several crystals of *N*-palmitoyl, *O*-octanoylethanolamine (NPOO) indicated the presence of two types of crystals from the same batch, indicating polymorphism. Therefore, both types were analyzed by single crystal X-ray diffraction and the crystal parameters are given in Table 2.1. Molecular structure of the α polymorph (NPOOα) is shown in the ORTEP plot given in Fig. 2.3A. It is clearly seen from this figure that the hydrocarbon portions of the two acyl chains (C8–C1, corresponding to the *O*-acyl chain and C13–C26, corresponding to the *N*-acyl chain) of the molecule are in all-*trans* conformation. The carbonyl group and the amide N–H are also in *trans* geometry. The torsion angle observed for the two acyl chain regions – excepting the C11–C12–C13–C14 angle, which is 68.6° – are all close to 180° and are fully in agreement with the above observation. The gauche conformation at the C12–C13 bond results in a distinct change in the chain direction leading to a bending of the molecule, thus giving it a bent structure, akin to the letter 'L'. In NAEs such as *N*-myristoylethanolamine (NMEA), *N*-palmitoylethanolamine (NPEA) and *N*-stearoylethanolamine (NSEA) a gauche conformation at the corresponding C–C bond results in a bending of the *N*-acyl chain giving an 'L' shape to the molecules in the crystalline state (Dahlén et al., 1977; Ramakrishnan & Swamy, 1999; Kamlekar & Swamy, 2006). Thus esterification of the hydroxyl group of NAE to produce *N*-, *O*-diacylethanolamine does not seem to affect the conformation of the *N*-acyl region.

N-Palmitoyl, *O*-octanoylethanolamine (NPOO) adopts an essentially similar structure in the β polymorph (NPOOβ). The C11–C12–C13–C14 torsion angle in NPOOβ is found to be -67.5°, which is slightly less than the value observed in the α

polymorph (NPOOα). This gauche conformation bends the NPOOβ molecule and gives it an 'L' shaped arrangement with both acyl chains coming off the two ends of the ethanolamine moiety. The two chains of the L-shaped molecule intersect at an angle of 114.5^{o} in the β form whereas the corresponding angle of intersection in the α polymorph is 114.3^{o}, which is slightly lower as compared to the β form.

Molecular structure of the α polymorph of *N*-palmitoyl, *O*-decanoylethanolamine (NPODα) is shown in the ORTEP plot given in Fig. 2.3B, and it is seen that it is isostructural with NPOOα. The other form of *N*-palmitoyl, *O*-decanoylethanolamine, namely NPODβ is isostructural with NPOOβ.

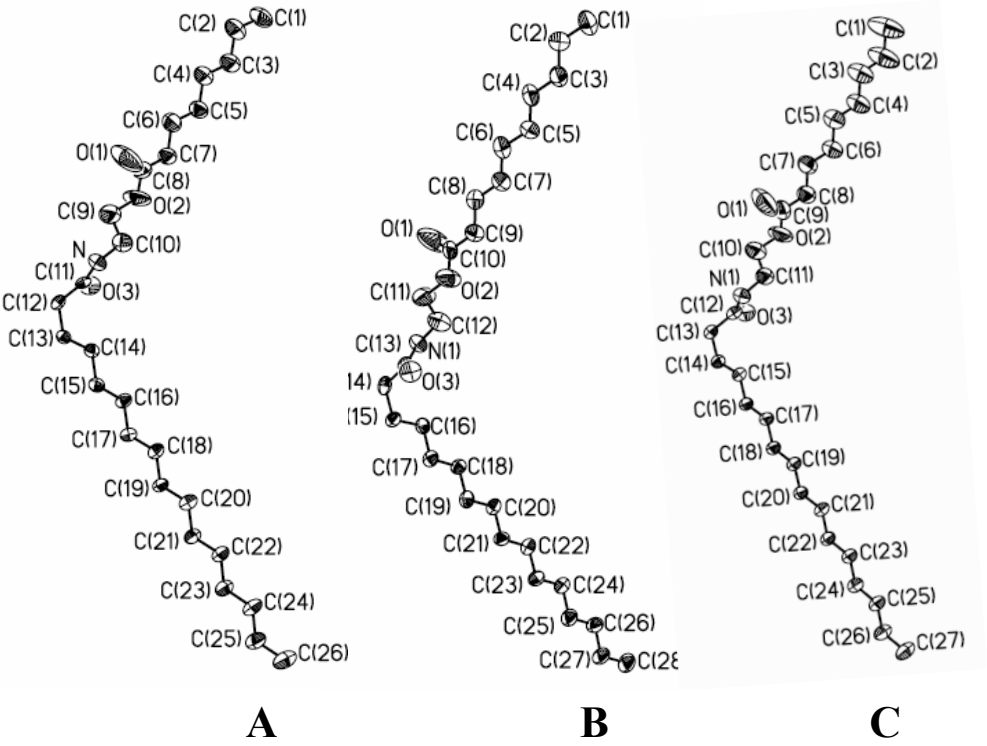

Fig. 2.3. ORTEP plots of the DAEs. (A) α polymorph of NPOO. (B) α polymorph of NPOD. (C) NPON.

The C13–C14–C15–C16 torsion angle in NPODα is found to be -70.0°, whereas the corresponding angle in the β polymorph is -69.0°. Both the polymorphs of NPOD also adopt an 'L' shape in the solid state due to the gauche conformation at the C14-C15 bond. The two acyl chains coming off the two ends of the ethanolamine moiety make an angle of 113.25^{o} with each other in NPODα and 113.8^{o} in NPODβ. In both the molecules the torsion angle at gauche conformation is very similar although in both cases the torsion angle in the α form is slightly higher than that in the β form. Similarly, the angle of intersection of the two acyl chains is also very similar in the α and β forms of both NPOD and NPOO.

Molecular structure of *N*-palmitoyl, *O*-nonanoylethanolamine (NPON) and *N*-palmitoyl, *O*-undecanoylethanolamine (NPOU) are similar to the β polymorph of NPOO and NPOD. The ORTEP plot of NPON is given in Fig. 2.3C and it is seen from the figure that this DAE with an odd *O*-acyl chain also adopts an L-shape in the solid state.

2.4.4. Molecular packing

Packing diagrams of NPOOα along the *b*-axis and *a*-axis are given in Fig. 2.4A and 2.5A, respectively. The NPOO molecules in the α polymorph are packed in layers that are stacked in such a way that the methyl groups of the *O*-acyl chains from one layer face the methyl groups of the *N*-acyl chains of the adjacent layer. As the *N*-acyl chain and *O*-acyl chain come together in one layer we refer to this as mixed packing arrangement. The methyl ends of the stacked layers are in van der Waals contacts with the closest methyl-methyl distance (C1-C1) between opposite layers and the same layer being 3.943 Å and 4.882 Å, respectively. The layer thickness (C1–C26 distance) in the structure of NPOOα is 28.05 Å and the all-*trans* *N*- and *O*-acyl chains of the molecule are tilted by 34.1° and 29.0°, respectively,

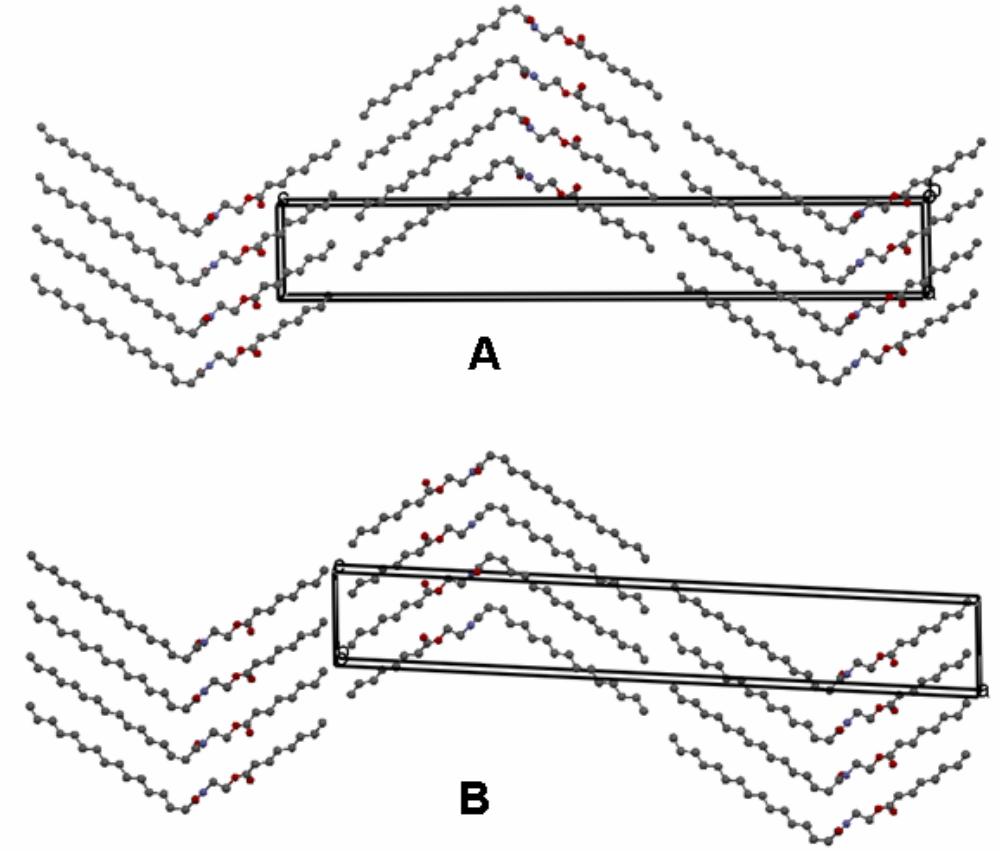

Fig. 2.4. Packing diagrams of NPOO. (A) A view along the *b*-axis of α polymorph, (B) A view along with *b*-axis of β polymorph.

with respect to the normal to the respective methyl end planes. These values are slightly lower than the range of the tilt angles with respect to the bilayer normal (35-37°) found in NMEA, NPEA and NSEA (Dahlén et al., 1977; Ramakrishnan & Swamy, 1999; Kamlekar & Swamy, 2006). In the stacked bilayers the *N*-acyl chain packs in one layer and the *O*-acyl chain in the other, which results in a mixed bilayer arrangement, with no mixing of *N*-acyl and *O*-acyl chains in the same layer. The molecular packing is very similar to that found in the crystal structures of 1,3-diacylglycerols (Larsson, 1963; Goto et al., 1995) and *N*-tetracosanoylphytosphingosine (Dahlén & Pascher, 1972), but differs significantly

from 1,2-diacylglycerols (Pascher & Sundell, 1981; Han et al., 1994), where the chain in the primary position bends at the carbonyl so that the molecule adopts a hairpin conformation with the *sn*-1 acyl chain lying next to the *sn*-2 chain.

Packing diagrams corresponding to the β polymorph of NPOO (NPOOβ) along the *b*-axis and *c*-axis are given in Figures 2.4B and 2.5B. The packing of NPOO molecules in the β polymorph is different from that found in the α polymorph. In NPOOβ the molecules are packed in layers in such a way that the methyl groups of the *O*-acyl chains from one layer face the methyl groups of the *O*-acyl chains of the next layer, instead of the methyl groups of the *N*-acyl chain of next layer as seen in the packing of NPOOα. Similarly the *N*-acyl chains from one layer face the *N*-acyl chains of the next layer. Since the *N*- and *O*-acyl chains pack in a symmetric fashion, we refer to this packing as symmetric packing arrangement. In NPOOβ the methyl ends of the stacked layers are in van der Waals contacts, with the closest methyl-methyl distance between opposite layers and the same layer being 3.918 Å and 4.866 Å, respectively. The layer thickness (C1–C26 distance) in NPOOβ is 27.93Å and the all-*trans N*- and *O*-acyl chains of the molecule are tilted by 34.1° and 28.8°, respectively, with respect to the normal to the respective methyl end planes.

The α polymorph of NPOD (NPODα) is isostructural with NPOOα and has a similar packing arrangement as observed in the crystal structure. The packing is of the mixed type where the methyl groups of the *O*-decanoyl chains from one layer face the methyl groups of the *N*-palmitoyl chains, with the closest methyl-methyl distance between opposite layers and the same layer being 3.916 Å and 4.882 Å, respectively. The layer thickness (C1–C28 distance) in NPODα is 29.98 Å and the all-*trans N*- and *O*-acyl chains of the molecule are tilted by 34.2° and 30.9°, respectively, with respect to the normal to the respective methyl end planes.

Similarly, the β polymorph of NPOD (NPODβ) is isostructural with NPOOβ and has a similar packing arrangement as observed in the crystal lattice of NPOOβ. The packing is of the symmetric type where the methyl groups of the *O*-decanoyl chains from one layer face the methyl groups of the *O*-decanoyl chains of the adjacent layer and *N*-palmitoyl chains from one layer face the methyl groups of the *N*-palmitoyl chains of the next layer. The closest methyl-methyl distance between the opposite layers and the same layer are 3.902 Å and 4.883 Å, respectively. The layer thickness (C1–C28 distance) in NPODβ is 30.07 Å and the all-*trans N*- and *O*-acyl chains of the molecule are tilted by 34.0° and 30.6°, respectively, with respect to the normal to the respective methyl end planes.

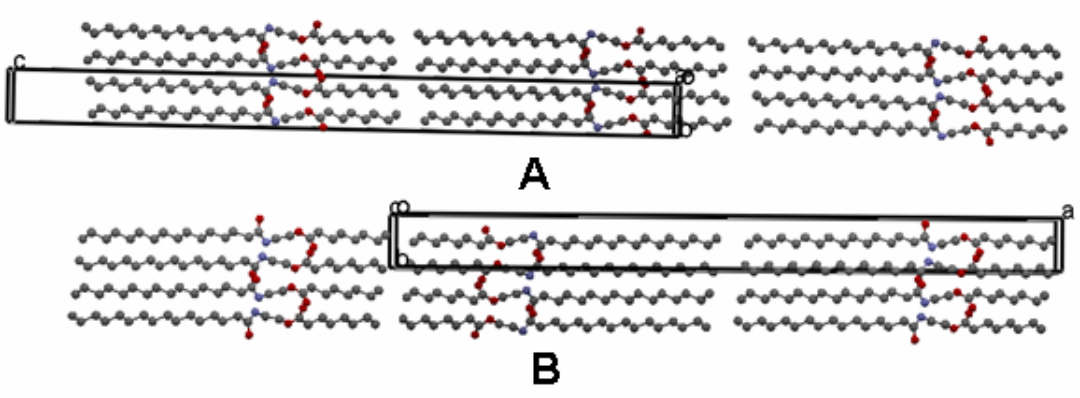

Fig. 2.5. Packing diagrams of NPOO. (A) A view along the *a*-axis of α polymorph, (B) A view along the *c*-axis of β polymorph.

The packing of NPON and NPOU are similar to that in the β polymorph of NPOO and NPOD. The acyl chains are packed in a symmetric manner, where the methyl groups of *N*-palmitoyl chains of one layer face the methyl groups of *N*-palmitoyl chains of the adjacent layer and methyl groups of odd *O*-acyl chains face the methyl groups of odd *O*-acyl chains of the next layer.

2.4.5. Subcell structure

The different lateral packing modes, adopted by hydrocarbon chains in lipid crystals are generally described by subcells that specify the relations between equivalent positions within the chain and its neighbors. Such chain packing modes fall into a relatively small number of hydrocarbon subcells with triclinic, monoclinic, orthorhombic, and hexagonal symmetry and their polymethylene planes can be mutually parallel or perpendicular with respect to their neighbors (Abrahamsson et al., 1978; Maulik et al., 1990). Examination of the hydrocarbon chain packing in the *N*-acyl chains and *O*-acyl chains of the α and β polymorphs of NPOO and NPOD revealed that the subcells in both these chains are of the orthorhombic type ($O_{\perp}$). The unit cell dimensions of these subcells are given in Table 2.5.

Table 2.5. Subcell dimensions of *N*- and *O*-acyl chains of DAEs.

	NPOO α form		NPOO β form		NPOD α form		NPOD β form	
	N-acyl chain	*O*-acyl chain	*N*-acyl chain	*O*-acyl chain	*N*-acyl chain	*O*-acyl chain	*N*-acyl chain	*O*-acyl chain
a(Å)	7.48(3)	7.76(1)	7.48(5)	7.74(1)	7.44(2)	7.64(2)	7.47(3)	7.65(6)
b(Å)	4.88(1)	4.88(1)	4.87(1)	4.87(1)	4.88(1)	4.88(1)	4.88(1)	4.88(1)
c(Å)	2.54(1)	2.53(1)	2.54(1)	2.52(1)	2.54(2)	2.54(1)	2.54(1)	2.54(1)

Generally in other two chain lipids such as 1, 3-diacylglycerols polymorphism arises from difference in subcell packing. In DAEs with mixed chains the polymorphs differ in the molecular packing along long axis. The subcell packing and molecular structure of the compounds in the two different polymorphic

forms are similar, but the two polymorphs differ in their packing arrangement. This type of polymorphism may therefore be referred to as packing polymorphism.

2.4.6. Molecular area

The area per each NPOO molecule in the bilayer plane in the crystal structures of the α and β polymorphs is 22.12 and 21.95 $Å^2$, respectively. In both α and β polymorphs of NPOD the area per molecule in the bilayer plane is 22.06 $Å^2$. These values are in the same range as those found with the NAEs whose 3-dimensional structures have been determined earlier, namely NPEA (21.99 $Å^2$ and 22.03 $Å^2$, respectively, for polymorphs α and β), NMEA (21.95 $Å^2$) and NSEA (21.99 $Å^2$) as well as some other two-chain lipids such as *N*-, *O*-dilauroylethanolamine, 2,3-dilauroyl-D-glycerol, 1,2-dipalmitoyl-sn-glycerol and 1-stearoyl-3-oleoyl-glycerol, whose molecular areas are in the range of 20.0-25.7 $Å^2$ (Dahlén et al., 1977; Pascher & Sundell, 1981; Han et al., 1994; Goto et al., 1995; Ramakrishnan & Swamy, 1999; Kamlekar & Swamy, 2006; Kamlekar et al., 2009).

2.4.7. Hydrogen bonding and intermolecular interactions

The molecular packing in the crystal structure of α polymorph of NPOO was examined carefully in order to understand the intermolecular interactions. The hydrogen bonding patterns in the crystal lattice, viewed along the *a*-, *b*- and *c*- axes, are shown in Figures 2.6A, 2.6B and 2.6C, respectively. Fig. 2.6A gives a view of the molecular packing together with the hydrogen bonds between the amide hydrogen and the carbonyl oxygen atoms of adjacent layers in the same leaflet of the bilayer. These N–H···O hydrogen bonds are formed between the amide N–H group of one molecule and the amide carbonyl oxygen of an adjacent NPOO molecule. All these H-bonds are identical, with an N–O distance of 2.87Å, and H···O distance of 2.00 Å and an N–H···O angle of 169°. This is very similar to the

value of 167° observed for the N–H···O angle in the crystal structure of NPEA (α polymorph) (Kamlekar & Swamy, 2006), and the values of 166.7° and 168° seen in the crystal structures of NMEA (Ramakrishnan & Swamy, 1999) and DLEA (Kamlekar et al., 2009).

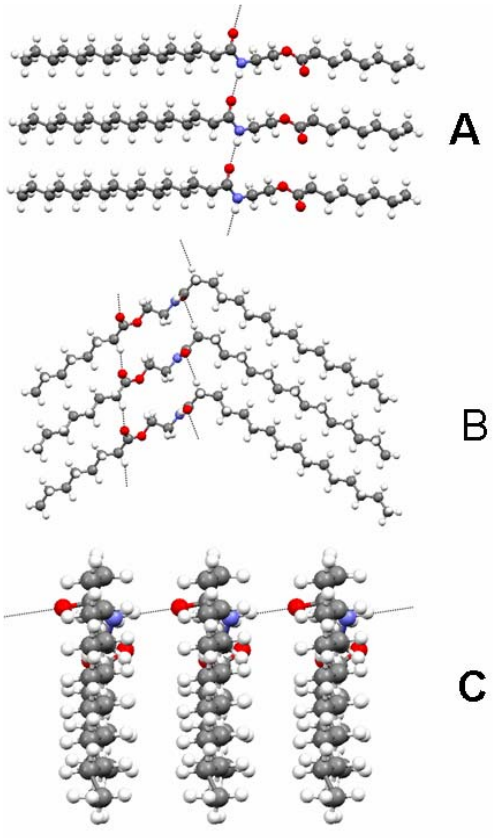

Fig. 2.6. Hydrogen bonding pattern in the crystal lattice of α polymorph of NPOO. (A) A close view along the *a*-axis displaying N-H···O type hydrogen bonding. (B) A close view along the *b*-axis displaying two C-H···O type hydrogen bonds. (C) A close view along the *c*-axis displaying two N-H···O type hydrogen bonds.

Fig. 2.6B gives a view of two weak C–H···O type hydrogen bonds observed in the crystal lattice of NPOOα. One of these is formed between O3 (oxygen atom

of the amide carbonyl group) of one molecule and one of the H-atoms on C12 (carbon atom α- to the amide carbonyl) of an adjacent molecule in the same layer. All the C–H···O hydrogen bonds between O3 and C12 in the crystal lattice are identical, with a C–O distance of 3.64 Å, an H···O distance of 2.67 Å and a C–H···O angle of 178°. The second C–H···O bond is formed between O1 (the ester carbonyl oxygen) of one molecule and one of the H-atoms on C7 (carbon atom α- to the ester carbonyl group) of an adjacent molecule in the same layer. All the hydrogen bonds between O1 and C7 are also identical, with a C–O distance of 3.38 Å, H···O distance of 2.59 Å and a C–H···O angle of 138°. Very similar hydrogen bonding patterns have been observed in the β form of NPOO as well as in the α and β polymorphs of NPOD.

2.4.8. Lattice energy calculations

Lattice energies of the α and β polymorphs of NPOO and NPOD were computed using the COMPASS/Dreiding force fields in Cerius^2 program package in order to estimate their relative energies. These calculations yielded an overall energy of -68.0 kcal/mol in COMPASS force field and -76.0 kcal/mol in Dreiding force field for the α polymorph of NPOO. For the β polymorph of NPOO the overall energy was computed as -69.0 kcal/mol in COMPASS force field and -76.75 kcal/mol in Dreiding force field. Similarly for the α polymorph of NPOD the calculated lattice energy is -72.5 kcal/mol in COMPASS force field and -80.25 kcal/mol in Dreiding force field. For the β polymorph of NPOD the overall computed energy is -73.0 kcal/mol in COMPASS force field and -81.0 kcal/mol in Dreiding force field. These results from lattice energy calculations indicate that both α and β polymorphs of each DAE (NPOO or NPOD) have comparable lattice energies.

2.4.9. Correlation of crystal structure and thermodynamic properties

It was reported earlier that 1,3-diacylglycerols exhibit higher transition temperature, transition enthalpy and transition entropy as compared to 1,2-diacylglycerols (Goto et al., 1995; Kodali et al., 1990). In 1,2-diacylglycerols the acyl chains lie side by side and have a hairpin conformation (Pascher et al., 1981; Han et al., 1994) whereas 1,3-diacylglycerols form an extended structure with the two chains separated in a 'V' formation with a dihedral angle of 94^{o} between the two acyl chain planes (Goto et al., 1995). It was proposed that the V-shaped conformation results in a more comfortable chain packing in 1,3-diacylglycerols as compared to 1,2-diacylglycerols (Goto et al., 1995). In DAEs the two chains are oriented with respect to each other at an angle of 113 – 114.5°, adopting an L-shaped geometry, which may further assist better packing. Our data also support that compared to the hairpin conformation, the lipid molecules pack better in a V- or L-shaped conformation. This may be reflected in higher ΔH_{inc} and ΔS_{inc} for DAEs as compared to NAEs. It may also be noted that transition temperature of DAEs are higher compared to diacylglycerols of same fatty acyl chainlength, although for the same acyl chains the latter have higher molecular weights as compared to the former.

2.4.10. Polymorphism in other 'L' shaped lipids

Our earlier studies have shown that diacylethanolamines with matched acyl chains adopt an 'L' shape in the solid state (Kamlekar et al., 2009). Here we have shown that diacylethanolamines with mixed acyl chains also adopt an 'L' shape in the solid state. Similar 'L' shaped structures have been found in the crystal structures of other two chain lipids such as 1,3-diacylglycerols (Larsson, 1963; Hybl and Dorset, 1971; Goto et al., 1995) and *N*-tetracosanoylphytosphingosine (Dahlén and

Pascher, 1972), where two acyl chains were segregated from the head group. Different spectroscopic and calorimetric methods have been employed to characterize polymorphism in the L-shaped lipids and it was shown earlier that 1,3-diacylglycerols (Malkin et al., 1937; Baur et al., 1949), ceramides (Raudenkolb et al., 2003, 2005) and diacylethanolamines (Kamlekar et al., 2009) can exhibit polymorphism in the solid state. Now the question that arises is regarding the structure of different polymorphic forms in L-shaped lipids! Is there any generality in the polymorphism of different L-shaped lipids?

In the present study the crystal structures of two polymorphic forms of NPOO have been solved, which have been referred to as α form and β form. The next even chain homolog of this compound, i. e., *N*-palmitoyl, *O*-decanoylethanolamine (NPOD) also exhibits similar polymorphism. Existence of the same type of polymorphism in the homologous series strongly suggests that similar polymorphic forms can exist in the entire series of molecules (DAEs). If we look closely at the packing motif of a two chain lipid, where the two chains are coming off the two sides of the head group, the lipid molecules can pack in at least two different ways. Panel 2 of Fig. 2.7A and 2.7B shows cartoon depiction of the two types of packing possibilities. In the first type the next molecule of an L or I (where the angle of intersection of two acyl chains is ca. 180°) shaped lipid can be oriented in such a way that the 1st acyl chain of the lipid will interact with the 2nd acyl chain of next molecule and 2nd acyl chain will interact with 1st acyl chain in the next layer, resulting in a mixed type chain packing. Due to the presence of mixed type chain packing the thickness of the bilayer will be the same in the entire lattice (Fig. 2.7A). This type of packing arrangement has been observed in the α polymorphs of NPOO and NPOD. In another type the next molecule can pack in such a manner that the 1st acyl chain will interact with the 1st acyl chain of the next

molecule and the 2nd acyl chain will interact with the 2nd acyl chain in the next layer, resulting in a symmetric type chain packing (Fig. 2.7B). In this type of packing the bilayer thickness is not the same in the entire lattice; the lattice will be composed of two types of bilayer thickness. This type of packing arrangement has been observed in the β polymorph of NPOO and NPOD.

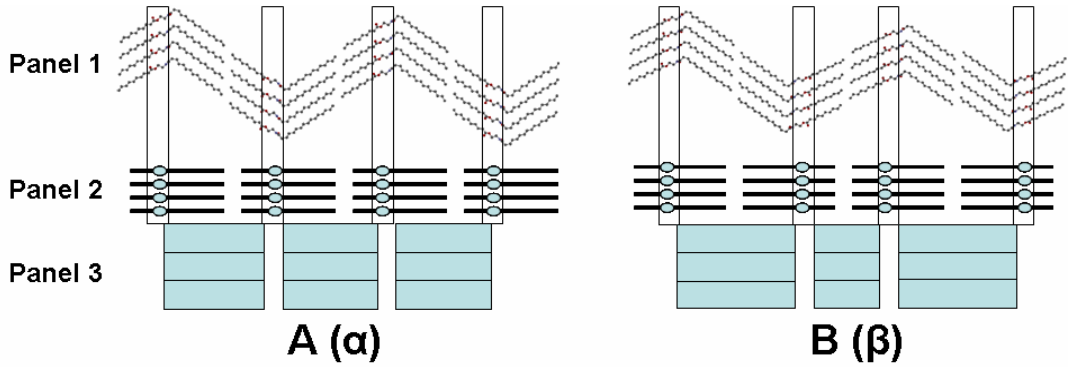

Fig. 2.7. Polymorphism in 'L' shaped lipids. Panel 1A & 1B, packing of α and β polymorph of NPOD, respectively. Panel 2A & 2B, cartoon depiction of two types of possible acyl chain packing. Panel 3A, one type of hydrophobic brick in α form. Panel 3B, two types of hydrophobic bricks in β form.

Panel 3 of Fig. 2.7A and 2.7B shows that hydrophobic regions of the diacyl lipid – which we refer to here as 'hydrophobic bricks' – are stacked against each other with favorable hydrophobic interactions. It may be seen that in the α form the same type of hydrophobic bricks repeat in the entire lattice (Panel 3 Fig. 2.7A), whereas in the β form two types of hydrophobic bricks alternate (Panel 3 Fig. 2.7B). If the two acyl chains of the lipid are identical and if the head group is symmetrical then we will get only one type of hydrophobic brick in the lattice. In this particular case both α and β type polymorphic forms may not be observed (e,g., matched chain 1,3-diacylglycerols). Except the above special case, α and β type polymorphism may be expected to be seen in all 'L' shaped lipids. The present

study establishes the existence of α and β type polymorphic forms in DAEs and strongly suggests that similar polymorphic structures may exist in other L-shaped lipids such as 1,3-diacylglycerols and ceramides. In α and β type polymorphic forms, if the hydrophilic interactions at head group are similar and the average length of the hydrophobic brick is also the same in two forms, they may have comparable lattice energy. The lattice energy calculations of the α and β polymorphs of DAEs also support the above argument. This suggests that at least two polymorphic forms should be present in an L-shaped lipid.

2.4.11. Even-odd alternation in transition temperatures and calorimetric properties

It is interesting to note that the phase transition temperatures and calorimetric properties (ΔH_t and ΔS_t) of DAEs exhibit an even-odd alternation. Similar trends were observed in the transition temperatures and physical properties of long-chain hydrocarbons, fatty acids and *N*-acylethanolamines in the solid phase, as well as for the chain melting phase transition temperatures of NAEs in the hydrated state (Larsson, 1986; Ramakrishnan & Swamy, 1998; Marsh & Swamy, 2000). Such alternation can be explained on the basis of packing of the hydrocarbon chains. To investigate this phenomenon in detail, the crystal structure of odd and even chain DAE have been compared. It was reported earlier that the melting point alternation in *n*-alkanes can be rationalized in terms of a simple geometrical model (Boese et al., 1999). The shape of *N*-palmitoyl, *O*-octanoylethanolamine (even *N*- and *O*-acyl chain) can be approximated to a rectangle, whereas the shape of *N*-palmitoyl, *O*-nonanoylethanolamine (even *N*- and odd *O*-acyl chain) can be approximated to a trapezoid in two dimension (Fig. 2.8). It has been shown schematically in Fig. 2.8 that the rectangle can be packed more tightly than a trapezoid, where similar packing will create some void space (marked in black).

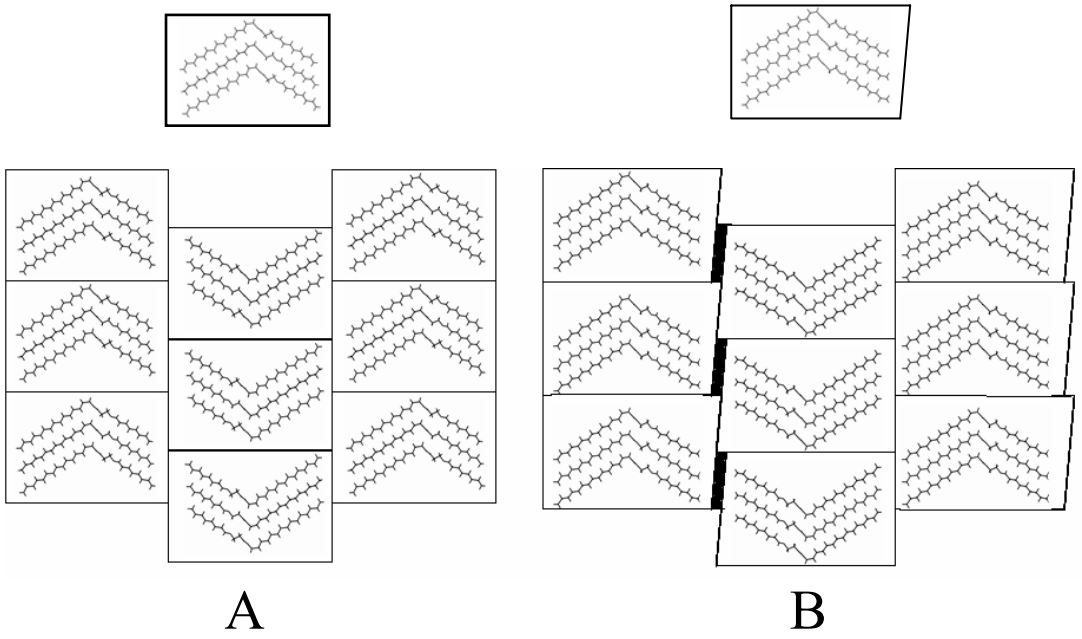

Fig. 2.8. Schematic representation of (A) the packing of an even *N*-, *O*- diacylethanolamine and (B) diacylethanolamine with an even *N* -acyl chain and odd *O*-acyl chain.

Table 2.6. Distance between the terminal C-atoms between the layers in diacylethanolamine with even and odd *O*-acyl chains.

Compound	*O*-methyl to *O*-methyl distance (opposite layer)	*O*-methyl to *O*-methyl distance (same layer)	*N*-methyl to *N*-methyl distance (opposite layer)	*N*-methyl to *N*-methyl distance (same layer)
NPOO	3.875 Å	4.866 Å	3.918 Å	4.866 Å
NPON	4.070 Å	4.883 Å	3.917 Å	4.883 Å
NPOD	3.902 Å	4.883 Å	3.906 Å	4.883 Å
NPOU	4.092 Å	4.890 Å	3.904 Å	4.890 Å

Therefore the distance between the closest methyl groups in opposite layer (C1-C1) will be more in case of DAEs with odd *O*-acyl chains as compared to the DAEs in which both *N*- and *O*- acyl chains are even (Table 2.6). Thus, DAEs with even *N*- and *O*-acyl chains have optimal intermolecular contact at both ends,

whereas DAEs with odd *O*-acyl chain and even *N*-acyl chain possess the optimal intermolecular interaction on one side and at the other end the distances between terminal methyl groups are longer. This leads to a less dense packing in DAEs with odd *O*-acyl chain, which is also evidenced from the packing coefficient. The packing coefficient for NPOO is 64.9%, which is higher than the values observed for NPON (63.2%) [β polymorphs have been considered since packing of β polymorph and NPON are similar]. Similarly, packing coefficient of NPOD is 64.8%, which is also higher than NPOU (63.6%). These results suggest that the acyl chains in DAEs with both even chains are packed more tightly than the DAEs with odd *O*-acyl chains and as a consequence odd-even alternation is observed in DAEs with mixed acyl chains.

Chapter 3

Structure and Phase Behavior of *O*-Acylethanolamines

3.1. Summary

Recent studies show that *O*-acylethanolamines (OAEs), structural isomers of the putative stress-fighting lipids, namely *N*-acylethanolamines (NAEs), can be derived from NAEs and are present in biological membranes under physiological conditions. In view of this, a homologous series of OAEs with even chainlengths (*n*=12-20) have been synthesized and the phase behavior and crystal structure have been investigated. Single-crystal X-ray diffraction studies show that the molecular packing of OAEs is modulated by the counterions. The OAE molecules with chloride, bromide and iodide counterion are organized in a tilted tail-to-tail fashion, similar to the arrangement in a bilayer membrane; whereas trifluoroacetate induces interdigitation in acyl chain packing. As a representative OAE, *O*-stearoylethanolamine (OSEA) has been investigated in detail and the thermotropic phase transitions its dispersions in water and in 150 mM NaCl were characterized using calorimetric, spectroscopic and turbidimetric studies. These studies revealed that when dispersed in water OSEA undergoes a cooperative phase transition centered at 53.8 ^{o}C from an ordered gel phase to a micellar structure whereas in the presence of 150 mM NaCl the transition temperature increases to 55.8 ^{o}C with retention of bilayer structure above the phase transition. These studies are relevant to understanding the role of salt on the phase properties of this new class of lipids.

3.2. Introduction

As indicated in Chapter 1, *O*-acylethanolamines (OAEs) containing different fatty acyl moieties may be present in biological membranes, with potentially interesting biological properties. In this regard it is of considerable interest to investigate the phase behavior and membrane interactions of OAEs and to identify their possible biological role. In this direction, in the present study, a series of OAEs with even chains have been synthesized and their phase behavior was characterized using differential scanning calorimetry (DSC), UV-Visible spectroscopy, fluorescence spectroscopy and spin-label ESR spectroscopy. In addition, the 3-dimensional structures of *O*-acylethanolamines with various counterions have been investigated by single-crystal X-ray diffraction and the molecular packing and intermolecular interactions in the crystal lattice have been analyzed.

Biological membranes are surrounded by an aqueous medium that contains ions and their interactions with cell membranes are crucial for membrane fusion, phase transitions, or transport across the membrane. Several studies on model membrane systems have revealed that ions have significant effects on the local and global properties of lipid bilayer (Aroti et al., 2007; Böckmann et al., 2003; Garcia-Manyes et al., 2005; Macdonald & Seelig, 1988; Pabst et al., 2007; Petrache et al., 2006; Sapia et al., 1994; Träuble & Eibl, 1974). It was also demonstrated that ionic strength can modulate the reorganization of lipids and membrane proteins in erythrocytes and affects membrane bending and shape of the erythrocytes (Glaser, 1982; Herrmann & Müller, 1986). In view of this, the effect of salt on the phase behavior of *O*-stearoylethanolamine has been investigated. Studies aimed at understanding the effect of salt (NaCl) concentration on the phase transition of the lipid suggest that salt can stabilize the lamellar structure of *O*-stearoylethanolamine (OSEA) even at higher temperatures.

3.3. Materials and methods

3.3.1. Materials

Fatty acids, 5-doxyl stearic acid, *N, N'*-dicyclohexylcarbodiimide (DCC) and 4-dimethylaminopyridine (DMAP) were purchased from Sigma-Aldrich (USA). Ammonium chloride (NH_4Cl), sulfuric acid and dioxane were obtained from Merck (Germany). Ethanolamine, BOC-anhydride (di-tert-butyl dicarbonate) and all the solvents were purchased locally. Milli-Q water was used in all experiments.

3.3.2. Synthesis of O-acylethanolamines

O-Acylethanolamine hydrochlorides (OAE.HCl) were synthesized by a minor modification of the procedure reported by Markey et al. (2000). Ethanolamine was blocked using BOC-anhydride and the protected ethanolamine was condensed with fatty acids using DCC as a coupling reagent. A catalytic amount of DMAP was used in the condensation reaction. The BOC-protected ester was then deblocked with 4M HCl in dioxane (prepared by dissolving dry HCl gas, which was produced from NH_4Cl and conc. H_2SO_4, into dioxane) to get the hydrochloride salt of *O*-acylethanolamine. To synthesize the trifluoroacetate, bromide and iodide salts of *O*-acylethanolamines, the BOC-protected esters were deblocked with trifluoroacetic acid, dry HBr (prepared by the reaction of tetralin with Br_2) and hydroiodic acid. Purity of the products was verified by IR and ^{1}H-NMR spectroscopy.

3.3.3. Differential scanning calorimetry

Differential scanning calorimetric studies were performed using a VP-DSC equipment (MicroCal LLC, Northampton, MA, USA). Accurately weighed lipid samples were dissolved in dry dichloromethane/methanol (1:1, v/v) and then the

solvent was removed under a stream of dry nitrogen gas. The resulting lipid film was vacuum desiccated for 5-6 hrs in order to remove residual traces of the solvent. The lipid was hydrated thoroughly with Milli-Q water or with 150 mM NaCl before performing the heating scans.

3.3.4. Turbidimetric studies

Samples for turbidimetric measurements were prepared by dispersing *O*-stearoylethanolamine hydrochloride (OSEA.HCl) in water or 150 mM NaCl. The sample was then hydrated fully by heating to about 65-70 °C in a warm water bath, with intermittent vortexing, followed by at least five cycles of freeze thawing, using liquid nitrogen and hot water (ca. 65 °C). After the last incubation in hot water, the sample was equilibrated to room temperature and transferred to a spectrometer cuvette. Turbidimetric measurements were performed at various temperatures between 25 and 65 °C using a Cary 100 UV-Visible spectrophotometer (VARIAN) equipped with a Peltier thermostat supplied by the manufacturer. Turbidity was measured by recording the optical density from 350 nm to 450 nm and turbidity at 400 nm was considered for further analysis.

3.3.5. ESR spectroscopy

Lipid dispersions of OSEA.HCl containing probe amounts of 5-SASL were prepared as follows. Measured volumes of OSEA.HCl stock solution (dissolved in chloroform-methanol mixture) and the spin-label stock solution were dispensed into glass sample tubes using a Hamilton syringe to yield 0.5 mol % spin label in the lipid dispersion. The solvent was evaporated by a gentle stream of dry nitrogen gas and the residual traces of the solvent were then removed by vacuum desiccation for a minimum of three hours. The samples were then hydrated with water or 150 mM

NaCl and kept in the dark at room temperature to reach equilibrium. Then the samples were centrifuged, and the pellets were transferred to glass capillaries. ESR spectra were recorded on a JEOL JES-FA 200 ESR spectrometer. Samples in 1 mm ID glass capillaries were placed in a standard quartz ESR tube containing light silicone oil for thermal stability. Temperature was measured with a fine-wire thermocouple positioned near the ESR tube.

3.3.6. Fluorescence spectroscopy

Fluorescence measurements were made on a SPEX FLUOROMAX-4 fluorescence spectrometer equipped with a temperature controller supplied by the manufacturer. Samples for fluorescence experiments were prepared essentially in the same manner as described above for ESR experiments, except that instead of spin probe pyrene was used. The lipid was then hydrated with water or with 150 mM NaCl and the optical density of the sample at 335 nm was kept less than 0.1. The lipid : pyrene ratio was kept as 400 : 1 and the final pyrene concentration was kept in the μM range. Samples were excited at 335 nm and emission spectra were recorded between 350 and 550 nm. Each spectrum was blank subtracted and was corrected for lamp intensity variation during measurement. The excitation and emission slit widths were set at 1.5 nm. Pyrene exhibits five bands in the spectrum and the intensity ratio of first and third band was considered for analysis.

3.3.7. Crystallization, X-ray diffraction and structure solution

Thin colorless crystals of different *O*-acylethanolamine hydrochlorides and *O*-myristoylethanolamine hydrobromide (OMEA.HBr) were grown from dichloromethane containing a trace of methanol. *O*-Acylethanolamine trifluoroacetate crystals were grown from diethyl ether. Crystals of *O*-

lauroylethanolamine hydroiodide (OLEA.HI) and *O*-myristoylethanolamine hydroiodide (OMEA.HI) were grown in chloroform. X-ray diffraction measurements were carried out as described in Chapter 2. The crystal parameters are given in Tables 3.1, 3.2 and 3.3.

Table 3.1. Crystallographic data for *O*-acylethanolamine hydrochlorides at 298 K.

	OLEA.HCl	**OMEA.HCl**	**OPEA.HCl**	**OSEA.HCl**
Formula	$C_{14}H_{30}ClNO_2$	$C_{16}H_{34}ClNO_2$	$C_{18}H_{38}ClNO_2$	$C_{20}H_{42}ClNO_2$
Crystal system	Orthorhombic	Orthorhombic	Orthorhombic	Orthorhombic
Space group	$P2_12_12_1$	$P2_12_12_1$	$P2_12_12_1$	$P2_12_12_1$
a (Å)	5.3969(17)	5.381(5)	5.3924(15)	5.382(5)
b (Å)	5.4004(18)	5.392(5)	5.3942(15)	5.410(5)
c (Å)	60.66(2)	67.30(6)	73.35(2)	79.98(7)
Z	4	4	4	4
V ($Å^3$)	1768.0(10)	1953(3)	2133.5(10)	2328(3)
D_{calc} (g cm^{-3})	1.051	1.047	1.046	1.038
R_1	0.0971	0.1183	0.1633	0.167
wR_2	0.2118	0.2730	0.4140	0.432
GooF	1.062	1.137	1.084	1.36
μ (mm^{-1})	0.213	0.198	0.186	0.175
Tilt angle (degree)	42.2	43.1	43.8	44.2

Table 3.2. Crystallographic data for *O*-acylethanolamine trifluoroacetates at 298K.

	OLEA.TFA	**OMEA.TFA**	**OPEA.TFA**	**OSEA.TFA**
Formula	$C_{16}H_{30}F_3NO_4$	$C_{18}H_{34}F_3NO_4$	$C_{20}H_{38}F_3NO_4$	$C_{22}H_{42}F_3NO_4$
Crystal system	Triclinic	Triclinic	Triclinic	Triclinic
Space group	*P-1*	*P-1*	*P-1*	*P-1*
a (Å)	6.237(3)	6.227(3)	6.2245(5)	6.2141(8)
b (Å)	8.742(4)	8.752(3)	8.7807(7)	8.7802(11)
c (Å)	19.052(9)	20.798(8)	22.3911(19)	24.097(3)
α	100.188(8)	78.142(8)	80.5080(10)	97.474(2)
β	95.447(8)	82.998(8)	88.303(2)	92.780(2)
γ	103.164(7)	76.741(8)	76.795(2)	103.223(2)
Z	2	2	2	2
V ($Å^3$)	985.5(8)	1076.3(7)	1175.08(17)	1264.9(3)
D_{calc} (g cm^{-3})	1.204	1.189	1.169	1.159
R_1	0.0778	0.1039	0.0815	0.1228
wR_2	0.2925	0.3102	0.2866	0.3123
GooF	1.108	1.029	1.032	1.150
μ (mm^{-1})	0.103	0.099	0.095	0.092

Table 3.3. Crystallographic data for hydroiodide and hydrobromide salts of *O*-acylethanolamines at 298 K.

	OLEA.HI	**OMEA.HI**	**OMEA.HBr**
Formula	$C_{14}H_{30}INO_2$	$C_{16}H_{34}INO_2$	$C_{16}H_{34}BrNO_2$
Crystal system	Triclinic	Triclinic	Orthorhombic
Space group	*P-1*	*P-1*	$P2_12_12_1$
a (Å)	5.4369(18)	5.4554(15)	5.5046(16)
b (Å)	6.350(2)	6.3836(17)	5.5072(16)
c (Å)	26.115(8)	28.972(8)	65.590(19)
α	85.740(5)	87.348(4)	90.0
β	87.863(5)	84.716(4)	90.0
γ	79.551(5)	79.283(4)	90.0
Z	2	2	4
V ($Å^3$)	883.9(5)	986.7(5)	1988.3(10)
D_{calc} (g cm^{-3})	1.395	1.344	1.177
R_1	0.1023	0.0926	0.1812
wR_2	0.2250	0.2369	0.4861
GooF	1.215	1.136	1.542
μ (mm^{-1})	1.809	1.626	2.070
Tilt angle (degree)	51.7	51.7	44.5

3.4. Results

3.4.1. X-ray diffraction studies

Description of the structure: The molecular structure of *O*-lauroylethanolamine hydrochloride (OLEA.HCl) is shown in the ORTEP plot given in Fig. 3.1. It is clearly seen from this figure that the hydrocarbon portion (C4−C14) of the acyl chains is in all-*trans* conformation and the torsion angles observed for the acyl chain region are all close to 180°. The all-*trans* conformation of the acyl chain region, gives the molecule a linear geometry.

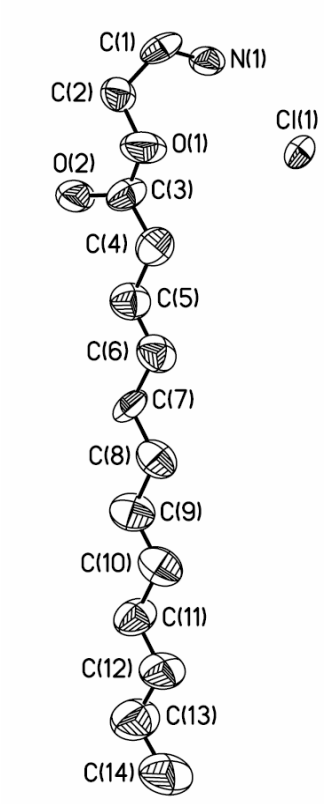

Fig. 3.1. An ORTEP plot showing the molecular structure of *O*-lauroylethanolamine hydrochloride.

In NAEs such as *N*-myristoylethanolamine, *N*-palmitoylethanolamine and *N*-stearoylethanolamine, existence of a single gauche conformation in the acyl chain region results in a bending of the *N*-acyl chain, giving an 'L' shape to the molecules in the crystalline state (Dahlén et al., 1977; Ramakrishnan & Swamy, 1999; Kamlekar & Swamy, 2006). Thus, there is a significant difference in the acyl chain conformation, due to which the molecular geometry changes from a bent structure in the NAEs to a linear structure in OLEA.HCl.

Molecular packing: Packing diagram of OLEA.HCl along the *b*-axis is given in Fig. 3.2A. The OLEA.HCl molecules are packed in a head-to-head (and tail-to-tail) manner in stacked bilayers. The methyl ends of the stacked bilayers are in van der Waals contacts, with the closest methyl-methyl contact distance (C14-C14) between the opposing layers and within the same layer being 4.08 Å and 5.39 Å, respectively. The bilayer thickness (N1-N1 distance) of OLEA.HCl is 34.3 Å and the all-*trans* acyl chains are tilted by 42.2° with respect to the bilayer normal, which is considerably higher than the tilt angles of 34.5-37° observed in the crystal structures of NAEs (Ramakrishnan & Swamy, 1999; Kamlekar & Swamy, 2006). The relatively high tilt angle in OLEA.HCl as compared to NAEs may be due to the presence of the Cl^- anion. This suggests that acyl chain packing may be modulated by the counter anions. Different counterions may exert different effects depending on their size and other properties.

To investigate this further crystal structures of *O*-lauroylethanolamine with iodide and trifluoroacetate counterions have been solved. It was observed that iodide induces more tilt in the acyl chain as compared to chloride, whereas trifluoroacetate induces interdigitation in the acyl chain (Fig. 3.2 B & C). The structures of *O*-myristoylethanolamine with chloride, bromide, iodide and trifluoroacetate have also been solved and it was observed that with increase in size

from chloride to iodide the tilt angle with respect to bilayer normal increases gradually and trifluoroacetate, which is the bulkiest among the anions used, induces interdigitation in the acyl chain.

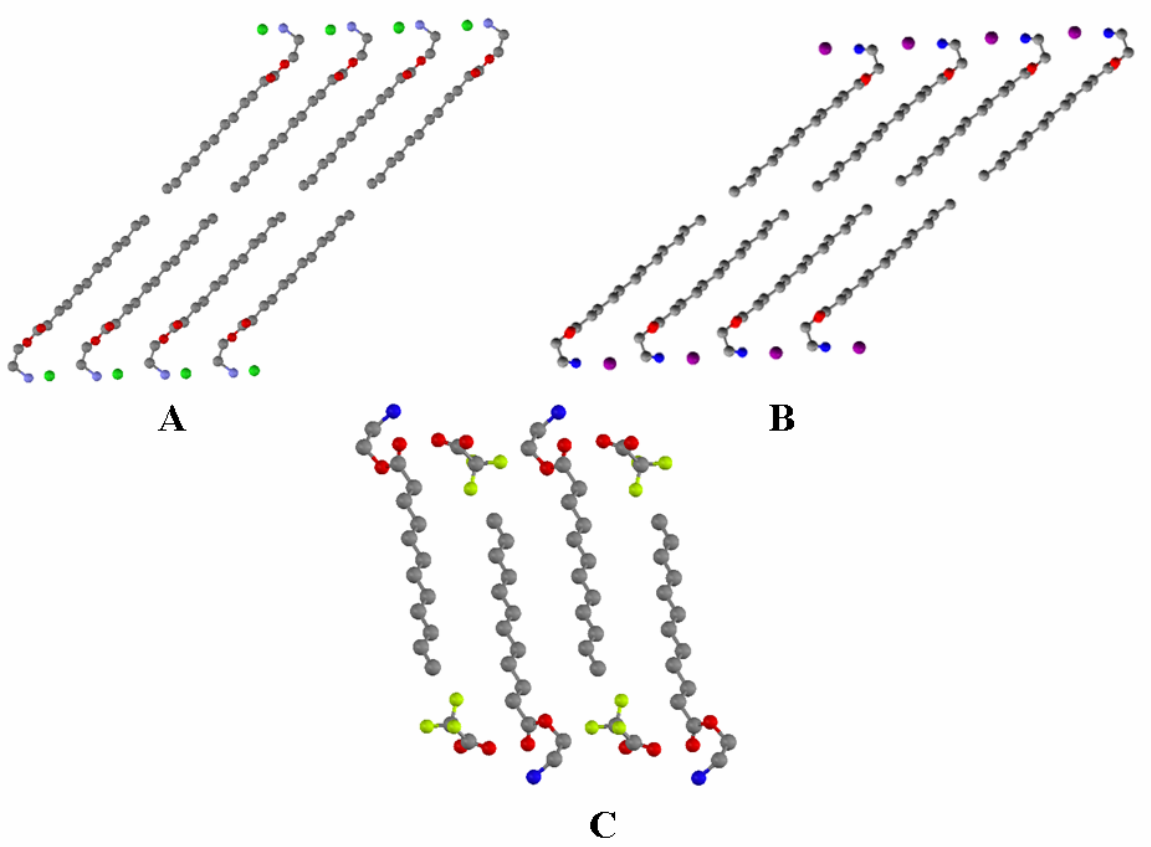

Fig.3.2. Packing diagrams of *O*-lauroylethanolamine with various counterions. A) Chloride ion induces tilt in acyl chain. B) Iodide ion induces more tilt as compared to chloride. C) Trifluoroacetate induces interdigitation in acyl chain. Color legends: grey, carbon; blue, nitrogen; red, oxygen; greenish yellow, fluorine; green, chloride; violet, iodide.

Hydrogen bonding and intermolecular interactions: To understand the intermolecular interactions in OLEA.HCl, the molecular packing in the crystal lattice was examined from various angles. The observed hydrogen bonding pattern

in the crystal lattice is shown in Fig. 3.3. Fig. 3.3A depicts that each chloride ion is hydrogen bonded to three N-H hydrogens and the chloride ion acts as a bridge between the head groups coming from opposite layers and adjacent layers. This results in the formation of three distinct hydrogen bonds by each chloride ion, with the hydrogen bond distance (H···Cl) and angle of the three types of N-H···Cl interactions being 1.93 Å, 2.02 Å, and 2.03 Å, and 168.8°, 172.9°, and 160.9° respectively. The three types of N-H···Cl interactions give rise to a hydrogen bonding motif in the head group region, which is topologically similar to the arrangement observed in super black phosphorous (Ermer & Eling, 1994) (Fig. 3.3B).

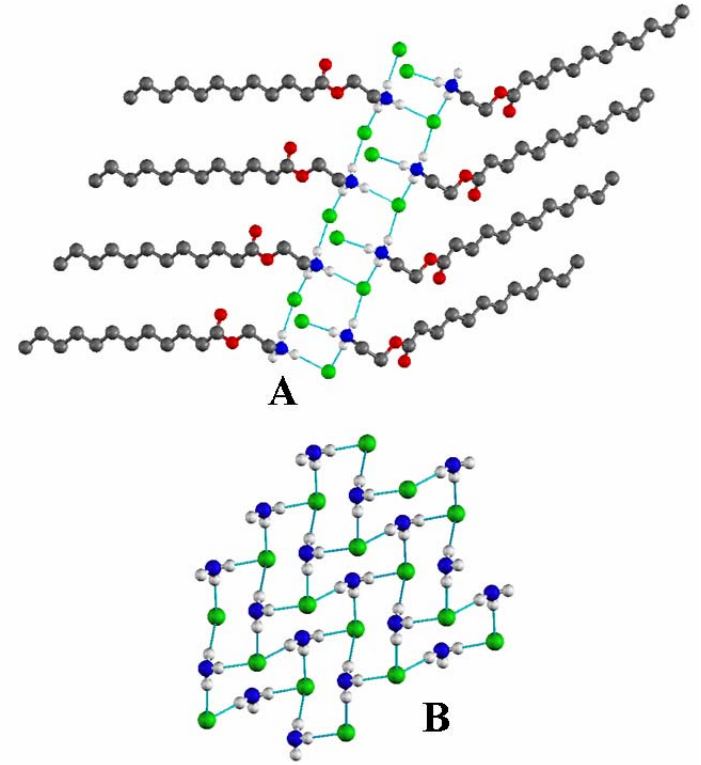

Fig. 3.3. Hydrogen bonding pattern in the crystal lattice of OLEA.HCl. (A) A close-up view displaying N-H···Cl type hydrogen bonding. (B) Hydrogen bonded motif involving N-H···Cl interactions is topologically similar to super-black phosphorous. Color legends: grey, carbon; blue, nitrogen; white, hydrogen; green, chloride.

The crystal structure, packing and hydrogen bonding interactions of *O*-palmitoylethanolamine hydrochloride (OPEA.HCl) and *O*-stearoylethanolamine hydrochloride (OSEA.HCl) are similar to those observed with OLEA.HCl. Similarly, as in OLEA.TFA, interdigitation of acyl chain has been observed in other OAEs, namely, *O*-palmitoylethanolamine trifluoroacetate and *O*-stearoylethanolamine trifluoroacetate.

3.4.2. Determination of CMC of OLEA.HCl

The CMC of OLEA.HCl was determined using an isothermal titration calorimeter (VP-ITC, Microcal Inc., Northampton, MA) by measuring the enthalpy changes resulting from dilution of the lipid solution into water at 25°C. Titration profiles resulting from sequential injections of 10µl aliquots of 100 mM OLEA.HCl solution into a 1440 µl reaction cell initially containing water were measured. The dependence of the enthalpy change per mole of surfactant (ΔH_i) injected into the reaction cell on the lipid concentration in the reaction cell was calculated by integration of the heat flow versus time profiles (Fig. 3.4). Initially, a series of relatively large endothermic peaks was observed when the lipid was injected into the reaction cell. These enthalpy changes result from micelle dissociation because the lipid concentration in the reaction cell is initially below the CMC (Bijma et al., 1997). The endothermic nature of these peaks ($\Delta H>0$) indicates that demicellization must lead to an increase in the overall entropy of the system, since micelle dissociation is thermodynamically favorable below the CMC ($\Delta G<0$), therefore $T\Delta S>\Delta H$. This entropy increase may be attributed to the disruption of water structure (release of counter-ions associated with the surfactant head-groups) when micelles breakdown to monomers (Bijma et al., 1997). After a certain number of injections, an appreciable decrease was noticed in peak height. A plot of the enthalpy versus injection number shows a sharp decrease in the enthalpy after

the 10th injection (Fig. 3.4, lower panel). This may be explained on the basis of the lipid concentration in the reaction cell exceeding the CMC, because of which the micelles injected into the reaction cell no longer dissociate. The enthalpy change above the CMC is therefore solely due to micelle dilution effects. The CMC of OLEA.HCl was determined from the inflexion point in the ΔH_i versus lipid concentration curves as 7.3 ± 0.2 mM.

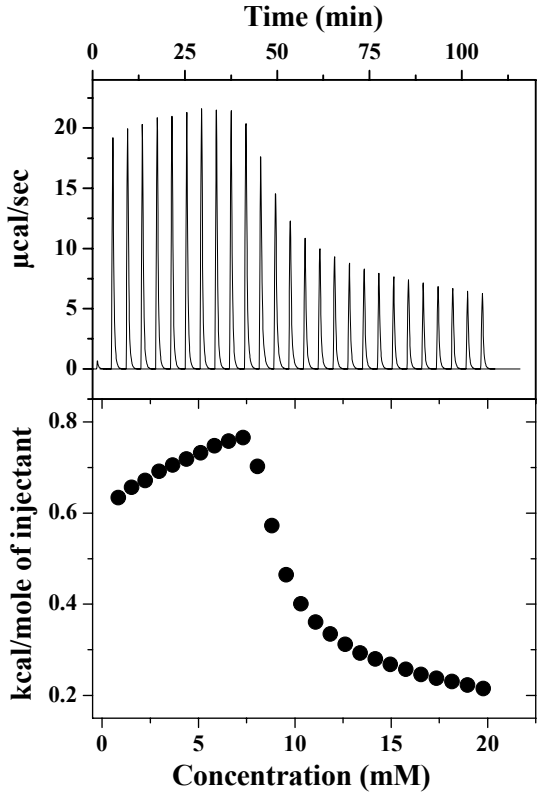

Fig. 3.4: ITC profile of dilution OLEA.HCl. The upper panel shows raw data for the injection of 100 mM OLEA.HCl into water. The lower panel shows the integrated data obtained from the raw data shown in upper panel. The difference in enthalpy between the two sections of the curve at the cmc represents the enthalpy of micellization. From the curve the obtained enthalpy of micellization is 0.4 kcal.mol^{-1}.

3.4.3. Differential scanning calorimetry

O-Acylethanolamines (OAEs) contain a basic moiety (-NH_2 group), which can exist in the protonated or free state depending upon the pH of the environment. Since *O*-acylethanolamines are not stable at basic pH (Markey et al., 2000) and in view of the acidic pH of endosomes and ischemic tissues (Murphy et al., 1984; Rybak & Murphy, 1998; Boomer & Thompson, 1999), we have synthesized *O*-acylethanolamines as the hydrochloride and characterized their phase transition.

Differential scanning calorimetry of O-acylethanolamines in excess water: The hydrated OAEs with even chainlengths (*n*=14-20) higher than lauroyl yielded turbid suspensions which become optically clear at higher temperature. This suggested that these compounds undergo a phase transition from a phase of high turbidity (possibly gel phase) to a phase where aggregates are small (micelles) and do not scatter visible light. In order to characterize the thermotropic transition differential scanning calorimetric (DSC) studies were performed with OAEs of higher chainlengths (*n*=14-20). Fig. 3.5 shows the second heating scan of OAEs and it shows that the phase transition temperature increases with acyl chainlength. The thermodynamic parameters such as transition temperature (T_t), enthaplpy of transition (ΔH_t), entropy of transition (ΔS_t) and the width at half maximum of the transition ($T_{1/2}$) associated with the phase transition, obtained from an analysis of DSC thermograms are listed in Table 3.4. While T_t increases with increase in acyl chainlength, ΔH_t and ΔS_t are not linerly dependent on chainlength. Also, it is clearly seen from Fig. 3.5 and Table 3.4 that the $T_{1/2}$ also varies with acyl chainlengths. For OMEA.HCl and OPEA.HCl the transition is broad, resulting in higher $T_{1/2}$ as compared to OSEA.HCl and *O*-arachidylethanolamine hydrochloride (OAEA.HCl), for which the transition is sharp. These results suggest that the phase

properties of OAEs depend on the acyl chainlength. In the present study the phase behavior of OSEA.HCl has been investigated in detail by various biophysical approaches.

Table 3.4. Thermodynamic parameters obtained from DSC studies on *O*-acylethanolamine hydrochlorides with even chainlengths. Samples were dispersed in water.

Acyl chainlength, n	T_t **(°C)**	$T_{1/2}$ **(°C)**	ΔH_t (kcal.mol^{-1})	ΔS_t (cal.mol^{-1}.K^{-1})
C_{14}	32.0 ± 0.37	2.46 ± 0.32	9.18 ± 0.59	30.09
C_{16}	43.3 ± 0.19	3.19 ± 0.19	11.07 ± 0.49	34.99
C_{18}	53.8 ± 0.37	0.57 ± 0.19	5.27 ± 0.73	16.12
C_{20}	66.0 ± 0.24	0.37 ± 0.10	6.36 ± 0.70	18.76

Differential scanning calorimetry of OSEA.HCl in the presence of salt: In order to understand the effect of ionic strength on the phase transition of OSEA.HCl, calorimetric studies were performed at various concentrations of NaCl. A representative heating thermogram recorded in 150 mM NaCl is shown in Fig. 3.5 and the thermodynamic parameters obtained are listed in Table 3.5. These data show that increasing the salt concentration results in an increase in the phase transition temperature (T_t), whereas the corresponding width at half maximum of the transition ($T_{1/2}$) decreases. Since the transition temperature does not change above 150 mM NaCl further studies regarding the salt concentration dependence of the phase behavior and phase transition have been carried out at the same concentration of NaCl. It is noteworthy that this ionic strength is physiologically relevant. The increase in T_t in presence of salt suggests that salt may stabilize the lamellar phase whereas the decrease in $T_{1/2}$ with increase in the salt concentration

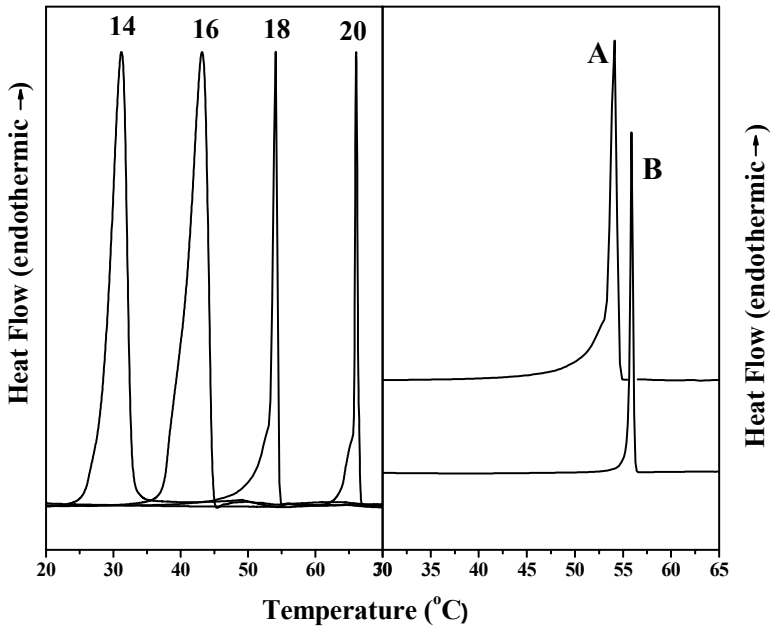

Fig. 3.5: Left panel, DSC heating thermograms of *O*-acylethanolamines with even chainlengths dispersed in water. Right panel, DSC heating thermograms of *O*-stearoylethanolamine hydrochloride dispersed in (**A**) water and (**B**) 150 mM NaCl.

Table 3.5. Thermodynamic parameters obtained from DSC studies on OSEA.HCl. Samples were dispersed in distilled water containing the indicated concentration of sodium chloride.

NaCl (mM)	T_t (°C)	$T_{1/2}$ (°C)	ΔH_t (kcal.mol^{-1})	ΔS_t (cal.mol^{-1}.K^{-1})
0	53.8 ± 0.37	0.57 ± 0.19	5.27 ± 0.73	16.12
25	55.24 ± 0.16	0.43 ± 0.04	6.35 ± 0.12	19.32
50	55.58 ± 0.24	0.34 ± 0.02	4.92 ± 0.07	14.97
150	55.81 ± 0.24	0.36 ± 0.06	5.45 ± 0.80	16.57
250	55.84 ± 0.10	0.30 ± 0.04	5.77 ± 1.24	17.54

shows that the phase transition becomes sharper. Saturated diacylphosphatidylcholines are known to exhibit sharp, thermotropic lamellar gel-liquid crystalline phase transitions with increase in temperature. The widths at half height ($T_{1/2}$) of these sharp transitions range between 0.10 and 0.32° for lamellar gel-liquid cryatalline phase transition in phosphatidylcholines (n=13-20) (Yeagle, 2005). The $T_{1/2}$ of 0.57 °C observed for the phase transition of OSEA.HCl in water (Table 3.5) is higher than the value obtained for the gel-liquid crystalline phase transition in hydrated distearoylphosphatidylcholine (DSPC) (T_t = 55.3 ^oC, $T_{1/2}$ = 0.24) (Lewis et al., 1987). The comparison with DSPC is appropriate since both DSPC and OSEA.HCl have identical (stearoyl) acyl chains in the hydrophobic region. The higher $T_{1/2}$ observed here for OSEA.HCl in water suggests that the phase transition is broader and hence may not correspond to a lamellar gel-to-liquid crystalline transition, which in phosphatidylcholines is a rather sharp transition. Additionally, as the solution becomes transparent at high temperature, it is likely that OSEA.HCl exists as micelles above the phase transition i. e., the transition taking place in water corresponds to a lamellar gel-to-micellar phase transition. In the presence of 150 mM NaCl the $T_{1/2}$ and the T_t values obtained from DSC studies for OSEA.HCl (T_t = 55.8 ^oC, $T_{1/2}$ = 0.24) are comparable to those corresponding to the gel-liquid crystalline phase transition of DSPC indicated above. Since the T_t increases and $T_{1/2}$ decreases and the sample remain turbid above phase transition, it is clear that salt has a significant effect on the phase transition and the phase structure above the transition. In order to investigate this in more detail, and to characterize the high temperature phases, turbidimetric and spectroscopic studies were performed.

3.4.4. Turbidimetric studies on OSEA.HCl

To investigate the salient features of the phase transition of OSEA.HCl, tubidimetric studies have been performed, monitoring the turbidity at 400 nm as a function of temperature using a spectrophotometer. Fig. 3.6 depicts the change in turbidity of OSEA.HCl in water and in 150 mM NaCl. In both environments the turbidity at low temperature was relatively high, which decreases with increase in temperature. Near the phase transition temperature the turbidity exhibits a sharp decrease upon increase of temperature and thereafter remains at a constant level. The midpoint of the steeply declining region was taken as the phase transition temperature (T_t). The T_t values obtained from the turbidimetric studies were 51.5 and 54.5 °C, respectively, for measurements performed in water and in 150 mM NaCl. These values are in good agreement with the values obtained from the DSC studies, presented above.

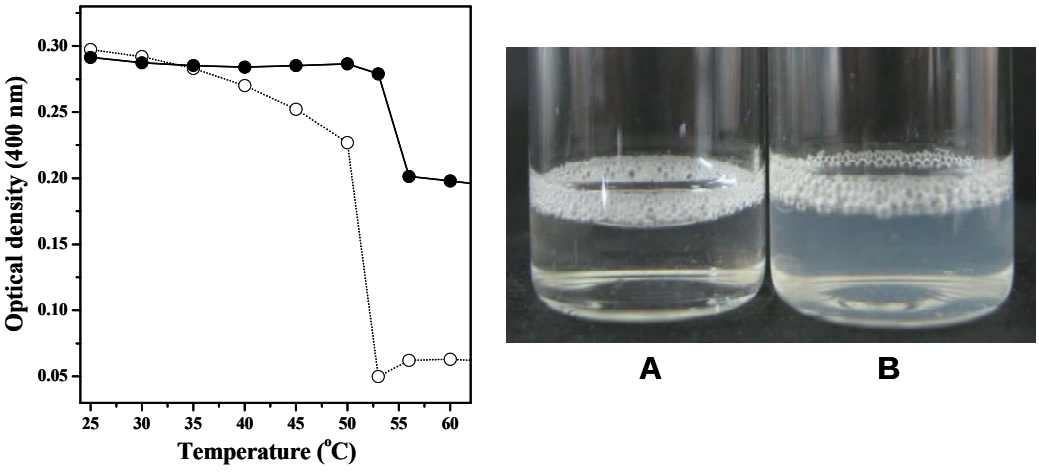

Fig. 3.6: Left panel, turbidimetric study of the thermotropic phase transition of OSEA.HCl dispersed in water (○) and in 150 mM NaCl (●). Lipid concentration was 1 mg/ml for both samples. Right panel, a snapshot of OSEA.HCl above phase transition. (**A)** Dispersed in water, (**B)** dispersed in 150 mM NaCl.

From Fig. 3.6 it can be clearly seen that above phase transition temperature turbidity of the sample in water is significantly lower than that of the sample prepared in 150 mM NaCl. The difference in turbidity is not due to difference in the lipid concentration since identical concentrations of OSEA.HCl were used in these two experiments. Visual inspection indicated that above phase transition the sample prepared in water is clear to the naked eye (Fig. 3.6A), suggesting that the aggregates are relatively small, which most likely correspond to micelles. Above phase transition temperature the sample in 150 mM NaCl exhibits a bluish turbidity, suggesting the presence of larger aggregates (Fig. 3.6B), which may correspond to liquid crystalline phase.

3.4.5. Spin-label ESR spectroscopy

ESR spectra of 5-doxyl stearic acid spin label (5-SASL) in OSEA.HCl in water and in 150 mM NaCl recorded at different temperatures are shown in Fig. 3.7A & 3.7B. At 25°C the spectra recorded in water and in 150 mM NaCl exhibit a pattern that is typical of fatty acid spin probes embedded in phospholipids bilayers (Kleinschmidt & Marsh., 1997; Sankaram & Thompson, 1990; Sapia et al., 1994). The outer hyperfine splitting ($2A_{max}$), which gives a measure of anisotropic motion of the probe, is 59.2 G and 56.8 G, respectively, in water and in 150 mM NaCl. The value of $2A_{max}$ at room temperature is close to the value exhibited by fatty acid spin labels bearing the nitroxide probe on the 5^{th} C-atom incorporated in the lamellar gel phase of lipids, suggesting that OSEA.HCl may adopt a lamellar gel phase in both the environments at room temperature (Sankaram & Thompson, 1990; Rama Krishna & Marsh, 1990; Marsh, 1980). As the temperature increases the $2A_{max}$ decreases in both the environments, consistent with the environment of the probe becoming more mobile at higher temperatures (Fig. 3.7C). In water, the spectra become more isotropic above the phase transition. Qualitatively similar spectra

have been obtained with octadecyl-trimethylammonium bromide (C_{18}TAB) micelles and other micelles using 5-SASL as a spin probe (Benatti et al, 2001). This suggests that in water OSEA.HCl may form some kind of micelles above the phase transition temperature. This observation is consistent with the results of the above turbidimetric studies, which could be interpreted in terms of the formation of micelles by OSEA.HCl above the phase transition. In 150 mM NaCl above phase transition temperature (55 °C) the $2A_{max}$ was found to be ca. 42.6 G, which is in the range expected for the 5-SASL in the liquid-crystalline phase of a bilayer membrane (Rama Krishna & Marsh, 1990; Marsh, 1980; Perez-Gil et al., 1995).

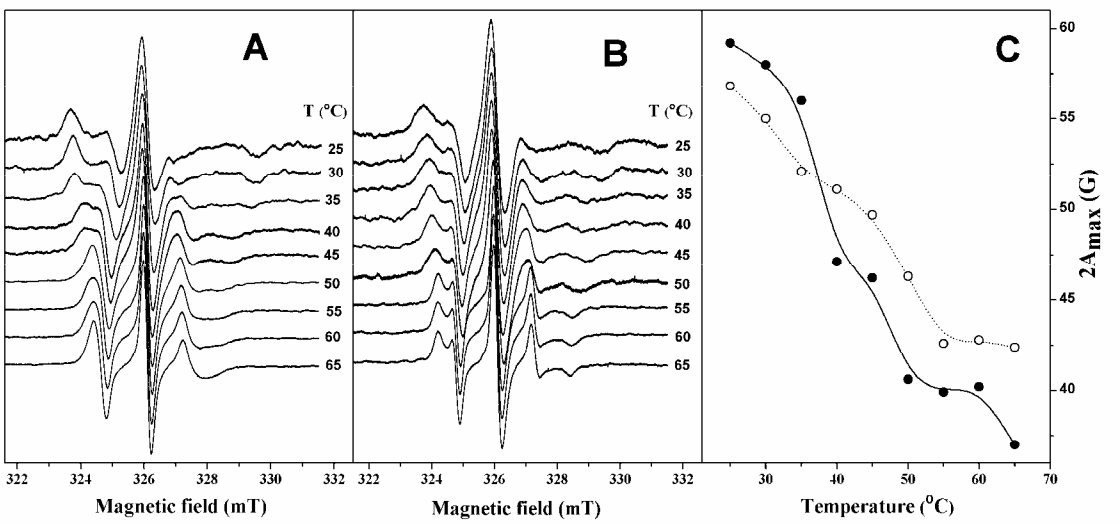

Fig. 3.7. A) ESR spectra of 5-SASL in OSEA.HCl dispersed in water. **B)** ESR spectra of 5-SASL in OSEA.HCl dispersed in 150 mM NaCl. **C)** Temperature dependence of $2A_{max}$ (G) in water (●) and in 150 mM NaCl (○). In A and B the temperature at which each spectrum was recorded is indicated.

Also, the spectra recorded above phase transition temperature display features that are characteristic of a fluid liquid crystalline phase with partially motionally averaged, axial hyperfine anisotropy (Sankaram & Thompson, 1990). These results are in agreement with OSEA.HCl undergoing a lamellar gel-phase to a fluid liquid-

crystalline phase transition in the presence of salt, instead of transforming to micellar phase as concluded above for the sample hydrated with water. Thus the ESR studies establish that presence of salt stabilizes the bilayer structure of OSEA.HCl.

3.4.6. Fluorescence spectroscopy

The relative intensities of vibronic bands in pyrene monomer fluorescence exhibit good correlation with polarity of the environment in which the probe is located (Kalyansundaram & Thomas, 1977). Higher values of I_1/I_3 peak ratio indicate higher polarity of the probe environment. In phospholipids, simple monitoring of the I_1/I_3 peak ratio allows determination of the gel-liquid crystalline phase transition temperature (Georghiou & Mukhopadhyay, 1981). The I_1/I_3 peak ratio of pyrene in OSEA.HCl decreases with increase in temperature (Fig. 3.8), suggesting that below the phase transition temperature (gel phase) pyrene is presumably located near the

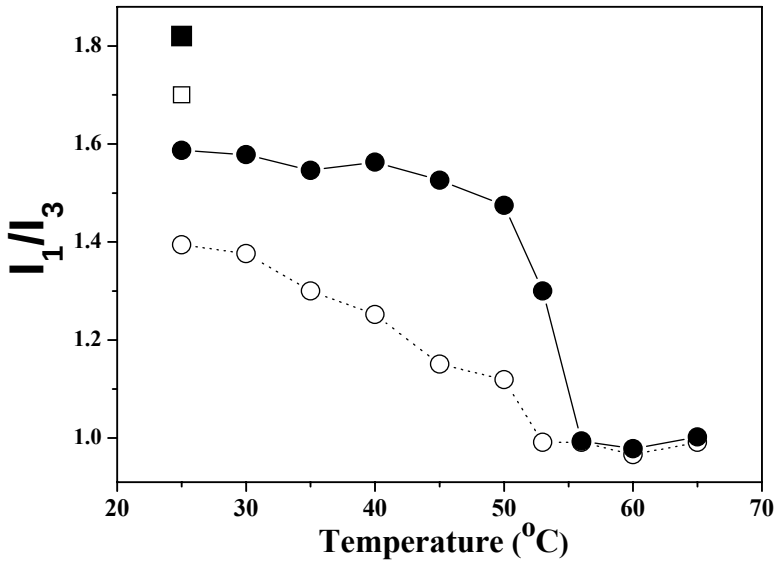

Fig. 3.8: Temperature dependence of polarity ratio (I_1/I_3) of pyrene in OSEA.HCl dispersed in water (○) and in 150 mM NaCl (●). Values of I_1/I_3 of pyrene alone in water (□) and in 150 mM NaCl (■) are also shown.

head group (polar) region, whereas above the phase transition temperature, it moves deeper into the hydrophobic region of the lipid aggregate. At room temperature (i.e., in the gel phase) I_1/I_3 peak ratio of OSEA.HCl in water and in 150 mM NaCl has values of 1.39 and 1.59, respectively. The higher value of peak ratio in 150 mM NaCl may be due to the fact that the environment becomes more polar in the presence of salt. It may also be possible that salt induces tighter packing of acyl chains and thus pyrene penetration to bilayer is further prohibited, resulting in its immobilization near the head group region.

3.4. Discussion

Research work done since the early 1960s has shown that long-chain *N*-acylethanolamines are present as minor components in a variety of organisms and their content increases dramatically under different types of stress (Schimd et al., 1990; Chapman, 2004). Additionally, it has been shown that NAEs can be transformed to *O*-acylethanolamines in acidic medium whereas the reverse transformation i.e., transformation of OAEs to NAEs takes place at basic pH (Markey et al., 2000). This suggested that OAEs are also likely to be present in biomembranes, especially under stress conditions when the content of NAEs increases quite significantly. Indeed this proved to be the case when *O*-arachidonylethanolamine was found to be present in brain tissues and it was reported that it can bind to both type-1 and type-2 cannabinoid receptors (Porter et al., 2002). In view of this, it would be interesting to investigate the structure, phase properties and membrane interactions of *O*-acylethanolamines and to compare them with those of *N*-acylethanolamines, which are structural isomers of OAEs. While several studies have been carried out on the phase behavior of aqueous dispersions of NAEs and their interaction with other membrane lipids with a view to correlate

their structure and phase behavior with the diverse biological activities exhibited by them (Ambrosini et al., 1993; Kamlekar et al., 2007, 2009; Marsh & Swamy, 2000; Ramakrishnan et al., 1997, 2002; Swamy et al., 2003), there have been no reports of similar studies on OAEs. In view of this lacuna, a homologous series of OAEs with even chainlengths have been synthesized and the phase behaviour and aggregation properties of one member of OAE family, OSEA.HCl in aqueous dispersions have been investigated. The results obtained are discussed here.

The self-aggregation of lipids and surfactants is an interesting phenomenon. Above a critical concentration these amphiphiles form aggregated structures and the aggregate morphology depends on the well-known packing parameter (P) as described by Israelachvili (1992):

$$P = v/l_c a_o$$

where v and l_c are the volume and chain length of the hydrophobic portion, respectively, and a_o is the optimal surface area occupied by the molecule at the hydrocarbon interface. For charged amphiphiles a_o is influenced considerably by the electrostatic repulsion between adjacent head groups in the aggregates and reducing the electrostatic repulsion can increase the value of P. Most short, single-chain surfactants have a P of less than one-third and consequently form spherical micelles. For membrane lipids and double-tailed surfactants, the volume of the hydrophobic group (v) is increased, resulting in a P value in the one-half to one range, and they will adopt a bilayer or vesicular phase.

The results obtained from calorimetric and spectroscopic techniques indicate that the structure of OSEA.HCl formed in aqueous dispersion depends on the ionic strength of the medium. In the absence of salt, due to electrostatic repulsion between the lipid head groups of adjacent layers OSEA.HCl takes up large amounts of water. Hydration of head group makes it large compared to the

tail which may induce the formation of an interdigitated gel or tilted lamellar gel phase at room temperature, which undergoes a phase transition with increase in temperature to yield most likely a micellar phase which was found to be optically clear in tubidimetric measurements (Fig. 3.6). In presence of salt the phase transition temperature increases with increase in the salt concentration and also the transition becomes sharp, which was evidenced by a decrease in the $T_{1/2}$ value (Table 3.5). The phenomenon may be due to better packing of the hydrocarbon chains as the electrostatic repulsion will be screened in presence of salt. The corresponding T_t and $T_{1/2}$ found in OSEA.HCl were 55.8 and 0.36 °C, respectively, which are close to the values obtained for the gel-liquid crystalline phase transition temperature of distearoylphosphatidylcholine (Lewis et al., 1987; Yeagle, 2005). The corresponding enthalpy of transition was 5.45 kcal.mol^{-1}, which is nearly half of the enthalpy of transition determined for the lamellar gel to liquid crystalline phase transition of DSPC (Lewis et al., 1987; Yeagle, 2005). This could be attributed to the fact that DSPC contains two fatty acyl chains, whereas OSEA.HCl is a single-chain lipid. Thus DSC data strongly suggests that in presence of 150 mM NaCl OSEA.HCl undergoes a lamellar gel to liquid crystalline phase transition, whereas in water above phase transition temperature a micellar phase is formed.

Spin-label ESR spectroscopy employing fatty acid or phospholipid spin labels bearing stable nitroxide spin probes have been used extensively to study the environment in the hydrophobic region of lipid aggregates and membranes (Rama Krishna & Marsh, 1990; Swamy & Marsh, 1994; Swamy et al., 2000). The outer hyperfine splitting ($2A_{max}$) of the probe provides information regarding the structure and dynamics of lipid aggregates. The observed $2A_{max}$ values of 5-doxylstearic acid embedded in OSEA.HCl dispersed in water and in 150 mM NaCl at low temperature (below phase transition) are comparable to the $2A_{max}$ values

obtained for this spin label in the lamellar gel phase of different lipids (Sankaram & Thompson, 1990; Rama Krishna & Marsh, 1990; Marsh, 1980). The ESR spectrum recorded above transition temperature in aqueous dispersions was considerably more isotropic, with a significantly reduced $2A_{max}$which is consistent with a micellar structure. In presence of 150 mM salt the ESR spectrum was relatively more anisotropic even after the phase transition and the obtained $2A_{max}$ values were in the range of values observed for this spin label in liquid crystalline phase (Rama Krishna & Marsh, 1990; Marsh, 1980; Perez-Gil et al., 1995). The ESR data and the bluish turbidity of the sample suggest the presence of liquid-crystalline phase above the phase transition temperature (Fig. 3.6 and Fig. 3.7).

Effect of salt on the phase behavior of *O*-stearoylethanolamine hydrochloride

The influence of ions on the structure and function of biological membranes is well recognized and the effects of ions on natural membranes as well as on model systems have been extensively investigated (Aroti et al., 2007; Böckmann et al., 2003; Garcia-Manyes et al., 2005; Macdonald & Seelig, 1988; Pabst et al., 2007; Petrache et al., 2006; Sapia et al., 1994; Träuble & Eibl, 1974). For a charged lipid in water, due to electrostatic repulsion the effective head group size of charged lipids increases, resulting in the formation of an interdigitated bilayer or a tilted bilayer structure in the gel phase. Above the phase transition, for some lipids the lamellar fluid phase will be unstable due to more open head group structure and it will most likely transform to a micellar phase. This type of phase transition has been characterized in surfactants, platelet activating factor and also in important derivatized lipids such as *N*-biotinyl phosphatidylethanolamines (Ohta et al., 2003; Alves et al., 2007; Feitosa et al., 2006; Horbaschek et al., 1998; Huang et al., 1986; Maurer et al., 1994; Swamy et al, 1993). Increase in the ionic strength of the aqueous solution of single-tailed ionic surfactants may result in a decrease in the

head group area, which increases the value of packing parameter *P* towards one, which stabilizes the bilayer gel phase and liquid crystalline phases. Here, it was observed that in presence of 150 mM NaCl the bilayer structure of OSEA.HCl is stabilized and the lipid does not undergo transition to a micellar phase at high temperature.

The salt induced lamellar phase stabilization seen here demonstrates that the phase behavior of OAEs may be modulated by ionic strength as described earlier with other lipids. It has been shown here that salt can help in stabilization of lamellar structure of the single chain lipid (OSEA.HCl) even at higher temperatures. The role played by salt has an important consequence on the stabilization of the bilayer structure of single tailed membrane components under stress or at extreme temperatures in extremophiles.

Structure and phase behavior

Previous biophysical studies suggest that *N*-acylethanolamines and their precursors, i.e., *N*-acylphosphatidylethanolamines stabilize the bilayer structure of phospholipids in which they are incorporated, most likely due to their strong tendency to form bilayer structure (Ambrosini et al., 1993; Domingo et al., 1993; Mercadal et al., 1995). The crystal structure of NAEs with different acyl chainlengths namely, *N*-stearoylethanolamine, *N*-palmitoylethanolamine and *N*-myristoylethanolamine also revealed that these molecules are packed in a bilayer fashion with tail-to-tail chain packing (Dahlén et al., 1977; Ramakrishnan & Swamy, 1999; Kamlekar & Swamy, 2006). *O*-Acylethanolamines are structural isomers of NAEs and analysis of the crystal structure of *O*-stearoylethanolamine hydrochloride revealed that the acyl chains in this lipid are also packed in a bilayer fashion (packing and intermolecular interaction of OSEA.HCl is similar to that in

OLEA.HCl). Although both NAEs and OSEA.HCl adopt a bilayer structure in the solid state the structure of individual molecules in these two classes of compounds is different. While NAEs adopt an L shape in the solid state, OSEA.HCl adopts a linear shape. The different shapes may lead to differences in the type of interaction with other membrane lipids such as phospholipids, lysolipids and cholesterol (will be discussed in Chapter 5).

The tilt angle with respect to bilayer normal in OSEA.HCl was found to be 44.4°, which is much higher than the values found in NAEs with different chainlengths (Dahlén et al., 1977; Ramakrishnan & Swamy, 1999; Kamlekar & Swamy, 2006). It was observed that if the tilt angle is more than 60° it induces interdigitation in the acyl chain packing (Yeagle, 2005). In OSEA.HCl the presence of Cl^- counterions may induce higher chain tilt as compared to NAEs and it is expected that in water, hydration will make the head group even bigger. Such increase in head group area may induce interdigitation or lead to large tilt in the chains with respect to bilayer plane.

Chapter 4

Thermotropic and Chaotropic Phase Transition in Bioactive *O*-Acylcholines

4.1 Summary

O-Acylcholines (OACs) exhibit interesting biological and medicinal activities. In view of this a homologous series of OACs with even chainlengths (n = 12 to 20) have been synthesized and their thermotropic phase transition have been characterized by differential scanning calorimetry. Linear least squares analyses yielded incremental values contributed by each methylene group to the transition enthalpy and entropy and the corresponding end contributions. The thermotropic phase transitions of *O*-stearoylcholine (OSC) dispersed in water, in 150 mM NaCl and in 150 mM NaI were characterized using calorimetric, spectroscopic and turbidimetric studies. These studies have revealed that when dispersed in water OSC undergoes a cooperative phase transition centered at 61.4 ^{o}C from an ordered gel phase to a micellar structure whereas in presence of 150 mM NaCl the transition temperature decreases to 37.7 ^{o}C, and in presence of 150 mM NaI the transition temperature increases to 64.6 ^{o}C. These studies suggest that ions play a definite role in the phase behavior and biological activity of OACs.

4.2. Introduction

As indicated in Chapter 1, *O*-acylcholines (OACs) with different fatty acyl chains have been found to exhibit interesting biological activities such as hemolysis (Cho & Proulx, 1969; 1971), toxicity against mosquitofish at low concentration (2 ppm) (Goldberg et al., 1982) and inhibition of wheat embryo Ca^{2+}-dependent protein kinase (CDPK) (Jinsart et al., 1991). Besides these activities, OACs are of pharmacological interest, as they can modulate the blood pressure (Schneider & Timms, 1957), act as skin penetration enhancers for several drugs (Loftsson et al., 1989) and exhibit rapid antimicrobial activity against a wide range of microorganisms (Ahlström et al., 1995). Although a considerable amount of knowledge exists on the biological and pharmacological properties of OACs, very little is known regarding their supramolecular structure in solution, thermotropic and chaotropic phase behavior and interaction with other lipids. Towards that direction, in the present study a homologous series of *O*-acylcholine iodides (OACs) with even chains have been synthesized and their thermotropic phase transition using differential scanning calorimetry have been characterized. The phase behavior of one member of OAC family namely, *O*-stearoylcholine iodide (OSC) has been examined in presence of NaCl and NaI using differential scanning calorimetry, electron spin resonance, turbidimetry and fluorescence spectroscopy. The result suggests that ions have a definite role on the phase behavior of OSC and predict similar behavior in other OACs. Finally, the 3-dimensional structure and packing of various *O*-acylcholine iodides were determined by single crystal X-ray diffraction.

4.3. Materials and methods

4.3.1. Synthesis of O-acylcholines

OACs with even acyl chainlengths (*n* =12-20) were synthesized in two steps. In the first step fatty acid was condensed with *N*, *N'*-dimethylethanolamine using dicyclohexylcarbodiimide (DCC) as a coupling agent and 4-dimethylamino pyridine (DMAP) as a catalyst. Fatty acid (1.15 eq), *N*, *N'*-dimethylethanolamine (1.0 eq) and DMAP (0.5 eq) were taken in a round bottom flask and the mixture was azeotroped thrice with dry benzene. The mixture were dried under high vacuum and dissolved in dry dichloromethane. DCC (1.4 eq) was added to the reaction mixture at 0 °C. The reaction was stirred overnight raising the temperature from 0 °C to room temperature in an inert atmosphere. The condensation product (fatty acid ester of *N*, *N'*-dimethylethanolamine) was extracted with ethyl acetate and purified by column chromatography. The purified and dried ester was treated with 1.3 eq of methyl iodide at 0 °C for quaternization. The product was washed with dry ether three times and dried under vacuum. The purified OACs were characterized by IR and ^{1}H-NMR spectroscopy.

4.3.2. Crystallization, X-ray diffraction and structure solution

Thin needle type, colorless crystals of *O*-acylcholine iodides were grown at room temperature from moist chloroform. Initial cell indexing of several crystals of *O*-palmitoylcholine (OPC) indicated the presence of two types of crystals from the same batch, suggesting the presence of two different polymorphs in the crystalline state. Therefore, both types (α and β form) were analyzed by single crystal X-ray diffraction measurements and data reduction was carried out as described in Chapter 2. For *O*-lauroylcholine (OLC) and *O*-myristoylcholine (OMC) only β

form and for *O*-arachidylcholine (OArC) only α form have been obtained. The β form of *O*-stearoylcholine (OSC) was obtained from a mixture of chloroform, methanol and water. The crystal parameters of α and β forms of OACs are given in Table 4.1 and Table 4.2.

Table 4.1. Crystallographic data for β-form of *O*-acylcholines at 298 K.

	OLC β form	**OMC β form**	**OPC β form**	**OSC β form**
Formula	$C_{17}H_{36}NO_2I$, $0.5H_2O$	$C_{19}H_{40}NO_2I$, $0.5H_2O$	$C_{21}H_{44}NO_2I$, $0.5H_2O$	$C_{23}H_{48}NO_2I$, $0.5H_2O$
Crystal system	Triclinic	Triclinic	Triclinic	Triclinic
Space group	*P-1*	*P-1*	*P-1*	*P-1*
a (Å)	8.0288(14)	8.0024(13)	7.9952(16)	7.992(3)
b (Å)	9.6155(17)	9.6386(16)	9.6480(19)	9.634(4)
c (Å)	28.062(5)	30.573(5)	33.069(7)	35.413(14)
α	94.058(3)	93.852(3)	93.686(4)	86.398(7)
β	94.193(3)	95.594(3)	96.898(4)	84.785(8)
γ	90.040(3)	90.068(3)	90.103(4)	89.961(7)
Z	4	4	4	4
V ($Å^3$)	2155.2(6)	2341.5(7)	2527.1(9)	2709.9(19)
D_{calc} (g cm^{-3})	3.273	3.374	3.350	1.239
R_1	0.0834	0.0751	0.1303	0.1978
wR_2	0.2229	0.1993	0.3695	0.4841
GooF	1.087	1.118	1.116	1.083
μ (mm^{-1})	9.041	9.320	9.253	1.199

Table 4.2. Crystallographic data for α-form of *O*-acylcholines at 298 K.

	OPC α form	**OSC α form**	**OArC α form**
Formula	C_{21} H_{44} N O_2 I	C_{23} H_{48} N O_2 I	C_{25} H_{52} N O_2 I
Crystal system	Triclinic	Triclinic	Triclinic
Space group	*P-1*	*P-1*	*P-1*
a (Å)	5.7781(13)	5.767(5)	5.7852(8)
b (Å)	7.6435(17)	7.645(7)	7.6708(11)
c (Å)	28.435(7)	30.62(3)	32.717(5)
α	89.992(4)	83.104(14)	90.250(2)
β	86.695(4)	87.054(19)	91.811(2)
γ	89.313(4)	89.389(13)	90.763(2)
Z	2	2	2
V ($Å^3$)	1253.7(5)	1339(2)	1451.0(4)
D_{calc} (g cm^{-3})	1.244	1.234	1.203
R_1	0.0694	0.0663	0.0623
wR_2	0.1630	0.1841	0.1335
GooF	1.020	1.079	1.082
μ (mm^{-1})	1.29	1.212	1.121

4.3.3. Differential scanning calorimetry

DSC studies were performed essentially as described in Chapter 3. The lipid was hydrated thoroughly with Millipore water containing the desired concentration of NaCl or NaI before performing the heating scans. In all cases the second heating scan was considered for data analysis. Transition enthalpies were determined by integrating the peak area under the transition curves. Transition entropies were determined from the transition enthalpies assuming a first order transition according to the expression (Marsh, 1990):

$$\Delta H_t = T.\Delta S_t \qquad (4.1)$$

where T is transition temperature and ΔH_t values were taken at this temperature in order to calculate the corresponding ΔS_t values.

4.3.4. Turbidimetry, ESR spectroscopy and fluorescence spectroscopy

Samples for turbidimetric measurements, ESR and fluorescence measurements were prepared according to the procedures described in Chapter 3.

4.4. Results

4.4.1. Description of the structure

ORTEP diagrams of the molecular structure of the α and β polymorphs of *O*-palmitoylcholine (OPC) are shown in Fig. 4.1. It is seen from Fig. 4.1, that the hydrocarbon portion of the acyl chains of the α polymorph of *O*-palmitoylcholine (OPCα) is in all-*trans* conformation and the torsion angles observed for the acyl chain region are all close to 180°. The torsion angle observed for the C4–C5–O1–C6 is 131.1°, which makes a slight gauche conformation at the C4–C5 bond resulting in a bending of the molecule at the end.

O-Palmitoylcholine (OPC) adopts similar structure in the β polymorph (OPCβ). The C4–C5–O1–C6 torsion angle in OPCβ is found to be -167.0°, which is close to 180° and consequently the trans geometry extends up to the C4–C5 bond. The bending at head group occurs at C4-N1 bond whereas in the α form bending starts at C5-C4 bond. Therefore the shape of β form is more close to linearity than the α form and the length of OPC molecule in the α form should be little less than that observed in the β form. Consistent with this, the N1-C21 distance was found to be 22.91 Å in the β form whereas the corresponding distance in the α polymorph is 22.57 Å.

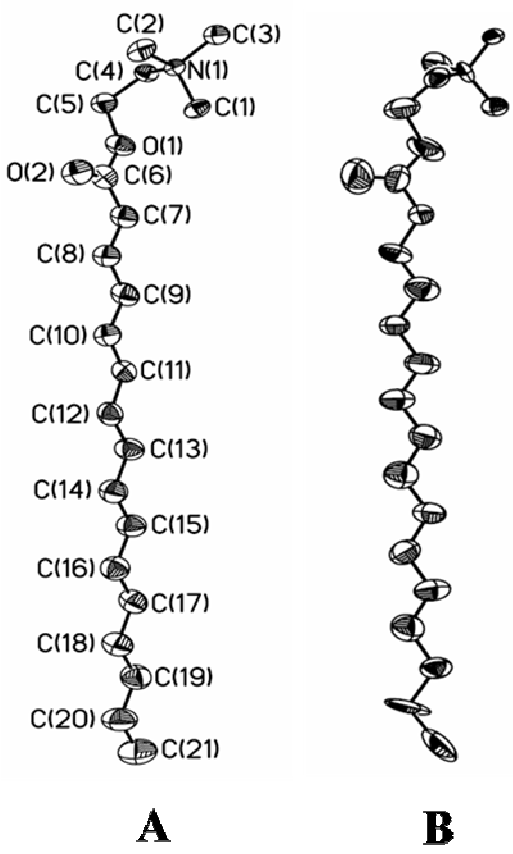

Fig. 4.1. ORTEP diagrams of *O*-palmitoylcholine. A) the α polymorph and B) the β polymorph. For clarity atom labels were deleted in the β form.

The molecular structures of α polymorph of *O*-stearoylcholine (OSCα) and *O*-arachidylcholine (OArCα) are similar to that of OPCα. The C4–C5–O1–C6 torsion angle in OSCα and OArCα is 131.80º and -130.35º and results in a bending of the C4-C5 bond. The structure of the other form of OSC, namely OSCβ is similar to that of OPCβ and the corresponding torsion angle was found to be -167.0. The N1-C23 distance in OSCβ is 25.2 Å and in the α form is 25.1 Å, which are consistent in the sense that the length of the β form is higher than the α form. The molecular structures of *O*-lauroylcholine (OLC) and *O*-myristoylcholine (OMC) are isostructural with the β form of OPC. The C4–C5–O1–C6 torsion angle in OLCβ and OMCβ are 171.9° and 163.4° respectively. For OLC and OMC no α form, and for OArC no β form, was been obtained, whereas OPC and OSC exist in two different polymorphic forms. These observations suggest that acyl chainlength may play a dominant role in polymorphism in this class of lipids.

4.4.2. Molecular packing

A packing diagram of the α polymorph of *O*-palmitoylcholine along the *a*-axis is given in Fig. 4.2A. OPC molecules in the α polymorph are packed in layers that are arranged in a head-to-head (and tail-to-tail) fashion in stacked bilayers. The methyl ends of the stacked layers are in van der Waals contacts with the closest methyl-methyl distance between opposite layers and the same layer being 3.91 Å and 5.78 Å, respectively. The bilayer thickness (carbonyl carbon-carbonyl carbon distance) in OPCα is 42.1 Å and the all-*trans* *O*-acyl chains of the molecule are tilted by 60.0° with respect to the normal to the respective methyl end planes. The higher chain tilt in OPCα is a consequence of large head group and the packing problem is overcome by the tilting of the hydrocarbon chains with respect to the bilayer normal. Other biologically relevant single chain lipids such as lysophosphatidic acid and lysophosphatidylethanolamine also have large head

group areas due to which they pack in a bilayer format with high tilt angle of the acyl chains with respect to the bilayer normal (Pascher et al., 1981; Pascher & Sundell, 1985).

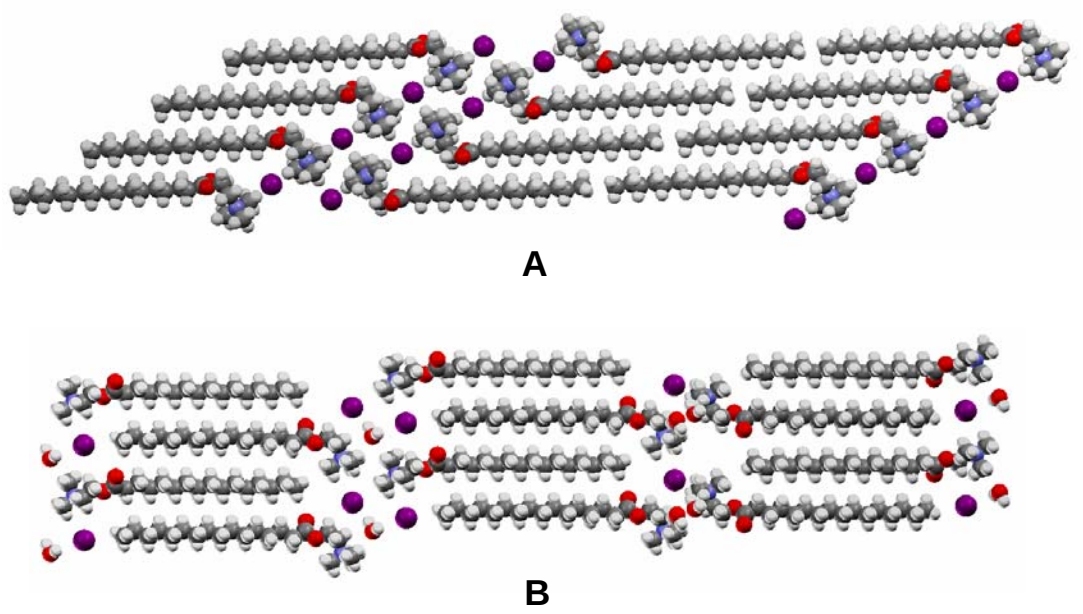

Fig. 4.2. Packing diagrams of *O*-palmitoylcholine along *a*-axis. A) α-polymorph packed in layers with tilted bilayer. B) β-polymorph packed in an interdigitated manner. Color legend: red, oxygen; blue, nitrogen; violet, iodine; grey, carbon.

The OPC molecules are packed in a head-to-tail manner with a common hydrocarbon chain matrix that is confined on both sides by a boundary layer of polar groups in the β form (Fig. 4.2B). This type of chain packing is known as interdigitation of acyl chains and in this way two hydrocarbon chains are accommodated per head group. In this packing mode one water molecule is also accommodated in the unit cell. The hydration of iodide and bulky choline moiety in the polar head group increases the molecular area to 38.5 $Å^2$, which become roughly twice of hydrocarbon chain cross section (~19.0 $Å^2$, observed for various lipids in the solid state) (Yeagle, 2005). Ratio of molecular area and hydrocarbon chain cross section in OPCβ also supports the formation of interdigitated bilayer.

The layer thickness (carbonyl carbon-carbonyl carbon distance) of OPCβ is 19.3 Å and the all-*trans* acyl chains are tilted by a virtually negligible angle of 1.1° with respect to bilayer normal.

The α polymorph of OSC and OArC are isostructural with OPCα and have a similar packing arrangement as observed in the crystal lattice of OPCα. They are packed in a head-to-head (and tail-to-tail) format in stacked tilted bilayers. The layer thickness in OSCα and OArCα is 47.2 Å and 52.4 Å, respectively, and the all-*trans* *O*-acyl chains of the molecules are tilted by 60.4° and 60.2°, respectively, with respect to the normal to the respective methyl end planes. Also, the packing arrangement of OLCβ, OMCβ and OSCβ are similar with that observed in OPCβ and they are packed with chain interdigitation. The layer thickness in OLCβ, OMCβ and OSCβ is 14.5, 16.9 and 21.8 Å respectively and the unit cell contains one water molecule. Therefore, in all the β forms hydration increases the size of the head group, which results in the packing of acyl chains in an interdigitated manner.

4.4.3. Differential scanning calorimetry of O-acylcholines

O-Acylcholine iodides (OACs) yielded turbid suspensions upon hydration and the suspensions settled down upon keeping for long time. The turbid suspensions become optically clear at higher temperature, suggesting that the amphiphile undergoes a phase transition from a phase of high turbidity (possibly lamellar gel phase) to a phase where aggregates are small (such as micelle), which do not scatter visible light. In order to characterize the thermotropic phase transitions, DSC studies were carried out on hydrated *O*-acylcholines (OACs) of even acyl chains (n = 12-20). OACs with different acyl chains exhibit a single, broad transition, except *O*-arachidylcholine which exhibits a minor transition before the main transition. Representative heating thermograms of OACs dispersed in

water are shown in Fig. 4.3. The transition temperatures (T_t), the widths at half maximum of the transition ($T_{1/2}$), transition enthalpies (ΔH_t) and transition entropies (ΔS_t) obtained from the heating thermograms are presented in Table 4.3. It is seen from this table that the thermodynamic parameters such as T_t, ΔH_t and ΔS_t increase with increase in chainlengths. A linear chainlength dependence was observed for ΔH_t and ΔS_t for the OACs of even chainlengths, indicating that structures of the phases formed by all OACs in aqueous dispersions are likely to be very similar. Therefore characterization of phase structure and phase transitions exhibited by one molecule in the series is likely to give an idea of the phase structures present in the entire homologous series. In view of this, further studies regarding the phase structure and phase transition were carried out with *O*-stearoylcholine iodide (OSC).

Table 4.3. Transition temperatures (T_t), transition enthalpies (ΔH_t), and transition entropies (ΔS_t) associated with the phase transition of hydrated *O*-acylcholines with even acyl chainlengths.

Acyl chainlength (n)	T_t (°C)	$T_{1/2}$ (°C)	ΔH_t (kcal.mol^{-1})	ΔS_t (cal.mol^{-1}.K^{-1})
C_{12}	38.3	2.40	7.1 ± 0.8	22.8
C_{14}	48.2	2.60	11.4 ± 1.2	35.5
C_{16}	56.2	2.50	15.4 ± 0.8	46.7
C_{18}	61.4	2.10	18.3 ± 0.3	54.7
C_{20}	67.3	0.90	21.7 ± 1.5	63.7

To understand the effect of salt (NaCl) on the phase transition, DSC studies were performed with OSC at various salt (NaCl) concentrations and the thermodynamic parameters obtained are listed in Table 4.4. Representative heating

thermograms in water and in 150 mM NaCl concentration are shown in Fig. 4.3. It has been observed that in presence of 25 mM NaCl the phase transition temperature (T_t) decreases from 61.4 to 39.9 °C and further increase in the salt concentration does not result in any significant change in the phase transition temperature. Therefore, further studies regarding the salt concentration dependence on the phase behavior and phase transition have been carried out at the physiological salt concentration (ca. 150 mM). The DSC results demonstrate that salt can modulate the phase transition properties of OSC and further spectroscopic studies were performed in order to characterize its phase behavior.

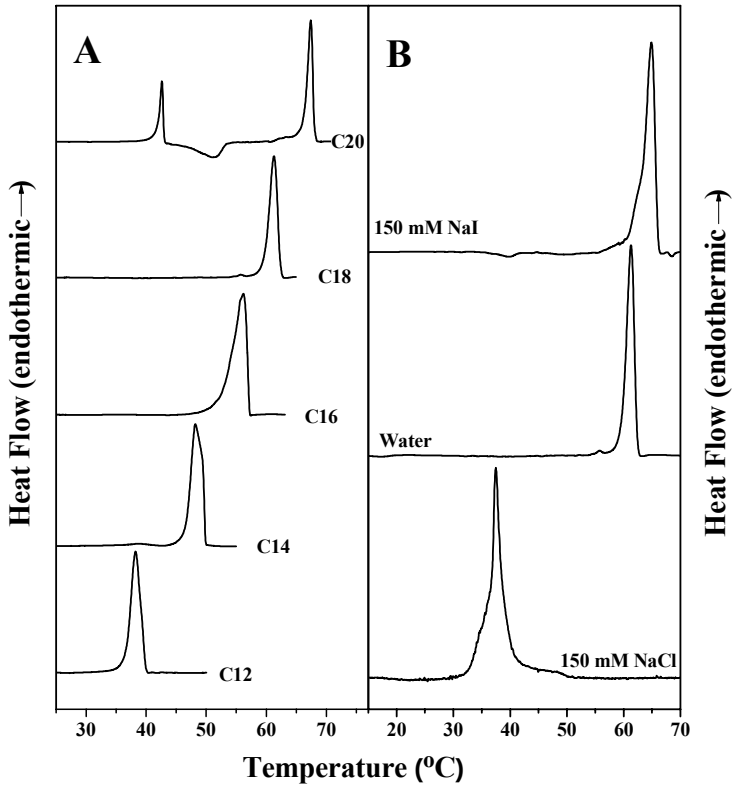

Fig. 4.3. DSC heating thermograms of *O*-acylcholines. A) Thermograms of OACs with even number of C-atoms in the acyl chains. B) Thermograms of *O*-stearoylcholine dispersed in water, 150 mM NaCl and 150 mM NaI.

Table 4.4: Thermodynamic parameters obtained from DSC studies on OSC. Samples were dispersed in distilled water containing the indicated concentration of sodium chloride.

NaCl (mM)	T_t (°C)	ΔH_t (kcal.mol^{-1})	ΔS_t (cal.mol^{-1}.K^{-1})
0	61.40 ± 0.12	18.3 ± 0.30	54.7
25	39.95 ± 0.05	10.0 ± 0.27	31.9
50	37.76 ± 0.02	8.7 ± 0.29	28.0
150	37.67 ± 0.24	8.4 ± 0.21	27.0
250	36.97 ± 0.69	8.1 ± 0.35	26.1
500	37.39 ± 0.29	6.4 ± 0.39	20.6
1000	38.57 ± 0.17	5.6 ± 0.63	18.0

4.4.4. Turbidimetric studies on OSC

To investigate the salient features of the phase transition of OSC, tubidimetric studies have been performed, monitoring the turbidity at 400 nm as a function of temperature using spectrophotometer. Fig. 4.4 depicts the change in turbidity of OSC in water and in 150 mM NaCl as a function of temperature. In both environments the turbidity at low temperature was relatively high and it decreases with increase in temperature. Near phase transition temperature the turbidity exhibits a sharp decrease upon increase of temperature and thereafter remains at a constant level. The midpoint of the steeply declining region was taken as the phase transition temperature (T_t). The T_t values obtained from the turbidimetric studies were 57.5 and 34.3 °C, respectively, for measurements performed in water and in 150 mM NaCl. These values are slightly lower than the values obtained from the

DSC study but are consistent with the DSC results in that phase transition temperature decreases by over 20º in the presence of 150 mM NaCl.

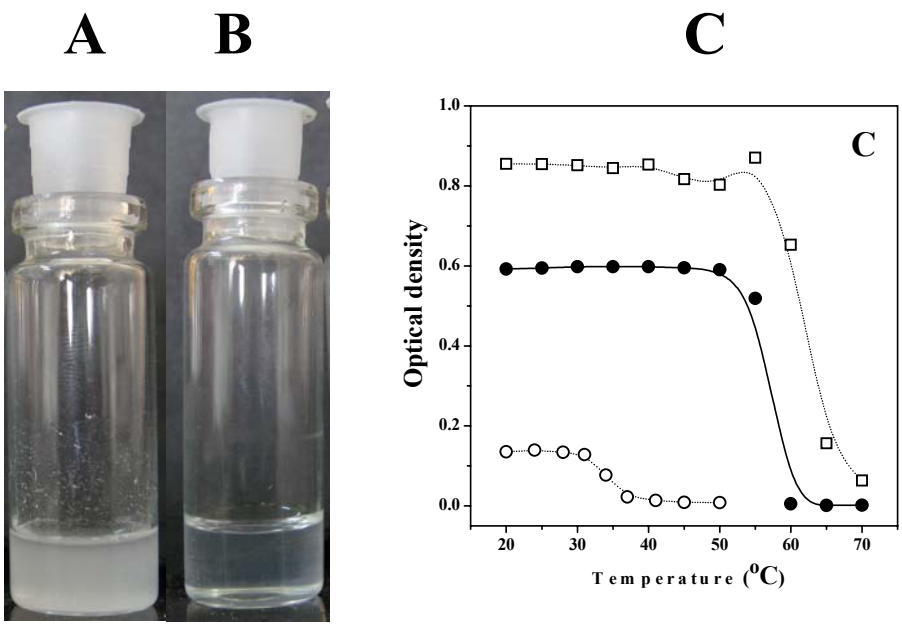

Fig. 4.4. Snapshot of OSC dispersed in (**A)** water and (**B)** in 150 mM NaCl. **C)** Turbidimetric study of the thermotropic phase transition of OSC dispersed in water (●), in 150 mM NaCl (○) and in 150 mM NaI (□). Lipid concentration was 1 mg/ml for all samples.

Now from Fig. 4.4C it can be clearly seen that turbidity of the sample before phase transition in water is much higher as compared to the turbidity of the sample prepared in 150 mM NaCl. Visual inspection also indicated that the sample (0.05 wt%) prepared in water is highly turbid as compared to the sample prepared in 150 mM NaCl (Fig. 4.4). The differences in turbidity are not due to differences in the lipid concentration since identical concentrations of OSC were used in these two experiments. This suggests that salt can modulate the phase structure, and consequently, phase transition temperature of OSC. Above the phase transition temperature in both environments and the sample was optically clear to the naked

eye. This indicates that the aggregates are relatively small and suggests that the phase is most likely composed of micelles.

4.4.5. Spin-label ESR spectroscopy

Spin-label ESR spectroscopy enables the study of specific environments within the lipid aggregates and membranes. The outer hyperfine splitting ($2A_{max}$), which gives a measure of anisotropic motion of the probe, provides information regarding the structure and dynamics of lipid aggregates. The ESR spectra of 5-SASL (5-doxyl stearic acid) incorporated at probe concentration in OSC, dispersed in water and in 150 mM NaCl recorded at different temperatures are shown in Fig. 4.5A & 4.5B. At 25 °C the spectra recorded in water and in 150 mM NaCl exhibit strong spin-spin broadening, clearly indicating that in this phase the acyl chains of the single chain lipid are tightly packed. The outer hyperfine splitting ($2A_{max}$) of 5-SASL in OSC was found to be 64.1G and 61.7G, respectively in water and in 150 mM NaCl. The value of the $2A_{max}$ obtained in water at room temperature is close to the value exhibited by the gel or crystalline phase of lipids and suggests that OSC may adopt a gel or crystalline phase. The $2A_{max}$ value observed in 150 mM NaCl is somewhat smaller and therefore most likely corresponds to the gel phase but not the crystalline phase. As the temperature increases the $2A_{max}$ decreases and near the phase transition temperature the value of $2A_{max}$ falls rapidly in both the environments. By monitoring the change in $2A_{max}$ with temperature it is possible to determine the phase transition temperature. From the ESR measurements the obtained phase transition temperature is 58 and 36 °C respectively, for measurements performed in water and 150 mM NaCl (Fig. 4.5C). The ESR data is also consistent with the lowering of phase transition temperature in presence of 150 mM NaCl. In both the environments the spectra become more isotropic after the phase transition temperature. Qualitatively similar spectra have been obtained for

5-SASL incorporated in octadecyl-trimethylammonium bromide (C_{18}TAB) micelle (Benatti et al, 2001) and other micelles. This suggests that in water and in 150 mM NaCl above the phase transition temperature, OSC forms some kind of micelles, as inferred from the turbidimetric studies.

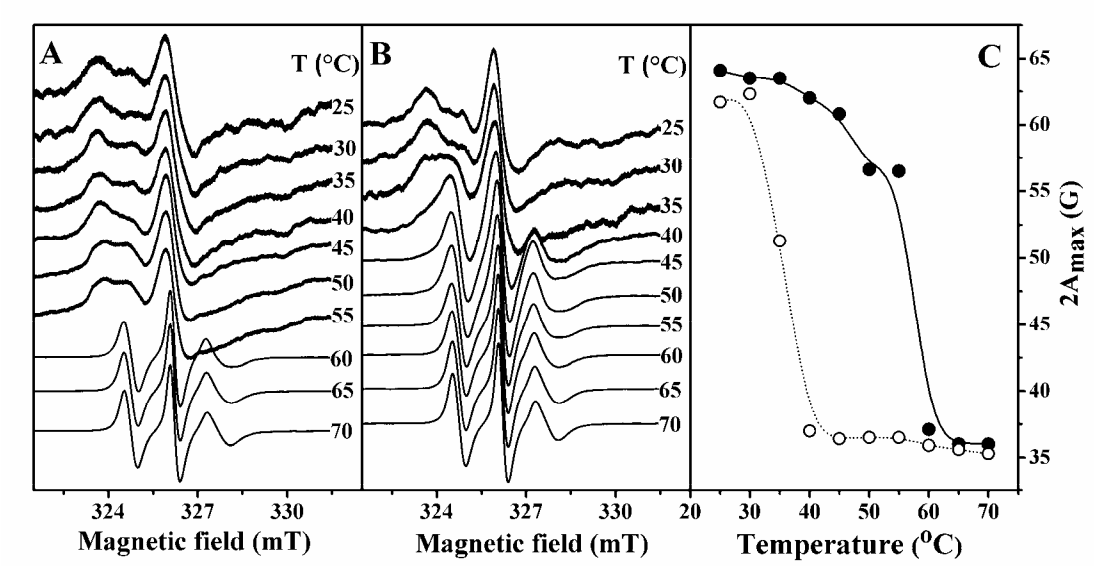

Fig. 4.5. **A)** ESR spectra of 5-SASL in OSC dispersed in water. **B)** ESR spectra of 5-SASL in OSC dispersed in 150 mM NaCl. **C)** Temperature dependence of $2A_{max}$ (G) in water (●) and in 150 mM NaCl (○). In A and B the temperature at which each spectrum was recorded is indicated.

4.4.6. Fluorescence spectroscopy

The phase transition temperature of OSC in 150 mM NaCl was further investigated by fluorescence spectroscopy using pyrene as a fluorescence probe. As mentioned in Chapter 3, the relative intensities of vibronic bands in pyrene monomer fluorescence spectrum allow one to determine the phase transition temperature (Georghiou & Mukhopadhyay, 1981).

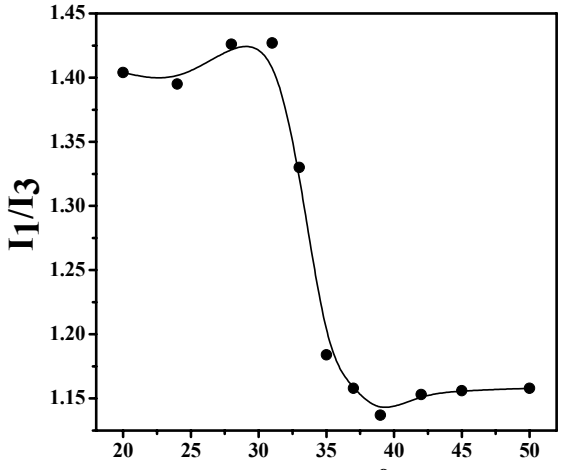

Fig. 4.6. Temperature dependence of polarity ratio (I_1/I_3) of pyrene in OSC dispersed in 150 mM NaCl.

The I_1/I_3 peak ratio of pyrene in OSC decreases with increase in temperature (Fig. 4.6), suggesting that below the phase transition temperature (gel phase) pyrene is presumably located near the head group (polar) region and above the phase transition temperature, pyrene moves deeper into the hydrophobic region of the lipid aggregate. From the steeply declining ratio of I_1/I_3 with temperature, the phase transition temperature was determined as 33.8 ºC, which is slightly lower than the transition temperature obtained from calorimetric studies. Thus the fluorescence spectroscopic studies are also consistent with the modulation of transition temperature of OSC in 150 mM NaCl. A similar fluorescence study with OSC in water could not be carried out due to high turbidity of the sample (see Fig. 4.4).

4.4.7. Calorimetric and turbidimetric studies in presence of 150 mM NaI

Further studies with OSC were performed in the presence of 150 mM NaI in order to investigate the role of iodide counterion in the phase behavior. DSC studies have shown that the phase transition temperature of OSC increases from 61.4 to 64.6 ºC in

presence of 150 mM NaI (Fig. 4.3). The phase transition temperature, obtained from turbidimetric studies also supports the increase in phase transition temperature in 150 mM NaI (Fig. 4.4). As the turbid solution becomes optically clear above the phase transition temperature, the transition most likely occurs from a lamellar gel phase to micellar phase in 150 mM NaI. An increase in the phase transition temperature in presence of salt (here 150 mM NaI) is expected since the electrostatic repulsion between adjacent head groups in the aggregates will be reduced (Trauble & Eibl, 1974), which is expected to result in a tightening of the acyl chain packing.

4.5. Discussion

4.5.1. Chainlength dependence of transition enthalpy and transition entropy

The chainlength dependence of transition enthalpy and transition entropy for the aqueous phase transitions of OACs of even chainlengths are given in Fig. 4.7A and Fig. 4.7B, respectively. The enthalpy and entropy data for OACs of even chainlengths could be fit well to expressions 4.2 and 4.3, given below (Larsson, 1986; Ramakrishnan et al., 1997; Ramakrishnan & Swamy, 1998):

$$\Delta H_t = \Delta H_o + (n\text{-}2)\,\Delta H_{inc} \qquad (4.2)$$

$$\Delta S_t = \Delta S_o + (n\text{-}2)\,\Delta S_{inc} \qquad (4.3)$$

where n is the number of C-atoms in the acyl chains and ΔH_o and ΔS_o are the end contributions to ΔH_t and ΔS_t, respectively, arising from the terminal methyl group and the polar region of the OAC molecule. ΔH_{inc} and ΔS_{inc} are the incremental values of ΔH_t and ΔS_t contributed by each CH_2 group. Linear least squares analysis of the chainlength-dependent values of ΔH_t and ΔS_t for the even chainlengths of OACs yielded the incremental values (ΔH_{inc} and ΔS_{inc}) and end contributions (ΔH_o and ΔS_o).

These values are listed in the Table 4.5. For the sake of comparison corresponding values obtained with NAEs and fatty acids are also given in this Table.

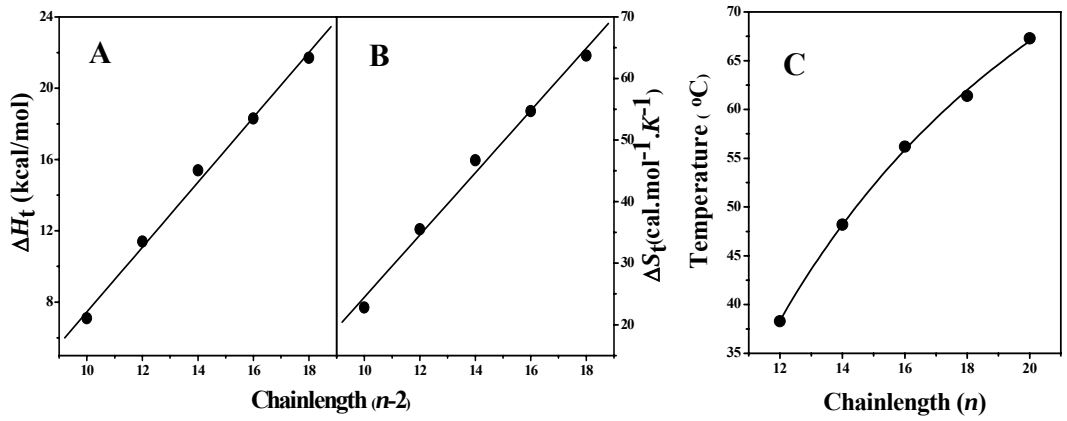

Fig. 4.7. Chainlength dependence of (A) transition enthalpies (ΔH_t), (B) transition entropies (ΔS_t) and (C) transition temperatures (T_t). Solid lines in A and B correspond to linear least square fits of the data to equations 4.2 and 4.3, respectively, whereas the solid line in C corresponds to non-linear least squares fit of the transition temperatures to equation 4.7.

Table 4.5. Incremental values (ΔH_{inc}, ΔS_{inc}) of chain length dependence and end contributions (ΔH_o, ΔS_o) to phase transition enthalpy and entropy of hydrated *O*-acylcholines of even chainlengths. Average values of transition enthalpy and transition entropy given in Table 4.3 have been used for the linear fitting of the data. Errors shown in parentheses are fitting errors obtained from the linear least squares analysis. For NAEs and fatty acids the values are taken from literature (Ramakrishnan et al., 1997; Larsson, 1986).

Lipid	ΔH_{inc}	ΔH_o	ΔS_{inc}	ΔS_o
OACs (Even chainlength)	1.82 (± 0.12)	-10.7 (± 1.9)	5.05 (± 0.27)	-26.0 (± 3.9)
NAEs (Even chainlength)	0.95 (± 0.06)	-0.52 (± 0.82)	2.37 (± 0.17)	3.1 (± 2.3)
Fatty acids (Even chainlength)	0.86 (± 0.05)	0.02 (± 0.51)	2.25 (± 0.16)	4.6 (± 1.8)

The ΔH_{inc} value of 1.82 kcal.mol^{-1} observed here for the OACs with even chainlengths indicates that the incremental enthalpy contributed by each CH_2 unit in the OACs is higher than that observed with the hydrated NAEs and dry fatty acids. Similarly, the ΔS_{inc} values obtained here for the OACs with even acyl chains are also considerably higher than the ΔS_{inc} values obtained for the NAEs and fatty acids (Table 4.5). These observations suggest that the acyl chains in OACs are packed more tightly.

4.5.2. Chainlength dependence of transition temperature

Although the data presented in Table 4.3 show that the transition temperatures increase with increase in acyl chainlength, the increase in the transition temperature (T_t) is not linearly proportional to the acyl chainlength. In order to understand this better the transition temperatures have been plotted as a function of acyl chainlength (Fig. 7C). From this figure it is seen that the T_t values increase in a smooth progression but with decreasing increments as the chainlength is increased. As the acyl chainlength increases, the total contribution from the polymethylene portion towards the total enthalpy and entropy of the phase transition will be sufficiently large that the end contributions are negligible in comparison. Therefore, at infinite acyl chainlength, equations 4.2 and 4.3 can be reduced to (Ramakrishnan et al., 1997):

$$\Delta H_t = (n\text{-}2)\Delta H_{inc} \qquad (4.4)$$

$$\Delta S_t = (n\text{-}2)\Delta S_{inc} \qquad (4.5)$$

Then the transition temperature for infinite chainlength, T_t^{∞}, will be given by:

$$T_t^{\infty} = \Delta H_{inc}/\Delta S_{inc} \qquad (4.6)$$

From the incremental enthalpy and entropy, the T_t^{∞} value for the OAC of even acyl chainlength has been estimated as 360.4 K. The chainlength dependence of the

transition temperatures of OACs of even acyl chainlengths was fitted to equation 4.7, predicted from the linear dependence of transition enthalpy and transition entropy given in equations 4.2 and 4.3 (Marsh, 1982, 1991):

$$T_t = \Delta H_t/\Delta S_t \quad = (\Delta H_{inc}/\Delta S_{inc})\,[1 - (n_o - n_o')/(n - n_o')] \qquad (4.7)$$

where n_o (= $-\,\Delta H_o/\Delta H_{inc}$) and n_o' (= $-\,\Delta S_o/\Delta S_{inc}$) are the chainlengths at which the transition enthalpy and transition entropy, respectively, extrapolate to zero. From the nonlinear least squares fit shown in Fig. 4.7C, it is evident that the transition temperatures of OACs with even chainlengths are described accurately by equation 4.7. In addition, the fitting parameters yielded the transition temperature at infinite chainlength (T_t^{∞}) for the OACs of even acyl chains as 390.7 K with χ^2 of 0.27.

As the OACs tend to form precipitates at room temperature, their solubility might be very low in this temperature range. Now if their solubility in water is too low and they tend to settle down from the water then the question that rises is, how they are biologically active?

An important characteristic of ionic lipids/surfactants is their tendency to precipitate from aqueous solutions, which can inhibit their activity and hence their use in many industrial applications. Thus the hydrated solid precipitate can be termed as 'denatured surfactants' in view of their lack of activity in this state. The 'denatured surfactant' or hydrated precipitate transforms to micelles above phase transition temperature, which was regarded as the Krafft temperature of the surfactant (Shinoda, 1963). It is desirable to examine ways of extending the temperature range over which finite sized aggregates are formed. It was shown earlier that introduction of an alcohol moiety in head group, increase in branching, unsaturation in acyl chain and counterion can modulate the Krafft temperature (Shinoda et al., 1972; Yang & Mantsch, 1986; Davey et al., 1998). The modulation of Krafft temperature with

counterion indicates that ions or chaotropes may have a definite role on the phase behavior of the lipid. Similar effect of different chaotropic ions on proteins has been examined and it was shown that the ions have a definite role on the salting out. Here, it was observed that in presence of 150 mM NaCl the phase properties of OSC have changed extensively and the phase transition temperature decreases significantly. Differential scanning calorimetric studies have revealed that the transition temperature drops from 61.4 to 37.7 ºC in presence of 150 mM NaCl. Results from turbidimetric, ESR and fluorescence spectroscopic studies are also consistent with the lowering of transition temperature of OSC in presence of 150 mM NaCl. In both the environments it was suggested that the phase above transition temperature is micellar, as the lipid dispersions were optically clear and have very low optical density as revealed from turbidimetric measurements (Fig. 4.4). The ESR spectra recorded above transition temperature in aqueous dispersions were more isotropic, which also support the micellar structure above the phase transition (Fig. 4.5). The lowering in transition temperature in presence of salt is unexpected as at high ionic strength (comparing 150 mM NaCl with water) the phase transition temperature generally increases due to screening of charges in the head group and closer packing of acyl chains. The reduction of phase transition temperature may be due to the fact that in presence of 150 mM NaCl the iodide counterions that interact with OSC will be replaced by chloride ions. Further support of the above argument comes from the calorimetric and turbidimetric studies of OSC in presence of 150 mM NaI, where the phase transition temperature increases as compared to the sample dispersed in water alone. The ionic strength will screen the charged head group and results in tighter chain packing, which is reflected in the increase in phase transition temperature and corresponding enthalpy of transition. Similar reports where cationic lipids with iodide counterion have more Krafft temperature than the chloride counterion has been

observed in cetyltrimethylammonium halides and *N*-alkylpyridinium halides (Knock & Bain, 2000; Perche et al., 1996).

The insolubilization of the lipid or surfactants below Krafft temperature is usually accompanied with the crystallization of alkyl chains of the surfactant molecules resulting in the formation of hydrated solids in excess water. The crystallization of the alkyl chains, which form bilayers composing the multilamella structure, is mainly driven by the van der Waals attraction among them. Molecules in OSC iodide crystal pack in an interdigitated manner that allows both close packing of the alkyl chains (leading to strong van der Waals interactions) and also close approach of the ionic group to the counterion (leading to a stronger Coulombic interaction) (Davey et al., 1998). Thus the interdigitated hydrated solid will be more stable as compared to the crystallized acyl chains in bilayer fashion. It was reported earlier that the interdigitated bilayer have a higher transition temperature and transition enthalpy as compared to normal bilayer (Swamy & Marsh, 1995). Since a change in Krafft temperature can be due to a change in the stability of hydrated solid, it is expected that crystallized lipids with interdigitated acyl chains will have more Krafft temperature.

The present result establishes that OACs in chloride salt environment probably have lower Krafft temperature and they will be in native form near body temperature, whereas in iodide environment it exists as denatured state. This fact will have an important consequence that nature designs chloride salt in the physiological fluid (KCl, NaCl), which may help to keep the lipids and surfactants in their native form at physiological temperature. In this context it is also noteworthy to mention that the denaturation of OACs and other cationic lipids (cetyltrimethylammonium halide, *N*-alkylpyridinium halide) also follows the famous Hofmeister series, where iodide acts as a chaotropic agent.

Chapter 5

Bilayer Formation by Equimolar Mixture of Lysophosphatidylcholine and *O*-Stearoylethanolamine

5.1. Summary

It has been shown by ^{31}P-NMR spectroscopy that *O*-stearoylethanolamine – a structural isomer of the stress-induced lipid, *N*-stearoylethanolamine – forms bilayer structure when mixed at 1:1 mole ratio with lysophosphatidylcholine. The equimolar mixture undergoes a thermotropic phase transition at 52.4 ºC from bilayer gel phase to a micellar structure as evidenced by differential scanning calorimetry, ^{31}P-NMR spectroscopy and turbidimetric studies. These results suggest that *O*-stearoylethanolamine can buffer the membranolytic effect of lysophosphatidylcholine.

5.2. Introduction

Phospholipase A_2 (PLA_2) hydrolyzes phosphatidylcholine at the *sn*-2 position to yield fatty acid and lysophosphatidylcholine. Physiologically, some of these fatty acids (e.g., arachidonic acid) function as precursors for a variety of hormones such as prostaglandins, leukotrienes, thromboxanes (Mayer & Marshall, 1993) and the other product lysophosphatidylcholine (LPC), is the immediate precursor of platelet-activating factor, a potent inflammatory mediator (Farooqui et al., 2004). Collective evidence from recent studies suggests that increased PLA_2 activity and PLA_2-generated mediators play a significant role in acute inflammatory responses in brain and in oxidative stress associated with neurological disorders such as ischemia, Alzheimer's disease, Parkinson's disease, and multiple sclerosis (Kalyvas & David, 2004; Phillis & O'Regan, 2004; Sun et al., 2004, Farooqui et al., 2006).

Due to the amphipathic property of LPC, it may also change membrane fluidity, permeability and stability. Earlier studies on biological systems have

shown that at lower concentration in the membrane, LPC promotes cell fusion (Howell & Lucy, 1969), whereas it is membranolytic at high concentrations and therefore its intracellular levels are under rigid control (Weltzien, 1979). In ischemic myocardium, LPC accumulates (Otani et al., 1989; Sedlis et al., 1993; Kinnaird et al., 1988) and leads to electrophysiological and mechanical dysfunction of the heart (Hoque et al., 1997; Woodley et al., 1991). It was shown that the presence of other lipid components (e.g. fatty acid, cholesterol) that have a molecular shape that is complementary to that of LPC can counteract the lipid membrane destabilizing effects of LPCs (Jain et al., 1980; Jain & Haas, 1981; Ramsammy & Brockerhoff, 1982). In this context it is of great interest to study the interaction between LPC with single chain membrane lipids.

In the present study, it has been shown that equimolar mixtures of egg lysophosphatidylcholine (ELPC) and *O*-stearoylethanolamine (OSEA) adopt a bilayer structure at room temperature, whereas the mixture of NAEs with ELPC forms micelle. The bilayer structure was characterized by ^{31}P-NMR and the morphology of the aggregates was imaged by atomic force microscopy (AFM). Finally the thermotropic phase behavior of the mixture was characterized by differential scanning calorimetry, ^{31}P-NMR spectroscopy and turbidimetric studies, which suggest that the bilayer undergoes a transition to a micellar phase above the transition temperature.

5.3. Materials and methods

5.3.1. Materials

Fatty acids, *N, N'*-dicyclohexylcarbodiimide (DCC) and 4-dimethylaminopyridine were purchased from Sigma-Aldrich (USA). Egg lysophosphatidylcholine (ELPC) was obtained from Avanti polar lipids. Ammonium chloride (NH_4Cl), sulfuric acid,

sodium chloride, EDTA, oxalyl chloride and dioxane were obtained from Merck (Germany). Ethanolamine, BOC-anhydride (di-tert-butyl dicarbonate) and all the solvents were purchased locally. Milli-Q water was used in all experiments.

5.3.2. Synthesis of O-stearoylethanolamine hydrochloride and N-acylethanolamines

O-Stearoylethanolamine hydrochloride (OSEA) was synthesized and characterized as described in Chapter 3. *N*-Myristoylethanolamine, *N*-palmitoylethanolamine and *N*-stearoylethanolamine were synthesized and characterized as reported earlier (Ramakrishnan et al., 1997).

5.3.3. ^{31}P-NMR Spectroscopy

Accurately weighed amounts of ELPC and OSEA or NAE were mixed to yield equimolar ratio and the mixture was dissolved in dichloromethane/methanol (1:1, v/v) mixture and the solvent was removed under dry nitrogen gas. The resulting lipid film was kept under vacuum for 5-6 hrs and then hydrated with 150 mM NaCl containing 0.2 mM EDTA. The sample was then subjected to at least five cycles of freeze thawing, using liquid nitrogen and hot water (ca. 65 °C) and then transferred to a 5 mm NMR tube. ^{31}P-NMR spectra were recorded at a frequency of 162 MHz on a Bruker Avance 400 FT-NMR spectrometer. Spectra were recorded using the zgpg30 pulse program provided by Bruker with ^{1}H decoupling with a decoupling power of 14db. The $\pi/2$ pulse width used was 9.5 μs for ^{31}P and the recycle delay was 1 sec. About 2048 to 4096 scans were accumulated for each spectrum and the free induction decay was processed using 100 Hz of line broadening in order to improve s/n ratio. Temperature was regulated by a thermostatted air-flow system. The spectral width was set to 400 ppm.

5.3.4. Atomic force microscopy

For AFM measurements, a drop of 0.2 mg/ml equimolar ELPC-OSEA solution in 150 mM NaCl was placed on a freshly cleaved mica sheet and dried immediately under nitrogen gas. The salt deposits were washed extensively by washing with Milli-Q water. The samples were once again dried with nitrogen gas. All the images were recorded in air under ambient conditions in semi-contact mode with a scan rate of 0.8 Hz using a SOLVER PRO-M AFM instrument (NTMDT, Moscow). The force was kept at the lowest possible value by continuously adjusting the set-point and feed-back gain during imaging. Image analysis was performed using NOVA software, supplied by NTMDT along with the instrument.

5.3.5. Differential scanning calorimetry

Differential scanning calorimetric studies were performed using a VP-DSC equipment (MicroCal LLC, Northampton, MA, USA). Accurately weighed lipid samples were dissolved in dry dichloromethane/methanol (1:1, v/v) and then the solvent was removed under a stream of dry nitrogen gas. The resulting lipid film was vacuum desiccated for 5-6 hrs in order to remove residual traces of the solvent. The lipid was hydrated thoroughly with 150 mM NaCl and subjected to differential scanning calorimetry essentially as described in Kamlekar & Swamy (2006a).

5.3.6. Turbidimetric studies

Samples for turbidimetric studies were prepared essentially as described in (Kamlekar & Swamy, 2006a) except that the lipid film was hydrated with 150 mM NaCl. Turbidimetric measurements were performed at various temperatures

between 25 and 60 °C using a Cary 100 UV-Visible spectrophotometer (VARIAN) equipped with a Peltier thermostat supplied by the manufacturer. Turbidity was measured by recording the optical density from 350 nm to 450 nm and turbidity at 400 mm was considered for further analysis.

5.4. Results and Discussion

It was mentioned in Chapter 3 that *O*-acylethanolamines are not stable at basic pH (Markey et al., 2000) and in view of the acidic pH of endosomes and ischemic tissues (Murphy et al., 1984; Rybak & Murphy, 1998; Boomer & Thompson, 1999), we have synthesized *O*-stearoylethanolamine hydrochloride and investigated its interaction with lysophosphatidylcholine by biophysical approaches.

5.4.1. ^{31}P-NMR spectroscopy

^{31}P-NMR spectra of equimolar mixtures of egg lysophosphatidylcholine (ELPC) with *O*-stearoylethanolamine hydrochloride (OSEA) and *N*-stearoylethanolamine, recorded at 25 ºC, are shown in Fig. 5.1. The spectrum of ELPC-OSEA mixture exhibits an asymmetric peak that is typical of bilayer structure (Cullis & De Kruijff, 1978). The effective chemical shift anisotropy (CSA) is found to be -67.5 ppm, which is in the range comparable with the CSA observed in saturated phosphatidylcholines and phosphatidylethanolamines in the gel phase (Kleinschmidt & Tamm, 2002; Kamlekar et al., 2007). On the other hand, the ELPC-NSEA mixture gave a sharp isotropic signal, which is similar to that obtained with LPC micelles (Mantsch & McElhaney, 1991; Frías et al., 2008).

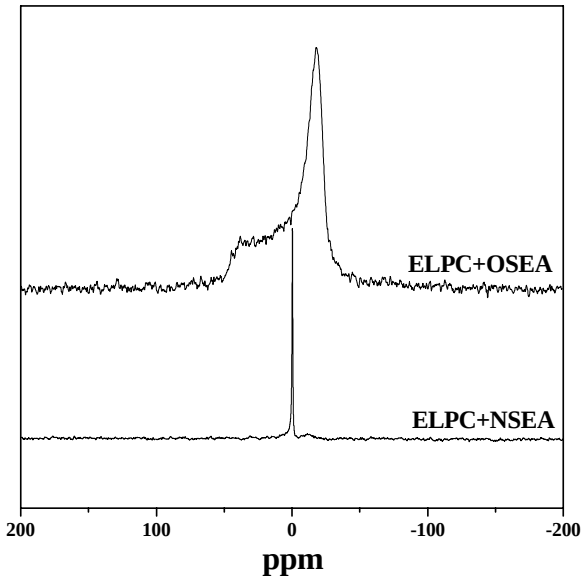

Fig. 5.1. ^{31}P-NMR spectra of equimolar ELPC-OSEA and ELPC-NSEA at 25 ºC.

This suggests that equimolar mixture of ELPC with NSEA, which is an isomer of OSEA does not adopt the bilayer structure. ^{31}P-NMR spectra of 1:1 mixtures of ELPC with other NAEs such as *N*-myristoylethanolamine and *N*-palmitoylethanolamine also gave sharp isotropic signals (not shown), indicating that NAE/lysophosphatidylcholine mixtures do not form the bilayer structure. It has been shown in Chapter 3 that the molecular structures of NSEA and OSEA exhibit significant differences; whereas NSEA has a bent L-shaped structure, OSEA adopts a linear structure and it was suggested that the difference in molecular structure may lead to difference in their interaction with other membrane lipids. Consistent with this, in the present study we have observed that these two lipids differ significantly in their interaction with ELPC.

5.4.2. Atomic force microscopy

Between the experimental macroscopic techniques and the theoretical atomistic approaches, atomic force microscopy (AFM) has proved to be a powerful technique that has allowed imaging of surfaces with sub-nanometric resolution (Garcia-Manyes et al., 2005). In order to characterize the surface topography of ELPC-OSEA mixture atomic force microscopic investigations were carried out in this study. The AFM image of an equimolar mixture of ELPC and OSEA in 150 mM NaCl, shown in Fig. 5.2A, is essentially very similar to the pattern observed in the AFM images of DMPC bilayers (Garcia-Manyes et al., 2005; Roiter et al., 2009; Lam et al., 2006). Using the Nova software provided by the AFM manufacturer the height of the layer obtained in Fig. 5.2A can be measured. Fig. 5.2B shows a cross section of the marked area shown in Fig. 5.2A in which, the layer height was measured to be 4.0 nm. The observed height of the layer (~4.0 nm) falls in the range of the height of a saturated lipid with fatty acyl chain (n=14 to 18) organized in bilayer fashion. Thus the atomic force microscopic data support bilayer formation by the equimolar mixture of ELPC and OSEA.

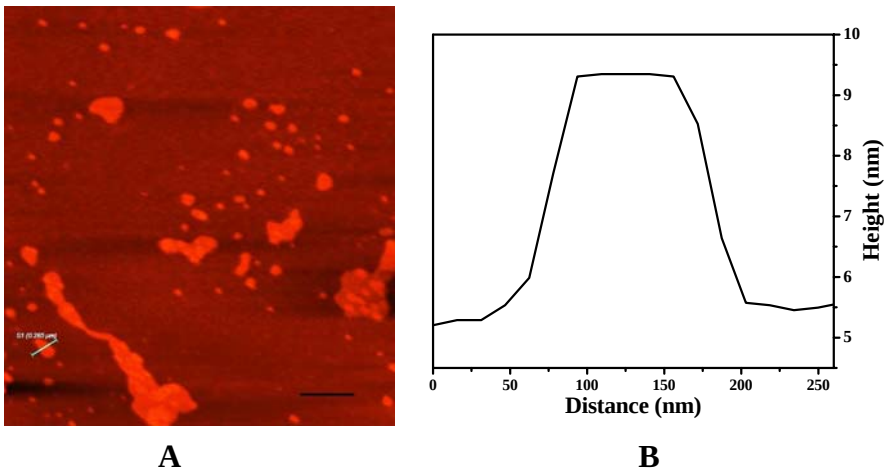

Fig. 5.2. A) AFM semicontact mode image of bilayers of equimolar ELPC-OSEA mixture. B) Cross-section profile of the marked area in A. The black bar corresponds to 500 nm.

5.4.3. Differential scanning calorimetry

Differential scanning calorimetric studies were performed in order to characterize the thermotropic phase transition of the equimolar mixture of ELPC and OSEA. The heating thermogram presented in Fig. 5.3A shows that the 1:1 mixture exhibits a major transition centered at 52.4°C and suggests that the bilayer undergoes a cooperative phase transition with increase in temperature. The transition is relatively broad, starting at 46 ºC and ending at 54 ºC with width at half maxima ($T_{1/2}$) of 3.4º. OSEA (100 mol%) and saturated diacylphosphatidylcholines dispersed in 150 mM NaCl have been shown to exhibit sharp, thermotropic lamellar-gel to liquid-crystalline phase transitions with increase in temperature (Chapter 3; Yeagle, 2005). The widths at half height ($T_{1/2}$) of these sharp transitions range between 0.10 and 0.32° for phosphatidylcholines (n=13-20) (Yeagle, 2005). The higher $T_{1/2}$ observed here for equimolar ELPC-OSEA mixture in 150 mM NaCl suggests that the phase transition is broader and hence may not correspond to a lamellar-gel to liquid-crystalline transition, which in OSEA and phosphatidylcholines is a rather sharp transition. Calorimetric measurements indicate that addition of 50 mol% ELPC to OSEA results in a decrease in the phase transition temperature from 55.8 to 52.4 ºC with concomitant broadening. The broadening of transition peak suggests that the thermotropic phase transition of equimolar mixture of ELPC and OSEA is complex and may be associated with major structural change during transition.

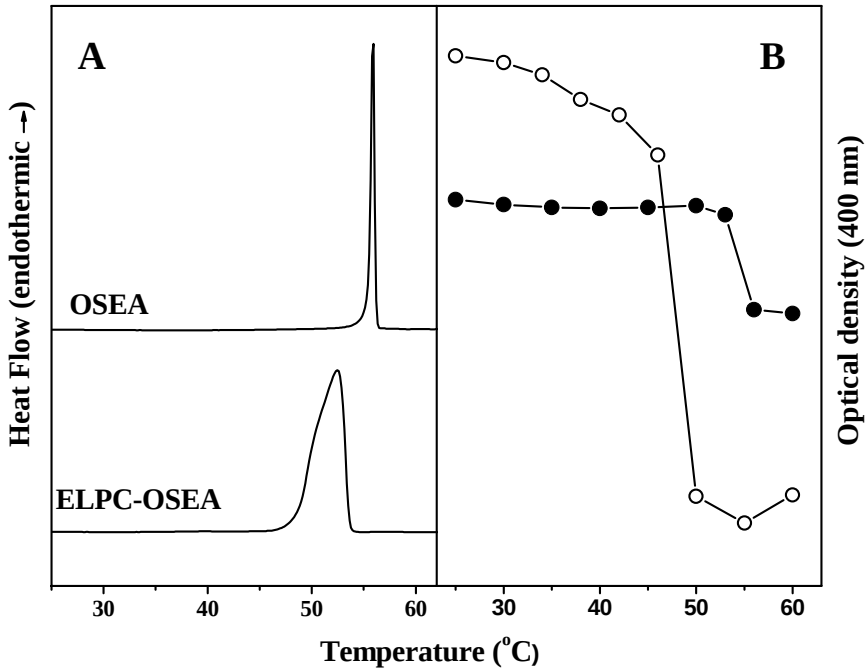

Fig. 5.3. A) DSC heating thermogram of equimolar ELPC-OSEA mixture dispersed in 150 mM NaCl. Heating thermogram of OSEA (100 mol%) taken from Chapter 3, is also plotted for comparison. B) Turbidimetric study of the thermotropic phase transition of ELPC-OSEA (○) and OSEA (●) dispersed in 150 mM NaCl. The temperature dependence of turbidity of OSEA (100 mol%) was taken from Chapter 3. The data points were connected by solid lines to guide the eye.

3.4. Temperature dependent ^{31}P-NMR spectroscopy

To get further structural insights on the aggregates formed near and above phase transition of equimolar mixtures of ELPC and OSEA, ^{31}P-NMR spectra were recorded at various temperatures (Fig. 5.4). Up to 40 ºC the sample shows anisotropic spectra that are characteristic of lamellar phase.

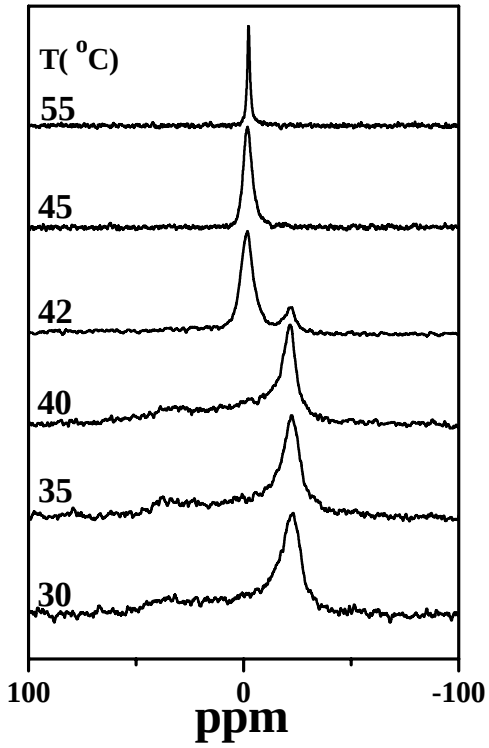

Fig. 5.4. ^{31}P-NMR spectra of equimolar ELPC and OSEA at various temperatures.

The overall shape of the spectra changes significantly near 42 ºC, now appearing as a superposition of two components with peaks centered near -1.7 ppm and -22.0 ppm (see Fig. 5.4). The isotropic signal centered at -1.7 ppm corresponds to micellar phase and the peak at -22 ppm may correspond to bilayer structure and suggests that at 42 ºC the two phases coexists. Upon heating to temperatures above 42 °C, the characteristic anisotropic pattern observed for lamellar structure disappears totally and the spectrum is composed of only isotropic signal. The spectra recorded at higher temperatures exhibit a sharp isotropic signal (Fig. 5.4).

These observations suggest that the equimolar ELPC-OSEA mixture transforms most likely into a micellar phase at high temperature.

5.4.5. Turbidimetry

The phase transition exhibited by the equimolar mixture of ELPC and OSEA was further characterized by turbidimetry, monitoring the turbidity at 400 nm as a function of temperature. Fig. 5.3B depicts the temperature dependence of the turbidity of a 1:1 mixture of ELPC and OSEA in 150 mM NaCl. The turbidity at low temperature was relatively high, which decreases with increase in temperature. Near phase transition temperature the turbidity exhibits a sharp decrease upon increase of temperature and thereafter remains at a constant level. The midpoint of the steeply declining region was taken as the phase transition temperature (T_t). The T_t value obtained from the turbidimetric studies is 48.5 °C, which is in good agreement with the T_t value of 52.4 ºC, obtained from the DSC measurements. From Fig. 5.3B it can also be noticed that above phase transition temperature turbidity of the sample is significantly lower and visual inspection of the equimolar ELPC-OSEA mixture indicated that above phase transition the sample is clear to the naked eye, suggesting that the aggregates are relatively small, and most likely correspond to micelles. For the sake of comparison between the turbidity of the equimolar ELPC-OSEA mixture and 100 mol% OSEA above phase transition temperature, the temperature dependence of turbidity of OSEA alone (data taken from Chapter 3) is also shown in Fig. 5.3B. The comparison shows that due to the formation of liquid-crystalline phase in 100 mol% OSEA the turbidity is relatively higher than the turbidity of the equimolar ELPC-OSEA mixture above the transition temperature. This suggests that addition of 50 mol% ELPC modulates the phase structure of OSEA above the phase transition. Our experimental result

suggest that the 1:1 mixture of ELPC and OSEA adopts the bilayer structure at room temperature, but the bilayer is unstable at high temperature since it undergoes a transformation to a micellar phase. In a phase transition from bilayer to micelle the lipid aggregates have to undergo significant reorganization, which is possibly reflected in the high $T_{1/2}$ of the transition.

The important outcome of the thermal phase transition of equimolar mixture of ELPC and OSEA is that the bilayer aggregate transforms to micellar phase slightly above the body temperature (ca. 37 °C). Now, if the mixture can encapsulate hydrophilic drugs then the mixture will be of potential use in thermo-triggerable drug delivery system for the treatment of solid tumor (Needham & Dewhirst, 2001). However, further studies are required regarding the phase diagram of ELPC and OSEA mixture and the encapsulation ability of the mixture.

5.4.6. Biological Implications

Lysophosphatidylcholine (LPC) is an endogenous phospholipid that gets released from the cell membrane by PLA_2–induced hydrolysis of a main membrane phospholipid, phosphatidylcholine and accumulates rapidly during myocardial ischemia (Otani et al., 1989; Sedlis et al., 1993; Kinnaird et al., 1988). LPC produces potent, reversible, and localized cardiac effects, such as membrane depolarization, modulation of the cardiac Na^+ current (Sato et al., 1993; Watson & Gold, 1997; Han et al., 2004) and may be related to the development of hypertension (Wu et al., 2001; Han et al., 2004). In addition, because of the amphiphilic nature of LPC, it may change the physico-chemical properties of the cell membrane. Fink and Gross (1984) have reported that LPC changes the sarcolemmal molecular dynamics and increases membrane fluidity. In addition, exposure to concentrations of LPC well above its critical micellar concentration has

been reported to transiently increase permeability in plasma membranes (Sidik & Smerdon, 1990). The membraneolytic effects of LPC have been studied extensively in relation to lysis of red blood cells (Weltzien, 1979; Bierbaum et al., 1979). Their release from cell membrane and detergent like activity is likely to be due to the formation of non-bilayer aggregates (micelles) at physiological temperature. Several studies have shown that addition of amphiphiles that form bilayer structure when mixed with LPC modulate the physical properties of membranes containing LPC. For example, Jain et al. (1980) have shown that equimolar mixture of LPC and fatty acid forms bilayer and they have pointed out that LPC and fatty acids together retard hemolysis. They have also postulated that the viability of certain cell types and organelles in presence of considerable amount of LPC (De Oliveira Filgueiras et al., 1979) is due to the bilayer formation between fatty acid and LPC (Jain et al., 1980). In another study it was reported that an equimolar mixture of LPC and cholesterol forms a complex and it has been suggested that cholesterol can buffer the membranolytic effect of LPC (Ramsammy & Brockerhoff, 1982). Recently, it has been observed that arbutin, a plant pigment, forms bilayer structure with LPC and inhibits the detergent-like effect of LPC on DMPC liposomes (Frías et al., 2007, 2008). In this context it may be speculated that OSEA, which forms bilayer structure when mixed with ELPC at 1:1 (mole/mole) ratio, may act as body's own stress fighting response, and stabilizes the bilayer structure of membrane in stress, for example, under conditions which lead to the over expression of PLA_2.

Chapter 6

Structure and Design of Base-labile Catanionic Mixed Lipid System

6.1. Summary

Lipid based base triggerable system will be useful for colon specific targeted delivery of drugs and pharmaceuticals. In view of this two novel base triggerable mixed lipid systems, consisting of 1) a mixture of *O*-lauroylethanolamine hydrochloride (OLEA.HCl) and sodium dodecyl sulfate (SDS) and 2) a mixture of OLEA.HCl with sodium dodecylbenzene sulfonate (SDBS) have been designed. The aggregates formed near equimolar mixture of OLEA.HCl-SDS and OLEA.HCl-SDBS have shown lability at basic pH, indicating that the system may be useful for developing colon specific drug delivery system(s). Turbidimetric and isothermal titration calorimetric studies revealed that OLEA.HCl forms a 1:1 (mole/mole) complex with SDS. The molecular packing and intermolecular interactions in the OLEA-SDS 1:1 complex have been solved by single crystal X-ray diffraction. These studies are also likely to help in understanding the specific interaction between lipids in more complex system, e. g. biomembranes.

6.2. Introduction

Liposomal drug delivery systems that self-destruct upon application of a stimulus have gained considerable interest in the biomedical community because of the temporal and spatial specificity they can afford to the delivery of therapeutics. Liposomes which unload the drug when subjected to different types of stimuli, e.g., acid, radiation, heat and redox-potential have been designed during the last decade or so (Huang et al., 2006; Shum et al., 2001; Needham & Dewhirst, 2001; Ong et al., 2008). This occurs either by increasing the permeability of the drug through the membrane or by completely disrupting the supramolecular structure of the vesicular assembly under the condition of applied stimuli. Like other systems base-triggerable systems also attracted researchers due their applicability in colon specific drug delivery. The pH-responsive colon-specific systems are based on the reported luminal pH increase gradually along the small intestine (from 6.63±0.53 in the jejunum) reaching a peak at the ileocaecal junction (7.49±0.46) (Evans et al., 1988). The most commonly used system is a polymer, Eudragit S and was designed to dissolve above pH 7. This polymer was first used as a colon-targeted pH-responsive delivery agent and is still used for site-specific delivery of the anti-inflammatory drug mesalazine to the large intestine for the treatment of ulcerative colitis (Dew et al., 1982; McConnell et al., 2008). But there have been no reports on lipid based base-triggerable delivery systems for colon-specific drug targeting.

Mixtures of cationic and anionic single chain lipids can spontaneously form vesicles and several other phase structures (Kaler et al., 1989; Dubois et al., 2001). Such catanionic mixed lipid systems, also known as catanionic surfactants have been subjected to extensive experimental studies, since their preparation is easier, and the size, and charge of the aggregates can be tuned simply. In the present study, two base-triggerable catanionic mixed lipid systems, 1) a mixture of *O*-

lauroylethanolamine hydrochloride (OLEA.HCl) and sodium dodecyl sulfate (SDS) and 2) a mixture of OLEA.HCl with sodium dodecylbenzene sulfonate (SDBS) have been designed. The interactions between OLEA.HCl and SDS were investigated by turbidimetry and isothermal titration calorimetry (ITC). Dissociation of the aggregates formed by both mixed lipid systems at high pH indicated that the designed systems may be promising candidates for developing base-triggerable delivery systems. Finally, the molecular structure and intermolecular interaction of the catanionic mixed lipid system and OLEA.HCl were determined by single crystal X-ray diffraction. To the best of our knowledge, the present report is the first description on the determination of crystal structure of a mixed lipid system, although structural characterization of the lipids was started in the 1950s. It is likely that the packing and intermolecular interaction in the mixed lipid system will help to understand the specific interaction between the lipids in membrane microdomains.

6.3. Materials and methods

6.3.1. Materials

Lauric acid, sodium dodecyl sulfate (SDS), sodium dodecylbenzene sulfonate (SDBS), *N, N'*-dicyclohexylcarbodiimide (DCC) and 4-dimethylaminopyridine (DMAP) were purchased from Sigma-Aldrich (USA). Ammonium chloride (NH_4Cl), sulfuric acid and dioxane were obtained from Merck (Germany). Ethanolamine, BOC-anhydride (di-tert-butyl dicarbonate), solvents and other chemicals used were of analytical grade and were purchased locally. Milli-Q water was used in all experiments.

6.3.2. Synthesis of O-lauroylethanolamine hydrochloride

O-Lauroylethanolamine hydrochloride (OLEA.HCl) was synthesized as described in Chapter 3.

6.3.3. Turbidimetry

Turbidimetric measurements were performed at 25 °C using a Cary 100 UV-Visible spectrophotometer (VARIAN). The lipids at different ratios were mixed, vortexed and kept for 30 minutes. For the experiments at different pH, the aggregated catanionic mixed lipid at near equimolar mixture (45:55, mol/mol) were incubated for 30 minutes in various buffer systems: 20 mM KCl-HCl (pH 2.0), 20 mM citrate-phosphate (pH 3.0-6.0), 20mM Tris-HCl (pH 7.0-9.0) and 20 mM glycine-NaOH (pH 10.0). Turbidity was measured by recording the optical density from 350 nm to 450 nm and turbidity at 400 mm was considered for further analysis.

6.3.4. Isothermal titration calorimetry

An isothermal titration calorimeter (VP-ITC, Microcal Inc., Northampton, MA) was used to determine the interaction between OLEA.HCl and SDS at 25 ºC. Small (10 μl) aliquots of 0.5 mM SDS solution were added via a rotating stirrer syringe to 0.05 mM OLEA.HCl solution contained in a 1.445 ml sample cell. Each injection lasted 20 s and an interval of 240 s was given between successive injections. The solution in the reaction cell was stirred at a speed of 300 rpm throughout the experiments. Usually the first injection was found to be inaccurate; therefore, a 2 μl injection was added first and the resultant point was deleted before the analysis of remaining data.

For a system of one set of binding sites, the total heat evolved (or absorbed) during the binding process at the end of the i^{th} injection Q(i), is given by Equation (6.1) (Wiseman et al., 1989).

$$Q(i) = nP_t\Delta H_b V\{1+X_t/nP_t+1/nK_bP_t-[(1+X_t/nP_t+1/nK_bP_t)2-4X_t/nP_t]½\}/2 \quad (6.1)$$

where n is the stoichiometry of binding, P_t is the total concentration of lipid in cell, X_t is the concentration of lipid in syringe, V is the cell volume, K_b is the binding constant and ΔH_b is the binding enthalpy. The heat corresponding to the i^{th} injection, $\Delta Q(i)$, is equal to the difference between Q(i) and Q(i-1) and is given by Equation (6.2), which involves the necessary correction factor for the displaced volume (which is equal to the injection volume dV_i):

$$\Delta Q(i) = Q(i) + dV_i/2V[Q(i) + Q(i\text{-}1)] - Q(i\text{-}1) \quad (6.2)$$

The ITC unit measures $\Delta Q(i)$ value for every injection. These values are then fitted to equations (6.1) and (6.2) by a nonlinear least squares method using the data analysis program Origin® (MicroCal™). The fit process involves initial guess of n, K_b and ΔH_b which allows calculation of $\Delta Q(i)$ values as mentioned above for all injections and compares them with the corresponding experimentally determined values. Based on this comparison the initial guess of n, K_b and ΔH_b is improved and the process is repeated till no further significant improvement in the fit can be obtained. The thermodynamic parameters, ΔG_b and ΔS_b are calculated according to the basic thermodynamic Equations (6.3) and (6.4):

$$\Delta G_b = -RT\ln K_b \quad (6.3)$$

$$\Delta G_b = \Delta H_b - T\Delta S_b \quad (6.4)$$

6.3.5. Crystallization, X-ray diffraction and structure solution

An equimolar mixture of OLEA.HCl and SDS was dissolved in dichloromethane containing a trace of methanol and kept for crystallization. Thin, colorless plate-type crystal was used for the data collection. X-ray diffraction measurements were carried out at room temperature (ca. 25 °C) with a Bruker SMART APEX CCD area detector system using a graphite monochromator and Mo-Kα (λ = 0.71073 Å) radiation obtained from a fine-focus sealed tube.

Data reduction was done using Bruker SAINTPLUS program. Structure solution was carried out in the triclinic space group. Absorption correction was applied using Bruker SADABS program. The structure of OLEA-DS complex was solved successfully by direct methods in the space group *P*-1 and refinement was done by full matrix least-squares procedure using the SHELXL-97 program (Sheldrick, 1997). The refinement converged into a final R_1 = 0.089, wR_2 = 0.187 and goodness of fit = 1.04.

6.3.6. Crystal parameters of OLEA-DS complex

Molecular formula: $C_{26}H_{55}NO_6S$. Molecular formula weight: 509.8; Crystals were plate type and colorless. Crystal system, triclinic; Space group, Sg = *P*-1; Ambient temperature, T = 298(2) K; Radiation wavelength (λ) = 0.71073 Å; Minimum resolution = 0.84 Å; Radiation type, Mo-Kα; Radiation source, Fine-focus sealed tube; Radiation monochromator, graphite; Number of reflections collected, 9110; Unique reflections, 5199; Reflection with I > 2σ(I), 3077; Number of parameters, 310.

Unit cell dimensions (with standard deviation in parentheses):

a = 5.478(1), b = 7.272(1), c = 37.771(5) Å; α = 87.989(3), β = 89.759(2), γ = 88.604(2)º; Volume of the cell, V = 1503.3(4) Å^3; Number of molecules in the unit cell, Z = 2; $F_{(000)}$ = 564; Absorption coefficient, μ =0.144 mm^{-1}; T = 298(2) K.

6.3.7. Lattice energy calculations

Lattice energies of OLEA.HCl and OLEA-DS complex were determined using the Dreiding force field in Cerius^2 suite of programs (Accelrys Inc., San Diego, CA, USA; website: http://www.accelrys.com).

6.3.8. Dynamic light scattering and atomic force microscopy

DLS measurements of a near equimolar mixture of OLEA.HCl and SDBS were performed at a 90° scattering angle on a PDExpert (Precison Detectors, Inc. Bellingham, MA, USA) DLS instrument at a wavelength of 685 nm with a power of 30 mW. For AFM measurements, a drop of dilute solution of near equimolar mixture of OLEA.HCl and SDBS was placed on a freshly cleaved mica sheet and dried immediately under nitrogen gas. The deposits were washed with miliQ water and dried with nitrogen gas. All the images were recorded in air under ambient conditions in semi-contact mode with a scan rate of 0.8 Hz using a SOLVER PRO-M AFM instrument (NTMDT, Moscow). The force was kept at the lowest possible value by continuously adjusting the set-point and feed-back gain during imaging. Image analysis was performed using NOVA software, supplied by NTMDT along with the instrument.

6.3.9. Fluorescence measurement

Fluorescence measurements were made on a SPEX FLUOROMAX-4 fluorescence spectrometer. The near equimolar mixture of OLEA.HCl and SDBS in the buffer or desired pH was mixed and pyrene (THF solution) was added to the solution by maintaining the lipid : pyrene ratio at 400 : 1. The final pyrene concentration was in the μM range. The mixture was vortexed and kept for 30 minutes at room temperature. Samples were excited at 335 nm and emission spectra were recorded in the range between 350 and 550 nm. The excitation and emission slit widths were set at 1.5 nm. Pyrene exhibits five bands in the spectrum and the intensity ratio of first and third band was considered for analysis.

6.4. Result and discussion

6.4.1. Turbidity of the mixed solution of OLEA and SDS

The optically clear solution of *O*-lauroylethanolamine hydrochloride (OLEA.HCl) in water becomes turbid upon addition of negatively charged sodium dodecyl sulfate (SDS) in small aliquots from an aqueous solution. This suggests that both the lipids interact with each other and form larger aggregates. Since OLEA.HCl is cationic and SDS is anionic, mixing of two lipids may lead to the formation of catanionic mixed lipid system. This was further investigated by turbidimetry.

The turbidity of OLEA.HCl-SDS mixtures at constant overall concentration is shown in Fig. 6.1. Initially the turbidity increases with increase in SDS concentration and reaches a maximum level near X_{SDS} value of 0.4 to 0.6. At higher X_{SDS} turbidity again decreases with further increase in SDS concentration.

The higher turbidity near the X_{SDS} value of 0.5 suggests the formation of 1:1 complex between two lipids.

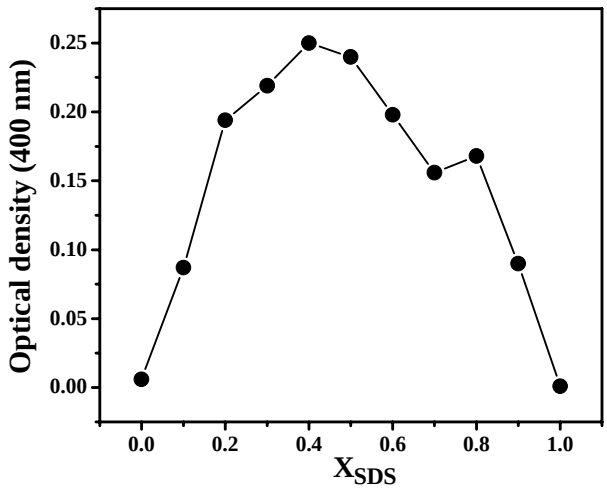

Fig. 6.1. Turbidity of various mixrues of OLEA.HCl and SDS.

6.4.2. Thermodynamics of interaction between OLEA.HCl and SDS

The formation of equimolar complex between OLEA.HCl and SDS as suggested by the turbidimetric study was further investigated by ITC. Experiments were carried out at sufficiently low concentration (below CMC) of both the lipids to avoid their self aggregation, which sometimes may complicate the data analysis. A representative calorimetric titration for the interaction of OLEA and SDS is given in the upper panel of Fig. 6.2. From the figure it is seen that the exothermic heat of binding decreases monotonically with successive injections until saturation is achieved. A plot of incremental heat released as a function of the ratio of SDS to OLEA.HCl is shown in the lower panels of Fig. 6.2, together with a non-linear least square fit of the data to equation 6.1.

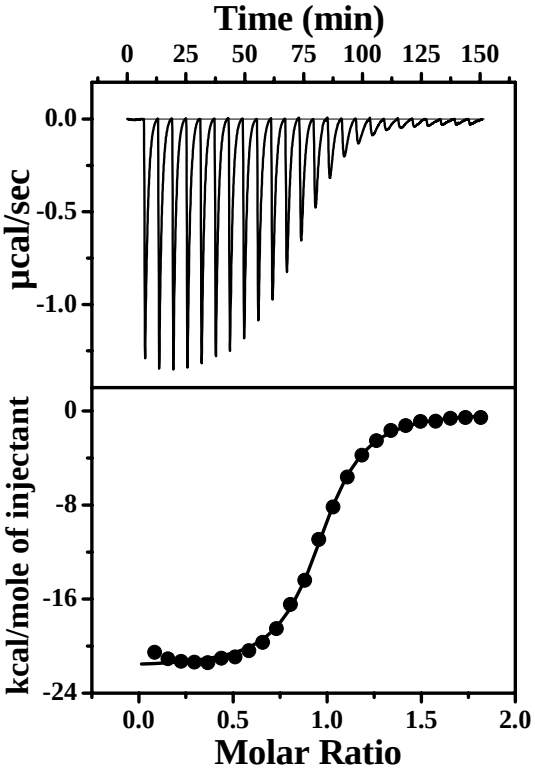

Fig. 6.2. ITC profile of interaction between OLEA.HCl and SDS at 25 ºC. The upper panel shows raw data for titration of 0.05 mM OLEA.HCl with 0.5 mM SDS. The lower panel shows the integrated data obtained from the raw data shown in upper panel, after subtracting the data from blank titration. The solid line in the bottom panel represents the best curve fit to the experimental data, using the '*one set of sites*' model from MicroCal Origin.

The experimental data could be fitted satisfactorily to a 'one set of sites' model available in the Origin software provided by the instrument manufacturer. The fits obtained for the data are shown as solid lines in the lower panels of Fig. 6.2. The fits yielded the values of various parameters such as stoichiometry of binding, n= 0.94 ± 0.12; binding constant K_b= 1.37E6 ± 0.09E6; enthalpy of binding, ΔH_b= -21.8 ± 1.0 kcal.mol^{-1} and entropy of binding, ΔS_b= -45.2 ± 3.75 cal.mol^{-1}.K^{-1}. The Gibbs free energy, ΔG_b obtained from equation 6.4 is -8.33 kcal.mol^{-1}. The stoichiometry of binding (n) was found to be near 1.0, indicating that OLEA and

SDS form a 1:1 (mol/mol) complex. As it forms an equimolar complex at low concentration, we expect that the first step of the formation of a catanionic mixed lipid system is the formation of a 1:1 complex and then the complex will self-assemble to form aggregated supramolecular structure above critical aggregation concentration.

6.4.3. Disruption of aggregate with pH

OLEA.HCl belongs to a class of lipids named as *O*-acylethanolamines (OAEs), which are ester derivatives of ethanolamine. OAEs with palmitoyl and arachidonyl acyl chains have been reported to be unstable at high pH and transforms to corresponding *N*-acylethanolamines via acyl chain migration (Markey et al., 2000). It is expected that like other OAEs, OLEA.HCl also would not be sufficiently stable at basic pH. Therefore the catanionic lipid aggregate formed by OLEA.HCl as a cationic lipid will be expected to be disrupted at high pH due to its transformation to *N*-lauroylethanolamine which may disturb the ionic as well as H-bonding interaction between the two oppositely charged lipids. Therefore, this catanionic mixed lipid aggregate system may be useful for the release of cargo at high pH such as in colonic delivery.

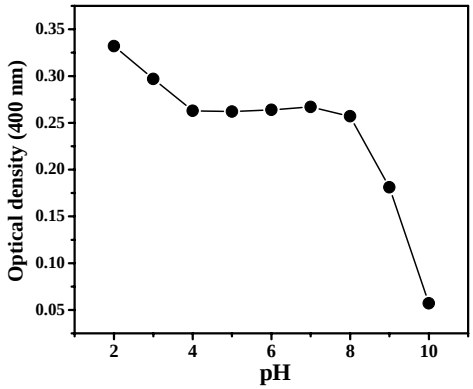

Fig. 6.3. Effect of pH on the turbidity of the aggregates formed by near equimolar mixture of OLEA.HCl and SDS.

Fig. 6.3 shows the turbidity of the equimolar OLEA.HCl-SDS mixtures at constant concentration with different pH. It is seen from this figure that turbidity of the sample decreases at high pH and suggests the disruption of aggregate with increase in pH. Unfortunately, the problem encountered in the system is that the formed catanionic mixed lipid system was not sufficiently stable for practical use. It tends to precipitation upon keeping for a long time and altering the lipid ratio from equimolar to near equimolar with slightly high percentage of cationic lipid or anionic lipid did not enhance the stability of the mixed lipid system. Although the mixture was not sufficiently stable, it provided a base system which can be modified to make stable base triggerable catanionic liposomes by fine-tuning the anionic lipid or by using other OAEs containing different acyl chains.

6.4.4. Description of the structure

The molecular structure of 1:1 complex of *O*-lauroylethanolamine and dodecyl sulfate (OLEA-DS) is shown in the ORTEP plot given in Fig. 6.4A, along with the atom numbering for all the non-hydrogen atoms. It is clearly seen from this figure that the hydrocarbon portion (C1−C12) of the acyl chains of dodecyl sulfate (DS) and OLEA (C16-C26) are in all-*trans* conformation. The torsion angles observed for the acyl chain region are all close to 180°. The gauche conformation of the C1-O4 bond of DS results in a minor bend at the head group region, although overall shape of the molecule is close to linearity. The all-*trans* conformation of the acyl chain portion of OLEA in the complex results in a linear geometry. In the complex both the linear molecules are oriented appropriately to facilitate hydrogen bond interaction between their hydrophilic groups and appreciable dispersion interaction between the hydrocarbon regions of the two molecules.

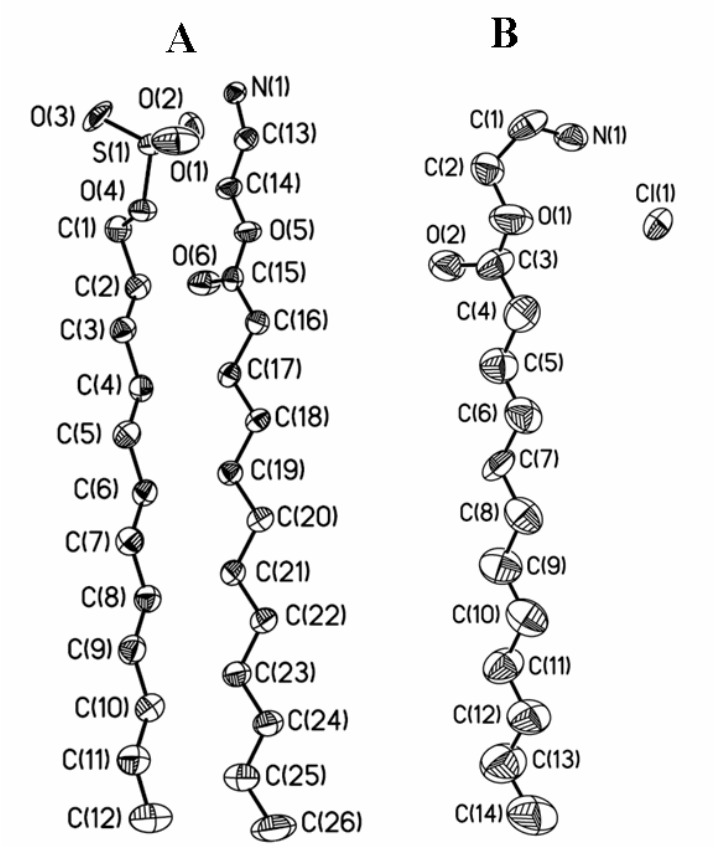

Fig. 6.4. A) An ORTEP plot showing the molecular structure of OLEA-DS (1: 1, mol/mol) complex. B) An ORTEP plot showing the molecular structure of *O*-lauroylethanolamine hydrochloride (to compare the structure of OLEA.HCl alone and in complex, taken from Chapter 3).

6.4.5. Molecular packing

Packing diagrams of the OLEA-DS complex along the *a*-axis and the *b*-axis are given in Fig. 6.5A and 6.5B, respectively. In the crystal the 1:1 complex of OLEA-DS unit repeats to form the entire lattice.

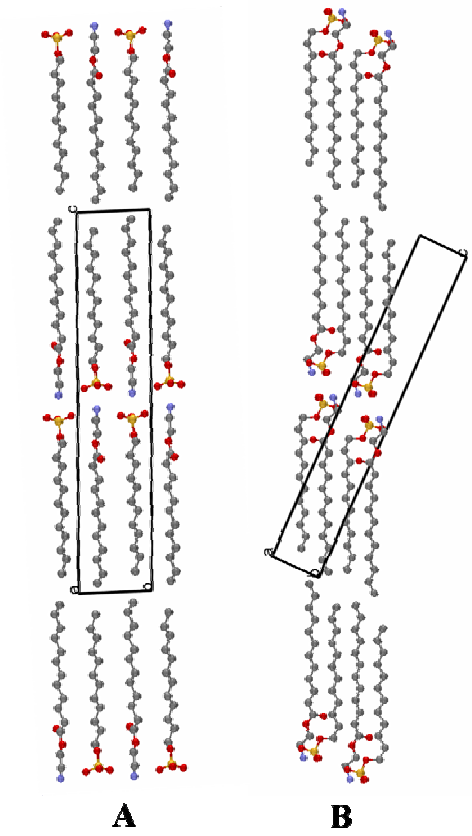

Fig. 6.5. Packing diagrams of OLEA-DS complex. (A) A view along the *a*-axis. (B) A view along the *b*-axis. Color code: grey, carbon; red, oxygen; blue, nitrogen; golden, sulfur.

The molecules are packed in layers that are stacked in such a way that the methyl groups of the *O*-lauroyl chains of OLEA from one layer face the methyl groups of the *O*-lauroyl chains of DS from the next layer. This chain packing is of the mixed type as *O*-lauroyl chains of DS from one layer face the *O*-lauroyl chains of OLEA from the next layer. The other possible chain packing is of the symmetric type, where *O*-lauroyl chain of OLEA could face the *O*-lauroyl chain of OLEA of next layer and *O*-lauroyl chain of DS could face the *O*-lauroyl chain of DS of the next layer. The length of the DS molecule is ~17.2 Å, which is slightly lower than the length of OLEA molecule (~18.3 Å). The difference of size may be responsible for

the mixed type chain packing. The methyl ends of the stacked bilayers are in van der Waals contacts, with the closest methyl-methyl (C12–C26) distance between opposite layers and the same layer being 3.93 Å and 4.26 Å, respectively. The bilayer thickness (C1–C15 distance) in the crystal structure of OLEA-DS is 31.8 Å and the all-*trans O*-lauroyl chains of OLEA and DS are tilted by 23.8° and 26.6°, respectively, with respect to the normal to the respective methyl end planes.

6.4.6. Subcell packing

The different lateral packing modes, adopted by hydrocarbon chains in lipid crystals are generally described by subcells that specify the relations between equivalent positions within the chain and its neighbors. Examination of the hydrocarbon chain packing in the acyl chains of OLEA-DS complex revealed that the hydrocarbon chains pack in the orthorhombic type ($O_{\perp}$), whereas the chain packing of OLEA.HCl was according to triclinic subcell ($T_{//}$) (Abrahamsson et al., 1978; Maulik et al., 1990). This shows that the chain packing is different between OLEA.HCl alone and in the complex with DS. The unit cell dimensions of $O_{\perp}$ subcell are a = 4.96 Å, b = 7.27 Å and c = 2.54 Å and $T_{//}$ subcell are a = 4.32 Å, b = 5.40 Å and c = 2.52 Å

6.4.7. Hydrogen bonding and intermolecular interactions

To understand the intermolecular interactions in OLEA-DS mixed lipid system, the molecular packing in the crystal lattice was examined from various angles. The observed hydrogen bonding pattern in the crystal lattice is shown in Fig. 6.6. Fig. 6.6A shows that each N-H hydrogen of OLEA is hydrogen bonded to one charged oxygen atom of the sulfate group of DS, resulting in three distinct H-bonds being formed by each OLEA molecule. These N-H···O type hydrogen bonds bridge the

head groups coming from opposite layers and adjacent layers. The hydrogen bond distance (H···O) and angle of the three types of N-H···O interactions are 1.93 Å, 2.02 Å, 2.03 Å and 168.8°, 172.9°, 160.9°, respectively. The hydrogen bonded network in the head group region adopts a pleated ladder-like structure (Fig. 6.6B).

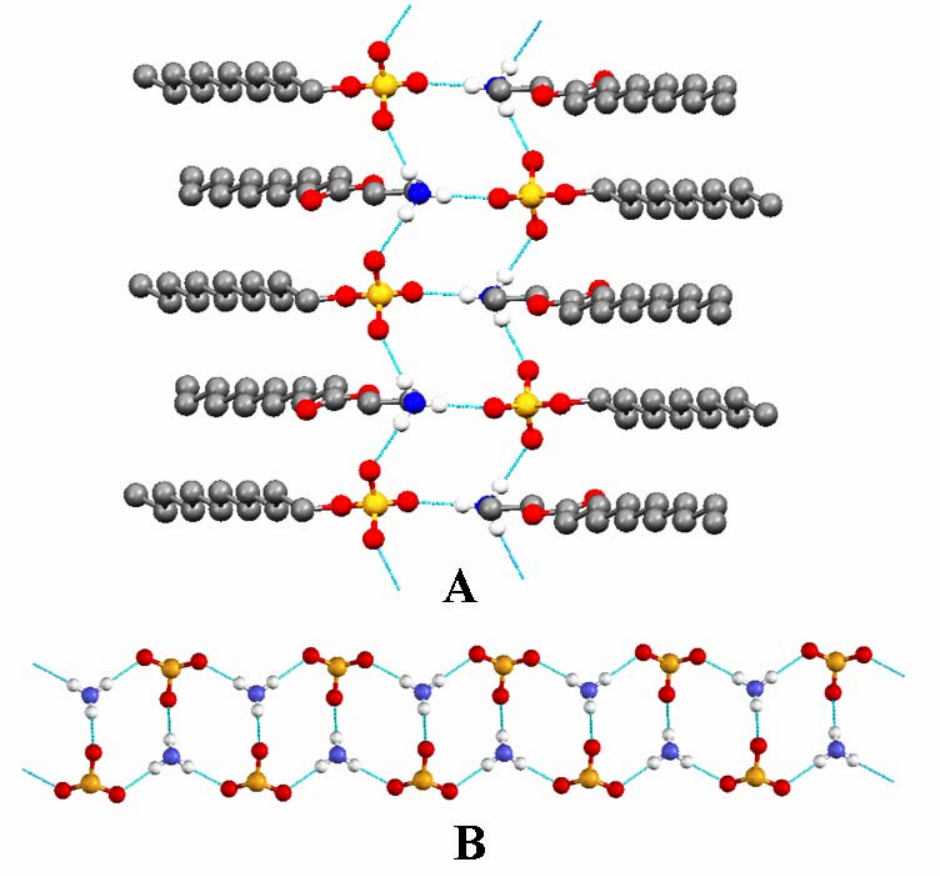

Fig. 6.6. Hydrogen bonding pattern in the crystal lattice of OLEA-DS complex. (A) A close-up view displaying N-H···O type hydrogen bonding. (B) Hydrogen bonded motifs involving N-H···O interactions, lead to the formation of a pleated ladder-like structure. Color code: grey, carbon; red, oxygen; blue, nitrogen; golden, sulfur; white, hydrogen.

6.4.8. Lattice energy calculation

Lattice energies of OLEA-DS complex and OLEA.HCl (parameters obtained from Chapter 3) were computed using the Dreiding force fields in Cerius^2 program package in order to estimate the lattice energies. The calculations yielded an overall energy of -124.7 kcal/mol for OLEA-DS complex and -99.4 kcal/mol for OLEA.HCl. This suggests that the equimolar complex is thermodynamically more stable than the single tail lipid. The higher lattice energy of the equimolar complex may be responsible for the high Krafft temperature of the system (see below).

6.4.9. Structure and phase behavior

Biological membranes are composed of a variety of different lipids and a knowledge of intermolecular interaction among them will help to understand their structure-activity relationship. The intermolecular interaction between two lipids can be investigated using various spectroscopic and calorimetric techniques. Among the different techniques single-crystal X-ray diffraction is the most powerful since it can provide precise information on the structure and packing of molecules at atomic resolution. Although the crystal structures of various membrane lipids and other lipids have been solved successfully, to the best of our knowledge there are no reports where the structure and packing of a mixed lipid system have been analyzed. This may be due to the difficulty of growing high quality-single crystals of lipid mixtures for X-ray diffraction. In addition, the diffraction patterns of lipids are dominated by strong subcell reflections arising from the regular hydrocarbon chain matrix, which complicate or sometimes hinder the structure solution (Pascher et al., 1992). Here, we have solved the structure of a mixed lipid system and the intermolecular interactions have been analyzed. The

hydrogen bonding belt between the head groups and dispersion interaction among the acyl chain as observed in the crystal structure of this mixed lipid system can help to understand the interaction in similar systems, such as lysophosphatidylcholine and fatty acid; lysophosphatidylcholine and cholesterol; *N*-myristoylethanolamine and cholesterol, where specific interaction between the two lipids have been observed (Jain et al., 1980; Ramsammy & Brockerhoff, 1982; Ramakrishnan et al., 2002).

The catanionic mixed lipid aggregates of OLEA.HCl and SDS have shown lability under basic condition and this system was expected to be a potential candidate for developing delivery agents to target colon. However, due to instability of the mixed aggregates, the system cannot be used for practical application. It was observed that the mixed aggregates tend to precipitate near equimolar mixture which may be due to the high Krafft temperature of the mixture. Krafft temperature is defined as the temperature above which the solubility of a surfactant/lipid increases dramatically in aqueous systems, and has been interpreted as the melting temperature of a hydrated solid surfactant (Shinoda, 1963; Tsujii & Mino, 1978). The insolubilization of the lipids or surfactants below Krafft temperature is usually accompanied by the crystallization of alkyl chains of the surfactant molecules inducing the formation of the hydrated solids in water. Therefore, change in Krafft temperature can be regarded as a change in the stability of hydrated solid and it is expected that crystallized lipids with higher lattice energy may possess higher Krafft temperature. The Krafft temperature of OLEA.HCl is well below room temperature and corresponding temperature for the equimolar mixture is much higher. The calculated lattice energy has shown that the complex possesses more lattice energy than OLEA.HCl alone. Therefore, the acyl chains are more tightly packed in the complex than in OLEA.HCl alone. Further support for

this comes from the packing coefficient, which has values of 65.6% and 60.7% for the complex and OLEA.HCl, respectively, suggesting that the acyl chains in the complex are packed more tightly than in OLEA.HCl. It is expected that branching in acyl chains and complex formation with mismatched chains may reduce the acyl chain packing and therefore the Krafft temperature of the system may be reduced. Further studies using different fatty acyl OAEs, other anionic surfactants and introduction of branching in the acyl chains are some of the approaches that can be employed to develop novel base-triggerable mixed lipid system for targeting colon.

In order to understand the effect of changing the anionic lipid on the stability of mixed lipid system, sodium dodecylbenzene sulfonate (SDBS) was used as an anionic lipid. The mixture of OLEA.HCl and SDBS yielded turbid suspensions and the suspensions were found to be are more stable than OLEA-SDS mixture. Therefore various physical studies including light scattering and imaging experiment have been carried out with the mixture.

6.4.10. Turbidity of the mixed solution of OLEA and SDBS

The turbidity of OLEA.HCl-SDBS mixtures at constant overall concentration is shown in Fig. 6.7. Initially the turbidity increases with increase in SDS concentration and reaches a maximum level when X_{SDBS} is 0.5. Above that turbidity again decreases with further increase in SDBS concentration. The higher turbidity near the X_{SDBS} value of 0.5 suggests the formation of 1:1 complex between two lipids.

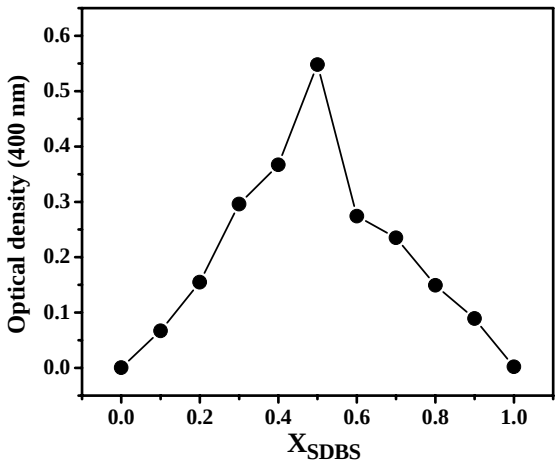

Fig. 6.7. Turbidity of various mixrues of OLEA.HCl and SDBS.

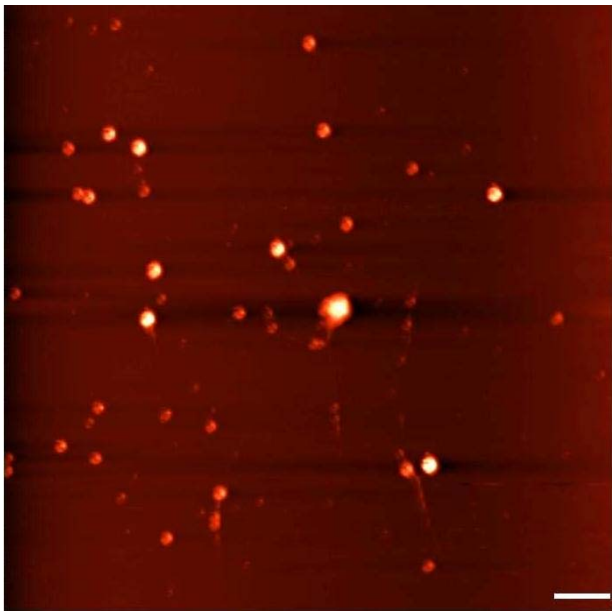

Fig. 6.8: AFM image of near equimolar mixture of OLEA.HCl and SDBS. The spherical structures seen in the figure indicate the formation of vesicular aggregates. Bar corresponds to 500 nm.

6.4.11. Dynamic light scattering and atomic force microscopy

DLS studies were carried out on dilute solutions of near equimolar (45:55, mol/mol) mixtures of OLEA.HCl and SDBS at 25 °C. The average R_h of the aggregate obtained from DLS data analysis is 258.0 ± 18.0 nm. To visualize the morphology of aggregates and corroborate the above DLS data, images of aggregates formed by near equimolar mixture of OLEA.HCl and SDBS samples using atomic force microscopy (AFM) have been recorded. Fig. 6.8 gives a representative AFM images of the mixture recorded at room temperature and shows the existence of vesicular aggregates. However, the size of the vesicles shown in the AFM picture appears to be somewhat smaller than the R_h values obtained from DLS measurements. This could be due to the fact that DLS measures average size of the aggregates present in solution.

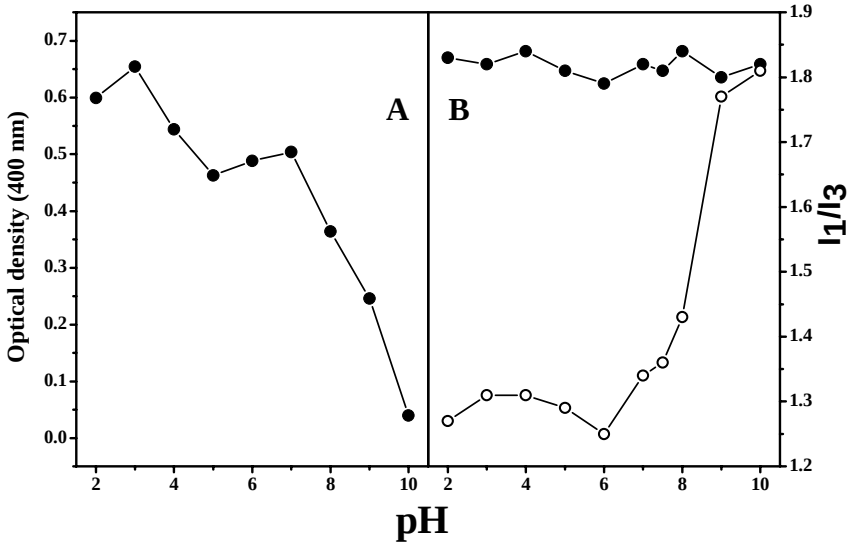

Fig. 6.9: A) Effect of pH on the turbidity of the aggregates formed by near equimolar mixture of OLEA.HCl and SDBS. B) Effect of pH of polarity ratio (I_1/I_3) of pyrene in near equimolar mixture of OLEA.HCl and SDBS (○). Values of I_1/I_3 of pyrene alone in same buffer (●) is also shown.

6.4.12. Disruption of vesicles at high pH

Fig. 6.9A shows the turbidity of near equimolar OLEA.HCl-SDBS mixtures of the same concentration at various pH. It is seen from this figure that turbidity of the sample decreases above pH 7.0 and suggests that the vesicular aggregates are disrupted at high pH. The disruption of the vesicles at high pH was further characterized by fluorescence spectroscopy using pyrene as a fluorescence probe. As mentioned in Chapter 3, pyrene exhibits five bands in the spectrum and the ratio of I_1/I_3 has a good correlation with the polarity of the environment (Kalyansundaram et al., 1977). In aqueous environment the I_1/I_3 value of the probe will be higher than when the probe is located in the hydrophobic environment.

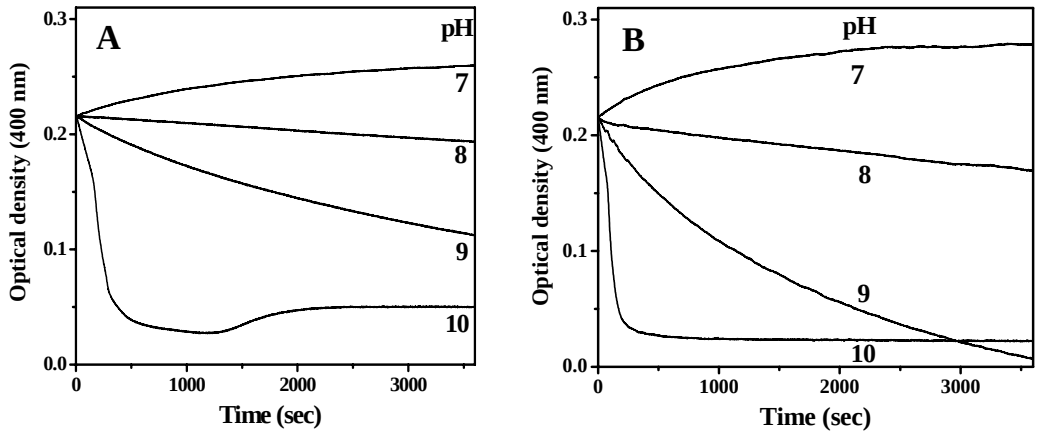

Fig. 6.10. Kinetics of disruption of vesicular aggregate from near equimolar mixtures of OLEA.HCl and SDBS in various pH at A) 25 ºC and B) 37 ºC.

The I_1/I_3 ratio of pyrene in near equimolar aggregates of OLEA.HCl-SDBS dispersed in different buffers is shown in Fig. 6.9B. It is seen from Fig. 6.9B that with increase in pH the I_1/I_3 value increases and at pH 10 the ratio is close to that of pyrene in buffer. This suggests that the vesicular aggregates are disrupted with increase in pH. Now, in order to characterize the kinetics of the vesicle disruption, turbidity of the equimolar mixture of OLEA.HCl-SDBS was monitored at 400 nm with time at various pH. Fig. 6.10A shows that the rate of disruption increases with pH and at physiological temperature (37 ºC) the rate is significantly higher as compared to the rate of disruption at 25 ºC (Fig. 6.10B).

Chapter 7

General Discussion and Conclusions

GENERAL DISCUSSION AND CONCLUSIONS

The work embodied in the thesis has been undertaken with the major objective to characterize several ethanolamine-based lipids such as DAEs, OAEs and OACs in order to understand their biophysical and biological properties. In pursuit of this goal single-crystal X-ray diffraction, DSC, ITC, spin-label ESR, ^{31}P-NMR, Fluorescence, DLS and atomic force microscopic studies have been carried out. The results obtained in these studies, reported in the preceding Chapters (2 through 6) clearly show that the objectives have been fulfilled to a large extent. The results obtained are discussed below.

A homologous series of *N*-, *O*-diacylethanolamines, which are biologically relevant lipids, have been synthesized and their thermotropic phase transitions have been characterized by differential scanning calorimetry. A linear dependence has been observed in the thermodynamic parameters, ΔH_t and ΔS_t associated with the chain-melting phase transitions. The structures of *N*-, *O*-diacylethanolamines with mixed acyl chains have been solved in two different polymorphic forms by single crystal X-ray diffraction. In polymorph α the chain packing is mixed, whereas in the β form chain packing is symmetric. It is proposed that similar kind of polymorphism may be present in other 'L' shaped lipids such as 1,3-diacylglycerols, ceramides, diacylethanolamines with matched chains, where polymorphism has been detected (or predicted) from spectroscopic and calorimetric studies but 3-dimentional structure at the atomic resolution have not been solved. The results also reveal that at least two polymorphic forms should exist in those lipids which adopt an L-shaped structure in the solid state. Comparison of the structure and packing of DAEs containing *N*-palmitoyl chains and even *O*-acyl chains with DAEs containing *N*-palmitoyl chains and odd *O*-acyl chains reveals

that the acyl chains of DAEs with both even chains are more closely packed as compared to the DAEs with one even and one odd acyl chains, which could be correlated to the odd-even alternation in the thermodynamic properties. In future, it will be interesting to synthesize DAEs with *N*-palmitoyl chains with longer *O*-acyl chains (*n*=17-20) and to characterize their thermotropic phase transition. Also, detection and characterization of α and β type polymorphic forms throughout the series will strengthen the proposal "atleast two polymorphic forms should be present in an L-shaped lipids".

In the studies reported in Chapter 3, a homologous series of OAEs with different counterions have been synthesized and crystal structures of several of them with various counterions have been solved. The result suggests that counterions can modulate the acyl chain packing; chloride, bromide and iodide were found to induce tilting in acyl chain to increasing levels, whereas the more bulky trifluoroacetate induces interdigitation in acyl chain packing. Biophysical investigations on the phase behavior of *O*-stearoylethanolamine dispersed in water and in 150 mM NaCl, indicate that in the absence of salt the lipid undergoes a lamellar gel to micellar phase transition, whereas in presence of salt it undergoes a lamellar gel to liquid-crystalline phase transition. The stabilization of bilayer structure of single tailed membrane components even at high temperature in presence of physiological salt concentration will be useful to understand the role of ionic strength on the membrane structure under stress, for example, at high temperatures in extremophiles. Small angle X-ray scattering experiments with hydrated OAEs of different fatty acyl chainlength will be an interesting future study to investigate the phase behavior of OAEs in more detail. Also the miscibility and interaction of OAEs including those with unsaturation in

the acyl chain with major membrane phospholipids (PCs and PEs) could be investigated.

In the work presented in Chapter 4, thermotropic phase transitions of a homologous series *O*-acylcholines, which are biologically relevant lipids, have been characterized by differential scanning calorimetry. A linear dependence has been observed in the thermodynamic parameters, ΔH_t and ΔS_t associated with the chain-melting phase transitions. The structures of two polymorphic forms (α and β form) of OACs have been solved by single crystal X-ray diffraction. The molecules in β form adopt an interdigitated bilayer-type arrangement with head-to-tail packing, whereas the molecules in the α form were found to be packed in a tilted bilayer format. The results from the studies in aqueous dispersion establish that OACs in chloride salt environment probably have lower Krafft temperature and they will be in native form near body temperature, whereas in iodide environment it exists as denatured state. This fact will have an important consequence that nature designs chloride salt in the physiological fluid (KCl, NaCl), which may help to keep the lipids and surfactants in their native form at physiological temperature. In this context it is also noteworthy to mention that the denaturation of OACs and other cationic lipids (cetyltrimethylammonium halide, *N*-alkylpyridinium halide) also follows the famous Hofmeister series, where iodide acts as a chaotropic agent. As the present result speculates the OACs with chloride counterion have lower Krafft temperature, it will be interesting to test the hypothesis and to investigate the phase behavior of OACs with chloride counterion.

In the work presented in Chapter 5 it has been shown *O*-stearoylethanolamine, a structural isomer of *N*-acylethanolamines, which are being studied for putative stress fighting role, forms bilayer structure at 1:1 mixture with

lysophosphatidylcholine. The equimolar mixture of lysophosphatidylcholine and *O*-stearoylethanolamine undergoes a phase transition at 52.4 ºC from bilayer to micellar structure as evidenced by differential scanning calorimetry, ^{31}P-NMR spectroscopy and turbidimetric studies. These results suggest that *O*-stearoylethanolamine can buffer the membranolytic effect of lysophosphatidylcholine. In future, the construction of a temperature-composition binary phase diagram of OSEA, LPC mixture will provide deeper insights into the mixed lipid system. The interaction of OAEs containing other fatty acyl chains, including unsaturated chains with LPC can also be investigated in order to generalize the role of OAEs on membrane stabilization.

The aim of the studies presented in Chapter 6 was to design a base-triggerable catanionic mixed lipid system and to determine the structure of a mixed lipid system. In this direction the interaction between OLEA.HCl and SDS has been characterized by ITC and turbidimetry, which indicate the formation of an equimolar complex between the two lipids. Disruption of aggregates formed by near equimolar mixtures of OLEA.HCl and SDS and OLEA.HCl and SDBS at high pH suggests that the present study can serve as a springboard for the design of novel base-triggerable systems for practical applications. The first crystal structure of a mixed lipid system has been solved by single crystal X-ray diffraction. The packing and intermolecular interaction between two lipids are expected to be relevant in understanding the specific interaction among the lipids in more complex system, e.g. in biomembranes.

References

REFERENCES

Abrahamsson, S., Dahlén, B., Löfgren, H. and Pascher, I. 1978. Lateral packing of hydrocarbon chains. *Progr. Chem. Fats Lipids* **16**: 125-143.

Ahlström, B., Chelminska-Bertilsson, M., Thompson, R.A. and Edebo. L. 1995. Long-chain alkanoylcholines, a new category of soft antimicrobial agents that are enzymatically degradable. *Antimicrob. Agents Chemother*. **39**: 50–55.

Akoka, S., Tellier, C., LeRoux, C. and Marion, D. 1988. A phosphorus magnetic resonance and a differential scanning calorimetry study of the physical properties of *N*-acylphosphatidylethanolamines in aqueous dispersions. *Chem. Phys. Lipids* **46**: 43-50.

Alves F.R., Zaniquelli, M.E.D., Loh, W., Castanheira, E.M.S., Real Oliveira, M.E.C.D. and Feitosa, E. 2007. Vesicle-micelle transition in aqueous mixtures of the cationic dioctadecyldimethylammonium and octadecyltrimethylammonium bromide surfactants. *J. Colloid Interface Sci.* **316**:132-139.

Ambrosini, A., Bertoli, E., Mariani, P., Tanfani, E., Wozniak, M. and Zolese. G. 1993. *N*-Acylethanolamines as membrane topological stress compromising agents. *Biochem. biophys. Acta* **1148**: 351-355.

Anderson, R.G. and Jacobson, K. 2002. A role for lipid shells in targeting proteins to caveolae, rafts, and other lipid domains. *Science* **296**:1821–1825.

Anacker, E.W. and Ghose, H.M. 1963. Counterions and micelle size. I. light scattering by solutions of dodecyltrimethylammonium salts. *J. Phys. Chem.* **67**:1713-1716.

Anacker, E.W. and Ghose, H.M. 1968. Counterions and micelle size. II. light scattering by solutions of cetylpyridinium salts. *J. Am. Chem. Soc*. **90**: 3161-3166.

Aroti, A., Leontidis, E., Maltseva, E. and Brezesinski, G. 2004. Effects of hofmeister anions on DPPC langmuir monolayers at the air-water interface. *J. Phys. Chem. B* **108**: 15238-15245.

Aroti, A., Leontidis, E., Dubois, M. and Zemb, T. 2007. Effects of monovalent anions of the hofmeister series on DPPC lipid bilayers part I: swelling and in-plane equations of state. *Biophys. J.* **93**: 1580–1590.

Arutyunova, L. B. 1961. Polymorphism in the higher normal fatty acids: Differential thermal analysis and infrared absorption spectra. *J. Struct. Chem.* **1**: 134-137.

Baur, F.J., Jackson, F.L., Kolp, D.G. and Lutto, E.S. 1949. The polymorphism of saturated 1,3-diglycerides. *J. Am. Chem. Soc*. **71**: 3363-3366.

Batchelor, J.D., Olteanu, A., Tripathy, A., and Pielak, G.J. 2004. Impact of protein denaturants and stabilizers on water structure. *J. Am. Chem. Soc*. **126**: 1958-1961.

Benatti, C.R., Feitosa, E., Fernandez, R.M. and Lamy-Freund, M.T. 2001. Structural and thermal characterization of dioctadecyldimethylammonium bromide dispersions by spin labels. *Chem. Phys. Lipids* **111**:93-104.

Bierbaum, T.J., Bouma, S.R. and Huestis, W.H. 1979. A mechanism of erythrocyte lysis by lysophosphatidylcholine. *Biochim. Biophys. Acta* **555**: 102–110.

Bijma, K., Engberts, J.B.F.N., Blandamer, M.J., Cullis, P.M., Last, P.M., Irlam, K.D. and Soldi, L.G. 1997. Classification of calorimetric titration plots for alkyltrimethylammonium and alkylpyridinium cationic surfactants in aqueous solutions. *J. Chem. Soc., Faraday Trans*. **93**: 1579-1584.

Böckmann, R.A., Hac, A., Heimburg, T. and Grubmüller, H. 2003. Effect of sodium chloride on a lipid bilayer. *Biophys. J.* **85**:1647-55.

Boese, R., Weiss, H.-C., Bläser, D. 1999. The melting point alternation in the short-chain *n*-alkanes: single-crystal X-ray analyses of propane at 30 K and of *n*-butane to *n*-nonane at 90 K. *Angew. Chem. Int. Ed.* **38**: 988-992.

Boomer, J. A., and Thompson. D. H. 1999. Synthesis of acid-labile diplasmenyl lipids for drug and gene delivery applications. *Chem. Phys. Lipids.* 99:145-153.

Boström, M., Williams, D.R.M. and Ninham, B.W. 2001. Specific ion effects: why DLVO theory fails for biology and colloid systems. *Phys. Rev. Lett.* **87**:168103.

Cacace, M.G., Landau, E.M. and Ramsden, J.J. 1997. The Hofmeister series: salt and solvent effects on interfacial phenomena. *Q. Rev. Biophys.* **30**:241–277.

Cantley, L.C. 2002. The phosphoinositide-3-kinase pathway. Science **296**:1655–1657.

Chanturiya, A.F., Chernomordik, L.V. and Zimmerberg, J. 1997. Flickering fusion pores comparable with initial exocytotic pores occur in protein-free phospholipid bilayers. *Proc. Natl. Acad. Sci. USA* **94**:14423–14428.

Cho, K. S. and Proulx. P. 1969. Lysis of erythrocytes by long-chain acyl esters of carnitine. *Biochim. Biophys. Acta* **193**: 30-35.

Cho, K. S. and Proulx. P. 1971. Studies on the mechanism of hemolysis by acyl carnitines, lysolecithins and acyl cholines. *Biochim. Biophys. Acta* **225**: 214-223.

Chapman, D. 1962. The Polymorphism of glycerides. *Chem. Rev*. **62**: 433-456.

Chapman, D. 1993. In Biomembranes Physical aspects (Shinitzky, M., Ed.) VCH Publishers Inc., New York. pp. 29-62.

Chapman, K.D., Tripathy, S., Venables, B. and Desouja, A.D. 1998. *N*-Acylethanolamines: Formation and molecular composition of a new class of plant lipids. *Plant Physiol.* **116**: 1163-1168.

Chapman, K.D. 2000. Emerging physiological roles for *N*-acylphosphatidylethanolamine metabolism in plants: signal transduction and membrane protection. *Chem. Phys. Lipids* **108**: 203-213.

Chapman, K.D. 2004. Occurrence, metabolism, and prospective functions of *N*-acylethanolamines in plants. *Prog. Lipid Res.* **43**: 302-327.

Chernomordik, L. 1996. Non-bilayer lipids and biological fusion intermediates. *Chem. Phys. Lipids* **81**: 221-230.

Clarke, R.J. and Lüpfert, C. 1999. Influence of anions and cations on the dipole potential of phosphatidylcholine vesicles: A basis for the hofmeister effect. *Biophys. J.* **76**: 2614–2624.

Collins, K.D., and Washabaugh, M.W. 1985. The Hofmeister effect and the behaviour of water at interfaces. *Q. Rev. Biophys*. **18**: 323–422.

Cullis, P.R. and De Kruijff, B. 1978. Polymorphic phase behaviour of lipid mixtures as detected by ^{31}P NMR. Evidence that cholesterol may destabilize bilayer structure in membrane systems containing phosphatidylethanolamines. *Biochim Biophys Acta* **507**: 207-218.

Cunningham, B. A., and L. J. Lis. 1986. Thiocyanate and bromide ions influence the bilayer structural parameters of phosphatidylcholines bilayers. *Biochim. Biophys. Acta* **861**: 237–242.

Dahlén, B. and Pascher, I. 1972. Molecular arrangements in sphingolipids. Crystal structure of *N*-tetracosanoylphytosphingosine. *Acta Cryst.* **B28**: 2396-2404.

Dahlén, B., Pascher, I. and Sundell, S. 1977. The crystal structure of *N*-(2-hydroxyethyl)-octadecanoate. *Acta. Chem. Scand.* **A31**: 313-320.

Davey, T.W., Ducker, W.A., Hayman, A.R. and Simpson, J. 1998. Krafft temperature depression in quaternary ammonium bromide surfactants. *Langmuir*. **14**: 3210-3213.

Davidsen, J., Jorgensen, K., Andresen, T.L. and Mouritsen, O.G. 2003. Secreted phospholipase A_2 as a new enzymatic trigger mechanism for localised liposomal drug release and absorption in diseased tissue. *Biochim. Biophys. Acta* **1609**: 95–101.

Davis, B. and Jordan. P. In: Karsa D. R. Industrial Applications of Surfactants, vol. II. Cambridge: Royal Society of Chemistry; 1990. p. 195–216.

De Oliveira Filgueiras, O.M., Van Den Besselaar, A.M.H.P. and Van Den Bosch, H. 1979. Localization of lysophosphatidylcholine in bovine chromaffin granules. Biochim. Biophys. Acta **558**: 73-84.

Devane, W.A., Hanus, L., Breuer, A., Pertwee, R.G., Stevensen, L.A., Griffin, G., Gibson, D., Mandelbaum, A., Etinger, A. and Mechoulam, R. 1992. Isolation and structure of a brain constituent that binds to the cannabinoid receptor. *Science* **258**: 1946-1949.

Dew, M.J., Hughes, P.J., Lee, M.G., Evans, B.K. and Rhodes, J. 1982. An oral preparation to release drugs in the human colon. *Br. J. Clin. Pharmacol.* **14**: 405–408.

Di, L. and Small, D. M. 1993. Physical behavior of the mixed chain diacylglycerol, 1-stearoyl-2-oleoyl-sn-glycerol: difficulties in chain packing produced marked polymorphism. *J. Lipid. Res*. **34**: 1611-1623.

Di, L. and Small, D.M. 1995. Physical behavior of the hydrophobic core of membranes: properties of 1-stearoyl-2-linoleoyl-*sn*-glycerol. *Biochemistry*. **34:** 16672-16677.

Domingo, J., Mora, M. and De Madariaga, M.A. 1993. Incorporation of *N*-acylethanolamine phospholipids into egg phosphatidylcholine vesicles: characterization and permeability properties of the binary systems. *Biochim. Biophys. Acta* **1148**: 308-316.

Drummond, D.C., Meyer, O., Hong, K., Kirpotin, D.B. and Papahadjopoulos, D. 1999. Optimizing liposomes for delivery of chemotherapeutic agents to solid tumors. *Pharmacol. Rev*. **51**: 691-743.

Dubois, M., Demé, B., Gulik-Krzywicki, T., Dedieu, J.-C., Vautrin, C., Désert, S., Perez, E. and Zemb, T. 2001. Self-assembly of regular hollow icosahedra in salt-free catanionic solutions. *Nature* **411**: 672-675.

Ermer, O. and Eling, A. 1994. Molecular recognition among alcohols and amines: super-tetrahedral crystal architectures of linear diphenol–diamine complexes and aminophenols. *J. Chem. Soc. Perkin Trans.* 2. 925-944.

Epand, R. M. and Bryszewska, M. 1988. Modulation of the bilayer to hexagonal phase transition and solvation of phosphatidylethanolamines in aqueous salt solutions. *Biochemistry* **27**: 8776–8779.

Epps, D.E., Schmid, P.C., Natarajan, V. and Schmid, H.H.O. 1979. *N*-acylethanolamine accumulation in infarcted myocardium. *Biochem. Biophys. Res. Commun.* **90:**628-633.

Epps, D.E., Natarajan, V., Schmid, P.C. and Schmid, H.H.O. 1980. Accumulation of N-acylethanolamine glycerophospholipids in infarcted myocardium. *Biochim. Biophys. Acta* **618**: 420-430.

Evans, D.F., Pye, G., Bramley, R., Clark, A.G., Dyson, T.J. and Hardcastle, J.D. 1988. Measurement of gastrointestinal pH profiles in normal ambulant human subjects. *Gut* **29**: 1035–1041.

Facci, L., Dal Toso, R., Romanello, S., Buriani, A., Skaper, S.D. and Leon, A. 1995. Mast cells express a peripheral cannabinoid receptor with differential sensitivity to anandamide and palmitoylethanolamide. *Proc. Natl. Acad. Sci. USA* **92**: 3376-3380.

Fahy, E., Subramaniam, S., Brown, H.A., Glass, C.K., Merrill, A.H., Murphy, Jr., R. C., Raetz, C.R.H., Russell, D.W., Seyama, Y., Shaw, W., Shimizu, T., Spener, F., van Meer, G., VanNieuwenhze, M.S., White, S.H., Witztum, J.L. and Dennis, E.A. 2005. A comprehensive classification system for lipids. *J. Lipid Res.* **46**: 839-861.

Farooqui, A.A., Ong, W.Y. and Horrocks, L.A. 2004. Neuroprotection abilities of cytosolic phospholipase A_2 inhibitors in kainic acid-induced neurodegeneration. *Curr Drug Targets Cardiovasc Haematol Disord* **4**: 85–96.

Farooqui, A.A., Ong, W-Y. and Horrocks, L.A. 2006. Inhibitors of brain phospholipase A_2 activity: their neuropharmacological effects and therapeutic importance for the treatment of neurologic disorders. *Pharmacol Rev*. **58**: 591–620.

Feitosa, E., Bonassi, N.M. and Loh, W. 2006. Vesicle-micelle transition in mixtures of dioctadecyldimethylammonium chloride and bromide with nonionic and zwitterionic surfactants. *Langmuir* **22**: 4512-4517.

Fink, K.L. and Gross, R.W. 1984. Modulation of canine myocardial sarcolemmal membrane fluidity by amphiphilic compounds. *Circ. Res*. **55**: 585-594.

Frías, M.A., Nicastro, A., Casado, N., Gennaro, A.M., Díaz, S.B. and Disalvo, E.A. 2007. Arbutin blocks defects in the ripple phase of DMPC bilayers by changing carbonyl organization. *Chem. Phys. Lipids* **147**: 22-29.

Frías, M.A., Winik, B., Franzoni, M.B., Levstein, P.R., Nicastro, A., Gennaro, A.M., Diaz, S.B. and Disalvo, E.A. 2008. Lysophosphatidylcholine–arbutin complexes form bilayer-like structures. *Biochim. Biophys. Acta* **1778**: 1259-1266.

Furutani, T., Ooshima, H. and Kato, J. 1997. Preparation of *N*-, *O*-diacylethanolamine from *N*-acylethanolamine using lipase preparations. *Enzyme Microb. Technol.* **20:** 214-220.

Ganley, O.H., Graessle, O.E. and Robinson, H.J. 1958. Anti-inflammatory activity of compounds obtained from egg yolk, peanut oil, and soybean lecithin. *J. Lab. Clin. Med.* **51**: 709-714.

Garcia-Manyes, S., Oncins, G. and Sanz, F. 2005. Effect of ion-binding and chemical phospholipid structure on the nanomechanics of lipid bilayers studied by force spectroscopy. *Biophys J.* **89**: 1812-26.

Georghiou, S. and Mukhyopadhyay, A.K. 1981. Phase transitions and cholesterol effects in phospholipid liposomes. A new method employing the enhancement of the O-O vibronic transition of pyrene. *Biochim. Biophys. Acta* **645**: 365-368.

Glaser, R. 1982. Echinocyte formation induced by potential changes of human red blood cells. *J. Membrane Biol.* **66**: 79-85.

Goldberg, A. S., Wasylyk, J., Renna, S., Reisman, H. and Nair, A. S. 1982. Isolation and structural elucidation of an ichthyocrinotoxin from the smooth trunkfish (Lactophrys triqueter Linnaeus). *Toxicon*. **20**: 1069-1074.

Goto, M., Honda, K., Di, L. and Small, D.M. 1995. Crystal structure of a mixed chain diacylglycerol, 1-stearoyl-3-oleyl-glycerol. *J. Lipid Res*. **36**: 2185-2190.

Guo, X. and Szoka, Jr. F.C. 2003. Chemical approaches to triggerable lipid vesicles for drug and gene delivery. *Acc. Chem. Res*. **36**: 335-341.

Gurau, M.C., Lim, S-M., Castellana, E.T., Albertorio, F., Kataoka, S. and Cremer, P. S. 2004. On the Mechanism of the Hofmeister Effect. *J. Am. Chem. Soc*. **126**: 10522-10523.

Han, G.W., Ruble, J.R. and Craven, B.M. 1994. The crystal structure of 1,2-dipalmitoyl-sn-glycerol at 123 K. *Chem. Phys. Lipids* **71**: 219-228.

Han, J.H., Cao, C., Kim; S.M., Piao, F.L. and Kim, S.H. 2004. Attenuation of lysophosphatidylcholine-induced suppression of ANP release from hypertrophied atria. *Hypertension* **43**: 243-248.

Han, L., Gao, J-R., Li, Z-M., Zhang Y. and Guo. W-M. 2007. Synthesis of new plant growth regulator: *N*-(Fatty acid) *O*-aryloxyacetyl ethanolamine. *Bioorg. Med. Chem. Lett*. **17:** 3231-3234.

Hansen, H.H., Ikonomidou, C., Bittigau, P. and Hansen, H.S. 2001a. Accumulation of the anadamide precursor and other *N*-acylethanolamine phopholipids in infant rat models of *in vivo* necrotic and apoptotic neural death. *J. Neurochem.* **76**: 39-46.

Hansen, H.H., Schmid, P.C., Bittigau, P., Lastres-Becker, I., Berrendero, F., Manzanares, J., Ikonomidou, C., Schmid, H.H.O., Fernandez-Ruiz, J.J. and Hansen, H.S. 2001b. Anandamide, but not 2-arachidonoylglycerol, accumulates during *in vivo* neurodegeneration. *J. Neurochem.* **78**: 1415-1427.

Hom, R.J. and Malkin, T. 1951. An X-ray and thermal examination of the glycerides. Part XI. The 1:2-diglycerides, and further observations on 1:3-diglycerides. *J. Chem. Soc*. 2663-2667.

Horbaschek, K., Hoffmann, H. and Thunig, C. 1998. Formation and properties of lamellar phases in systems of cationic surfactants and hydroxy-naphthoate. *J. Colloid Interface Sci.* **206**: 439–456.

Howell, J.I. and Lucy, J.A. 1969. Cell fusion induced by lysolecithin. *Febs lett*. **4**: 147-150.

Herrmann, A. and Müller, P. 1986. Ionic strength-dependent alterations of membrane structure of red blood cells. *Biosci. Rep.* **6**: 1007-1015.

Hilgemann, D.W. 2003. Getting ready for the decade of the lipids. *Annu. Rev. Physiol.* **65**: 697–700.

Hoque, A.N.E., Haist, J.V. and Karmazyn, M. 1997. Na^+-H^+ exchange inhibition protects against mechanical, ultrastructural, and biochemical impairment induced by low concentrations of lysophosphatidylcholine in isolated rat hearts. *Circ. Res.* **80**: 95–102.

Huang, C., Mason, J.T., Stephenson, F.A. and Levin, I.W.1986. Polymorphic phase behavior of platelet-activating factor. *Biophys. J.* **49**: 587-595.

Huang, Z., Guo, X., Li, W., MacKay, J.A. and Szoka. Jr. F.C. 2006. Acid-triggered transformation of diortho ester phosphocholine liposome. *J. Am. Chem. Soc.* **128**: 60-61.

Hybl, A., Dorset, D. 1971. The crystal structure of the 1,3-diglyceride of l l-bromoundecanoie acid. Acta Cryst. **B27**: 977-986.

Israelachvili, J.N. 1992. Intermolecular and Surface Forces; Academic Press: New York.

Jain, M.K., Van Echteld, C.J.A., Ramirez, F., De Gier, J., De Haas, G.H. and Van Deenen, L.L.M. 1980. Association of lysophosphatidylcholine with fatty acids in aqueous phase to form bilayers. *Nature* **284**: 486-487.

Jain, M.K. and Haas, G.H. 1981. Structure of 1-acyl lysophosphatidylcholine and fatty acid complex in bilayers. *Biochim. Biophys. Acta* **642**: 203-211.

Jendrasiak, G.L. 1972. Halide interaction with phospholipids: proton magnetic resonance studies. *Chem. Phys. Lipids* **9**: 133–146.

Jinsart, W., Ternai, B. and Polya, G. M. 1991. Inhibition and activation of wheat embryo calcium-dependent protein kinase and inhibition of avian myosin light chain kinase by long chain aliphatic amphiphiles. *Plant Sci.* **78**: 165-75.

Kaler, E.W., Murthy, A.K., Rodriguez, B.E. and Zasadzinski, J.A. 1989. Spontaneous vesicle formation in aqueous mixtures of single-tailed surfactants. *Science* **245**: 1371–1374.

Kalyanasundaram, K. and Thomas, J.K. 1977. Environmental effects on vibronic band intensities in pyrene monomer fluorescence and their application in studies of micellar systems. *J. Am. Chem. Soc.* **99**: 2039-2044.

Kalyvas, A. and David, S. 2004. Cytosolic phospholipase A_2 plays a key role in the pathogenesis of multiple sclerosis-like disease. *Neuron* **41**: 323–335.

Kamlekar, R.K and Swamy, M.J. 2006. Molecular packing and intermolecular interactioms in two structural polymorphs of *N*-palmitoylethanolamine, a Type-2 cannabinoid receptor agonist. *J. Lipid Res.* **47**: 1424-1433.

Kamlekar, R.K and Swamy, M.J. 2006a. Studies on the critical micellar concentration and phase transitions of stearoylcarnitine. *Biosci. Rep*. **26**: 387-398.

Kamlekar, R.K., Satyanarayana, S., Marsh, D. and Swamy, M. J. 2007. Miscibility and phase behavior of *N*-acylethanolamine/diacylphosphatidylethanolamine binary mixtures of matched acyl chainlengths (N=14, 16). *Biophys J*. **92:** 3968-3977.

Kamlekar, R.K., Tarafdar, P.K. and Swamy, M.J. 2009. Synthesis, calorimetric studies and crystal structures of *N*, *O*-diacylethanolamines with matched chains. J. Lipid Res. (Published online, doi:10.1194/jlr.M900105-JLR200)**.**

Karmali, P.P. and Chaudhuri, A. 2007. Cationic liposomes as non-viral carriers of gene medicines: resolved issues, open questions, and future promises. *Med. Res. Rev.* **27**: 696-722.

Kewitz, H. and Pleul. O. 1976. Synthesis of choline from ethanolamine in rat brain. *Proc. Natl Acad. Sci. USA*. **73**: 2181-2185.

Kinnaird, A.A., Choy, P.C. and Man, R.Y. 1988. Lysophosphatidylcholine accumulation in the ischemic canine heart. *Lipids* **23**: 32-35.

Kleinschmidt, J.H. and Marsh, D. 1997. Spin-label electron spin resonance studies on the interactions of lysine peptides with phospholipid membranes. *Biophys. J.* **73**: 2546–2555.

Kleinschmidt, J.H. and Tamm, L.K. 2002. Structural transitions in short-chain lipid assemblies studied by ^{31}P-NMR spectroscopy. *Biophys. J*. **83**: 994–1003.

Knock, M.M. and Bain, C.D. 2000. Effect of counterion on monolayers of hexadecyltrimethylammonium halides at the air−water interface. *Langmuir* **16**: 2857-2865.

Kodali, D. R., Fahey, D.A., and Small, D.M. 1990. Structure and polymorphism of saturated monoacid 1,2-diacyl-sn-glycerols. *Biochemistry* **29**: 10771-10779.

Kunz, W., Henle, J. and Ninham, B.W. 2004. About the science of the effect of salts: Franz Hofmeister's historical papers. *Curr. Opin. Colloid Int. Sci*. **9**: 19–37.

LaFrance, D., Marion, D. and Pézolet, M. 1990. Study of the structure of *N*-acyldipalmitoylphosphatidylethanolamines in aqueous dispersion by infrared and Raman spectroscopies. *Biochemistry* **29**: 4592-4599.

Lam, K.L.H., Ishitsuka, Y., Cheng, Y., Chien, K., Waring, A.J., Lehrer, R.I. and Lee, K.Y.C. 2006. Mechanism of Supported Membrane Disruption by Antimicrobial Peptide Protegrin-1. *J. Phys. Chem. B* **110**: 21282-21286.

Larsson, K. 1963. The crystal structure of the 1,3-diglyceride of 3-thiadodecanoic Acid. *Acta Cryst.* **16**: 741-748.

Larsson, K. 1986. Physical properties—structural and physical characteristics. *In* The lipid Handbook (Gunstone, F. D., Harwood, J. L. and Padley, F. B., Eds.), Chapman and Hall, London, pp. 321-384.

Lehninger, A.L., Nelson, D.L. and Cox, M.M. 1993. Principles of Biochemistry, CBS Publishers & Distributors, Delhi, 1013pp.

Leontidis, E. 2002. Hofmeister anion effects on surfactant self-assembly and the formation of mesoporous solids. *Curr. Opin. Colloid Int. Sci*. **7**: 81-91.

Leontidis, E., and Aroti, A. 2009. Liquid expanded monolayers of lipids as model systems to understand the anionic hofmeister series: 1. a tale of models. *J. Phys. Chem. B* **113**: 1447–1459.

Lewis, R.N.A.H., Mak, N. and McElhaney, R.N. 1987. A differential scanning calorimetric study of the thermotropic phase behavior of model membranes composed of phosphatidylcholines containing linear saturated fatty acyl chains. *Biochemistry* **26**: 6118-6126.

Li, X-M., Ramakrishnan, M., Brockman, H.L., Brown, R.E. and Swamy, M.J. 2002. *N*-Myristoylated phosphatidylethanolamine: Interfacial behavior and interaction with cholesterol. *Langmuir* **18**: 231-238.

Loftsson, T., Somogyi, G. and Bodor, N. 1989. Effect of choline esters and oleic acid on the penetration of acyclovir, estradiol, hydrocortisone, nitroglycerin, retinoic acid and trifluorothymidine across hairless mouse skin in vitro. *Acta Pharm. Nordica*. **1**: 279-86.

Loshchilova, E., and Karvaly, B. 1978. Laser Raman studies of molecular interactions with phosphatidylcholine multilayers. II. Effects of mono- and divalent ions on bilayer structure. *Biochim. Biophys. Acta* **514**: 274–285.

Lutton, E.S. and Fehl, A.J., 1970. The polymorphism of odd and even saturated single acid triglycerides, C_8-C_{22}. *Lipids* **5**: 90-99.

Macdonald, P.M., and Seelig, J. 1988. Anion binding to neutral and positively charged lipid membranes. *Biochemistry* **27**: 6769-75.

Malkin, T., Shurbagy, M.R.E. and Meara, M.L. 1937. An X-ray and thermal examination of the glycerides. Part III. The αα'-diglycerides. *J. Chem. Soc*. 1409-1413.

Mantsch, H.H. and McElhaney, R.N. 1991. Phospholipids phase transitions in model and biological membranes as studied by infrared spectroscopy. *Chem. Phys. Lipids* **57**: 213–226.

Markey, S.P., Dudding, T. and Wang, T.L. 2000. Base- and acid-catalyzed interconversions of *O*-acyl and *N*-acyl-ethanolamines: a cautionary note for lipid analyses. *J. Lipid Res.* 41:657-662.

Markin, V.S. and Albanesi, J.P. 2002. Membrane fusion: stalk model revisited. *Biophys. J.* **82**: 693–712.

Marsh, D. 1980. Molecular motion in phospholipids bilayers in the gel phaae: long axis rotation. *Biochemistry* **19:**1632-1637.

Marsh, D. 1982. Biomembranes. *In* Supramolecular Structure and Function. G. Pifat, and J. N. Herak, editors. Plenum Press, New York. 127-178.

Marsh, D. 1990. Handbook of Lipid Bilayers. CRC Press, Boca Raton, Florida, 387pp.

Marsh, D. 1991. Analysis of the chainlength dependence of lipid phase transition temperatures: Main and pretransitions of phosphatidylcholines; main and non-lamellar transitions of phosphatidylethanolamines. *Biochim. Biophys. Acta* **1062:** 1-6.

Marsh, D. 1991a. General features of phospholipid phase transitions. *Chem. Phys. Lipids* **57**: 109-120.

Marsh, D. and Swamy, M.J. 2000. Derivatised lipids in membranes. Physico-chemical aspects of *N*-biotinyl phosphatidylethanolamines, *N*-acylphosphatidylethanolamines and *N*-acylethanolamines. *Chem. Phys. Lipids* **105**: 43-69.

Maurer, N., Elmar, P., Fritz, P. and Otto, G. 1994. Phase behavior of the antineoplastic ether lipid 1-*O*-octadecyl-2-*O*-methylglycero-3-phosphocholine. *Biochim. Biophy.Acta* **1192**: 167-176.

Mayer, R.J. and Marshall, L.A. 1993. New insights on mammalian phospholipase A_2(s); Comparison of arachidonoyl-selective and -nonselective enzymes. *FASEB J*. **7**: 339-348.

McConnell, E.L., Short, M.D. and Basit, A.W. 2008. An *in vivo* comparison of intestinal pH and bacteria as physiological trigger mechanisms for colonic targeting in man. *J. Control. Release* **130**: 154-160.

Meers, P. 2001. Enzyme-activated targeting of liposomes. *Adv. Drug Delivery Rev*. **53**: 265–272.

Mercadal, M., Domingo, J.C., Bermudez, M., Mora, M. and De Madariaga, M.A. 1995. *N*-Palmitoylphosphatidylethanolamine stabilizes liposomes in the presence of human serum: effect of lipidic composition and system characterization. *Biochim. Biophys. Acta* **1235**: 281-288.

Moesgaard, B., Jaroszweski, J.W. and Hansen, H.S. 1999. Accumulation of *N*-acylethanolamine phospholipid in rat brains during post-decapitative ischemia: a ^{31}P NMR study. *J. Lipid Res.* **40**: 515-521.

Moreno, E., Cordobilla, R., Calvet, T., Cuevas-Diarte, M. A., Gbabode, G., Negrier, P., Mondieig, D., Oonk and H. A. J. 2007. Polymorphism of even saturated carboxylic acids from n-decanoic to n-eicosanoic acid. *New. J. Chem*. **31**: 947-957.

Maulik, P.R., Ruocco, M.J. and Shipley, G.G. 1990. Hydrocarbon chain packing modes in lipids: effect of altered sub-cell dimensions and chain rotation. *Chem. Phys. Lipids* **56**: 123-133.

Mouritsen, O.G. 2005. Life-as a Matter of Fat. The Emerging Science of Lipidomics. Springer-Verlag, Berlin.

Mulder, A. M. and Cravatt. B.F. 2006. Endocannabinoid metabolism in the absence of fatty acid amide hydrolase (FAAH): Discovery of phosphorylcholine derivatives of *N*-acyl ethanolamines. *Biochemistry* **45:** 11267-11277.

Murphy, R. F., Powers, S. and Cantor. C. R. 1984. Endosome pH measured in single cells by dual fluorescence flow cytometry: rapid acidification of insulin to pH 6. *J. Cell Biol.* **98:** 1757-1762.

Natarajan, V., Schmid, P.C. and Schmid, H.H.O. 1986. *N*-Acylethanolamine phospholipid metabolism in normal and ischemic rat brain. *Biochim. Biophys. Acta* **878**: 32-41.

Needham, D. and Dewhirst, M.W. 2001. The development and testing of a new temperature-sensitive drug delivery system for the treatment of solid tumors. *Adv. Drug Del. Rev*. **53**: 285-305.

Nguyen, D. and Bertrand, G.L. 1992. Calorimetric observations of the sphere-rod transition of tetradecyltrimethylammonium bromide and sodium dodecyl sulfate: Effects of electrolytes and non-electrolytes at 25 and 45 ºC. *J. Colloid Int. Sci*. **150**: 143-157.

Ninham, B.W., and Yaminsky, V. 1997. Ion binding and ion specificity: the Hofmeister effect and Onsager and Lifshitz theories. *Langmuir*. **13**: 2097–2108.

Ohta, A., Nakashima, S., Matsuyanagi, H., Asakawa, T. and Miyagishi, S. 2003. Krafft temperature and enthalpy of solution of *N*-acyl amino acid surfactants and their racemic modifications: effect of the counter ion. *Colloid Polym. Sci.* **282**:162-169.

Omta, A.W., Kropman, M.F., Woutersen, S. and Bakker, H.J. 2003. Negligible effect of ions on the hydrogen-bond structure in liquid water. *Science*. **301**: 347-349.

Ong, W., Yang, Y., Cruciano, A.C. and McCarley, R.L. 2008. Redox-triggered contents release from liposomes. *J. Am. Chem. Soc.* **130**: 14739-14744.

Otani, H., Prasad, M.R., Jones, R.M. and Das, D.K. 1989. Mechanism of membrane phospholipid degradation in ischemic-reperfused rat hearts. *Am J Physiol.* **257**: H252–H258.

Pabst, G., Hodzic, A., Strancar, J., Danner, S., Rappolt, M. and Laggner, P. 2007 Rigidification of neutral lipid bilayers in the presence of salts. *Biophys. J.* **93**:2688-2696.

Pascher, I. and Sundell, S. 1981. Glycerol conformation and molecular packing of membrane lipids. The crystal structure of 2,3-dilauroyl-D-glycerol. *J. Mol. Biol.* **153**: 791-806.

Pascher, I., Sundell, S. and Hauser, H. 1981. Polar group interaction and molecular packing of membrane lipids. The crystal structure of lysophosphatidylethanolamine. *J. Mol. Biol.* **153**: 807-824.

Pascher, I. and Sundell, S. 1985. Interactions and space requirements of the phosphate head group in membrane lipids. The crystal structure of disodium lysophosphatidate dihydrate. *Chem. Phys. Lipids* **37**: 241-250.

Pascher, I., Lundmark, M., Nyholm, P.G. and Sundell, S. 1992. Crystal structures of membrane lipids. *Biochim. Biophys. Acta* **1113**: 339-373.

Perche, T., Auvray, X., Petipas, C. and Anthore, R. 1996. Micellization of *N*-alkylpyridinium halides in formamide tensiometric and small angle neutron scattering Study. *Langmuir* **12**: 863-871.

Pérez-Gil, J., Casals, C. and Marsh, D. 1995. Interactions of hydrophobic lung surfactant proteins SP-B and SP-C with dipalmitoylphosphatidylcholine and dipalmitoylphosphatidylglycerol bilayers studied by electron spin resonance spectroscopy. *Biochemistry* **34**:3964-3971.

Petrache, H.I., Tristram-Nagle, S., Harries, D., Kucerka, N., Nagle, J.F. and Parsegian, V.A. 2006. Swelling of phospholipids by monovalent salt. *J. Lipid Res.* **47**:302-309.

Phillis, J.W. and O'Regan, M.H. 2004. A potentially critical role of phospholipases in central nervous system ischemic, traumatic, and neurodegenerative disorders. *Brain Res Rev*. **44**:13–47.

Porter, A.C., Sauer, J-M., Knierman, M.D., Becker, G.W., Berna, M.J., Bao, J., Nomikos, G.G., Carter, P., Bymaster, F.P., Leese, A.B. and Felder, C.C. 2002. Characterization of a novel endocannabinoid, virodhamine, with antagonist activity at the CB1 receptor. *J. Pharmacol. Exp. Ther.* **301**: 1020-1024.

Rama Krishna, Y.V.S. and Marsh, D. 1990. Spin label ESR and ^{31}P-NMR studies of the cubic and inverted hexagonal phases of dimyristoylphosphatidylcholine/myristic acid (1:2, mol/mol) mixtures. *Biochim. Biophys. Acta* **1024**: 89-94.

Ramakrishnan, M., Sheeba, V., Komath, S.S. and Swamy, M.J. 1997. Differential scanning calorimetric studies on the thermotropic phase transitions of dry and hydrated forms of *N*-acylethanolamines of even chainlengths. *Biochim. Biophys. Acta* **1329**: 302-310.

Ramakrishnan, M. and Swamy, M.J. 1998. Differential scanning calorimetric studies on the thermotropic phase transitions of *N*-acylethanolamines of odd chainlengths. *Chem. Phys. Lipids* **94**: 43-51.

Ramakrishnan, M. and Swamy, M.J. 1999. Molecular packing and intermolecular interactions in *N*-acylethanolamines: crystal structure of *N*-myristoylethanolamine. *Biochim. Biophys. Acta* **1418**: 261-267.

Ramakrishnan, M., Kenoth, R., Kamlekar, R.K., Chandra, M.S., Radhakrishnan, T.P. and Swamy, M.J. 2002. *N*-Myristoylethanolamine -Cholesterol (1:1) complex: First evidence from differential scanning calorimetry, fast-atom-bombardment mass spectrometry and computational modelling. *FEBS Lett.* **531**: 343-347.

Ramakrishnan, M., Tarafdar, P.K., Kamlekar, R.K. and Swamy, M.J. 2007. Differential scanning calorimetric studies on the interaction of *N*-acylethanolamines with cholesterol. *Curr. Sci.* **93**: 234-238.

Ramsammy L.S. and Brockerhoff, H. 1982. Lysophosphatidylcholine-cholesterol complex. *J. Biol. Chem*. **257**: 3570-3574.

Raudenkolb, S., Hübner, W., Rettig, W., Wartewig, S. and Neubert, R.H.H. 2003. Polymorphism of ceramide 3. Part 1: an investigation focused on the head group of *N*-octadecanoylphytosphingosine. *Chem. Phys. Lipids* **123**: 9-17.

Raudenkolb, S., Wartewig, S. and Neubert, R.H.H. 2005. Polymorphism of ceramide 6: a vibrational spectroscopic and X-ray powder diffraction investigation of the diastereomers of *N*-(α-hydroxyoctadecanoyl)-phytosphingosine. *Chem. Phys. Lipids* **133**: 89-102.

Rodriguez, C.H., Lowery, L.H., Scamehorn, J. F. and Harwell, J. H. 2001. Kinetics of precipitation of surfactants. I. Anionic surfactants with calcium and with cationic surfactants. *JSD* **4**: 1-14.

Roiter, Y., Ornatska, M., Rammohan, A.R., Balakrishnan, J., Heine, D.R. and Minko, S. 2009. Interaction of Lipid Membrane with Nanostructured Surfaces. *Langmuir* **25**: 6287-6299.

Rosen, M. J. Surfactants and interfacial phenomenon. third ed. New York: John Wiley; 2004.

Ronsin, G., Perrin, C., Guedat, P., Kremer, A., Camilleri, P. and Kirby, A. J. 2001. Novel spermine-based cationic gemini surfactants for gene delivery. *Chem Comm*. **21**: 2234-2235.

Rybak, S.L., and Murphy. R.F. 1998. Primary cell cultures from murine kidney and heart differ in endosomal pH. *J. Cell Physiol.* **176**: 216-22.

Rydall, J.R. and Macdonald, P.M. 1992. Investigation of anion binding to neutral lipid membranes using ^{2}H NMR. *Biochemistry* **31**: 1092-1099.

Sachs, J.N. and Woolf, T.B. 2003. Understanding the hofmeister effect in interactions between chaotropic anions and lipid bilayers: molecular dynamics simulations. *J. Am. Chem. Soc.* **125**: 8742-8743.

Sanderson, P.W., Lis, L.J., Quinn, P.J. and Williams, W.P. 1991. The Hofmeister effect in relation to membrane lipid phase stability. *Biochim. Biophys. Acta* **1067**: 43–50.

Sankaram, M. and Thompson, T.E. 1990. Interaction of cholesterol with various glycerophospholipids and sphingomyelin. *Biochemistry* **29**: 10670-10675.

Sapia, P., Coppola, L., Ranieri, G. and Sportelli, L. 1994. Effects of high electrolyte concentration on DPPC-multilayers: an ESR and DSC investigation. *Colloid Polym. Sci.* **272**: 1289-1294.

Sato, T., Arita, M. and Kiyosue, T. 1993. Differential mechanism of block of palmitoyl lysophosphatidylcholine and palmitoyl carnitine on inward rectifier K^+ channels of guinea-pig ventricular myocytes. *Cardiovasc Drugs Ther*. **7**: 575–584.

Sedlis, S.P., Hom, M., Sequeira, J.M. and Esposito, R. 1993. Lysophosphatidylcholine accumulation in ischemic human myocardium. *J Lab Clin Med.* **121**: 111–117.

Sheldrick, G. M., 1997. SHELXL97. Program for the refinement of crystal structures. University of Göttingen, Göttingen, Germany.

Scheul, H., Goldstein, E., Mechoulam, R., Zimmerman, A.M. and Zimmerman. S. 1994. Anandamide (arachidonylethanolamide), a brain cannabinoid receptor agonist, reduces sperm fertilizing capacity in sea urchins by inhibiting the acrosome reaction. *Proc. Natl. Acad. Sci. USA* **91**: 7678-7682.

Schmid, H.H.O., Schmid, P.C., and Natarajan, V. 1990. *N*-acylated glycerophospholipids and their derivatives. *Prog. Lipid Res.* **29**: 1-43.

Schmid, H.H.O., Schmid, P.C. and Natarajan, V. 1996. The *N*-acylation-phosphodiesterase pathway and signalling. *Chem. Phys. Lipids* **80**:133-42.

Schmid, H.H.O., Schmid, P.C. and Berdyshev, E.V. 2002. Cell signaling by endocannabinoids and their congeners: questions of selectivity and other challenges. *Chem. Phys. Lipids* **121**: 111-134.

Schneider, R. and Timms, A. R. 1957. Some aspects of the pharmacology of an homologous series of choline esters of fatty acids. *Brit. J. Pharmacol*. **12**: 30-38.

Shinoda, K. "Colloidal Surfactants", Academic Press, New York, N.Y., 1963, p 7.

Shinoda, K.; Hato, M. and Hayashi, T. 1972. The physicochemical properties of aqueous solutions of fluorinated surfactants. *J. Phys. Chem*. **76**: 909-914.

Shum, P., Kim, J-M. and Thompson, D.H. 2001. Phototriggering of liposomal drug delivery systems. *Adv. Drug Del. Rev*. **53**: 273-284.

Sidik., K. and Smerdon, M.J. 1990. Bleomycin-induced DNA damage and repair in human cells permeabilized with lysophosphatidylcholine. *Cancer Res*. **50**: 1613–1619.

Sudholter, E.J.R., Engberts, J.B.F.N. and De Jeu, W.H. 1982. Thermotropic liquid-crystalline behavior of some single- and double-chained pyridinium amphiphiles. *J Phys Chem.* 86:1908-1913.

Sun, G.Y., Xu, J.F., Jensen, M.D. and Simonyi, A. 2004. Phospholipase A_2 in the central nervous system: implications for neurodegenerative diseases. *J Lipid Res* **45**:205–213.

Stephenson, R.A. In: Karsa D. R. Industrial Applications of Surfactants, vol. II. Cambridge: Royal Society of Chemistry; 1990. p. 235–75.

Stetten, D. Jr. 1941. Biological synthesis of choline by rats on diets with and without adequate lipotropic methyl. *J. Biol. Chem.* **142**: 629-633.

Swamy, M.J., Würz, U. and Marsh, D. 1993. Structure of vitaminylated lipids in aqueous dispersion: X-ray diffraction and ^{31}P NMR studies of *N*-biotinylphosphatidylethanolamines. *Biochemistry* **32**: 9960-9967.

Swamy, M.J. and Marsh, D. 1994. Spin-label electron spin resonance studies on the dynamics of the different phases of *N*-biotinylphosphatidylethanolamines. *Biochemistry* **33**: 11656-11663.

Swamy, M.J. and Marsh, D. 1995. Thermodynamics of interdigitated phases of phosphatidylcholine in glycerol. *Biophys. J*. **69**: 1402-1408.

Swamy, M.J., Marsh, D., Ramakrishnan, M. 1997. Differential scanning calorimetry of chain-melting phase transitions of *N*-acylphosphatidylethanolamines. *Biophys. J*. **73**: 2556-2564.

Swamy, M.J., Ramakrishnan, M., Angerstein, B. and Marsh, D. 2000. Spin-label electron spin resonance studies on the mode of anchoring and vertical location of the *N*-acyl chain in *N*-acylphosphatidylethanolamines. *Biochemistry* **39**: 12476-12484.

Swamy, M.J., Ramakrishnan, M., Marsh, D. and Würz, U. 2003. Miscibility and phase behaviour of binary mixtures of *N*-palmitoylethanolamine and dipalmitoylphosphatidylcholine. *Biochim. Biophys. Acta* **1616**:174-183.

Träuble, H. and Eibl, H. 1974. Electrostatic effects on lipid phase transitions: membrane structure and ionic environment. *Proc. Natl. Acad. Sci. USA.* **71**:214-219.

Tsujii, K. and Mino, J. 1978. Krafft point depression of some zwitterionic surfactants by inorganic salts. *J. Phys. Chem.* **82**: 1610-1614.

Underwood, A.L. and Anacker, E.W. 1987. Counterion lyotropy and micelle formation. *J. Colloid Int. Sci.* **117**: 242-250.

Venance, L., Piomelli, D., Glowinski, J. and Giaume, C. 1995. Inhibition of anandamide of gap junctions and intercellular calcium signaling in striatal astrocytes. *Nature* **376**: 590-594.

Vanzi, F., Madan, B. and Sharp, K. 1998. Effect of the protein denaturants urea and guanidinium on water structure: A structural and thermodynamic study. *J. Am. Chem. Soc.* **120**: 10748-10753.

Washabaugh, M.W. and Collins, K.D. 1986. The systematic characterization by aqueous column chromatography of solutes which affect protein stability. *J. Biol. Chem.* **261**: 12477- 12485.

Watson, C.L. and Gold, M.R. 1997. Lysophosphatidylcholine modulates cardiac I(Na) via multiple protein kinase pathways. *Circ Res*. **81**: 387–395.

Weinreb, G. And Lentz, B.R. 2007. Analysis of membrane fusion as a two-state sequential process: evaluation of the stalk model. *Biophys. J.* **92**: 4012–4029.

Weltzien, H.U. 1979. Cytolytic and membrane- perturbing properties of lysophosphatidylcholine. *Biochim. Biophys. Acta* **559**: 259–287.

Wiseman, T., Williston, S., Brandts, J.F. and Lin, L.N. 1989. Rapid measurement of binding constants and heats of binding using a new titration calorimeter. *Anal. Biochem.* **179**: 131–137.

Woodley, S.L., Ikenouchi, H. and Barry, W.H. 1991. Lysophosphatidylcholine increases cytosolic calcium in ventricular myocytes by direct action on the sarcolemma. *J. Mol. Cell. Cardiol*. **23**: 671–680.

Wouters, J., Vandevoorde, S., Culot, C., Docquir, F. and Lambert, D. M. 2002. Polymorphism of *N*-stearoylethanolamine: differential scanning calorimetric, vibrational spectroscopic (FTIR), and crystallographic studies. *Chem. Phys. Lipids* **119**: 13-21.

Wu, R., Lemne, C., de Faire, U. and Frostegard, J. 2001. Antibodies to lysophosphatidylcholine are decreased in borderline hypertension. *Hypertension* **37**: 154–159.

Yang, P.W. and Mantsch, H.H.J. 1986. The critical micellization temperature and its dependence on the position and geometry of the double bond in a series of sodium octadecenoates. *Colloid Interface Sci*. **113**: 218-224.

Yeagle, P.L. (2005). The structure of biological membranes. 2nd edition. CRC press.

Zhang, Y., and Cremer, P.S. 2006. Interactions between macromolecules and ions: the Hofmeister series. *Curr. Opin. Chem. Biol*. **10**: 658–663.

Zou, Q., Bennion, B.J., Daggett, V. and Murphy, K.P. 2002. The molecular mechanism of stabilization of proteins by TMAO and its ability to counteract the effects of urea. *J. Am. Chem. Soc*. **124**: 1192-1202.

List of Publications

1. M. Ramakrishnan, **P. K. Tarafdar**, R. K. Kamlekar & M. J. Swamy*. Differential Scanning Calorimetric Studies on the Interaction of *N*-Acylethanolamines with Cholesterol. (2007) **Curr. Sci**. 93, 234-238.

2. M. J. Swamy*, **P. K. Tarafdar**, & R. S. Damai. Structure of Biological Membranes and Lipid-Protein Interactions. (2007) **Ann. Souvenir AP Akademi Sci.** P18-21.

3. **P. K. Tarafdar**, V. L. Vasudev, A. Kondreddy, A. R. Podile & M. J. Swamy*. Biophysical Investigations on the Aggregation and Thermal Unfolding of $Harpin_{Pss}$ and Identification of Leucine-Zipper-Like Motifs in Harpins. (2009) **Biochim. Biophys. Acta-Proteins and proteomics** 1794, 1684-1692.

4. **P. K. Tarafdar** & M. J. Swamy*. Polymorphism in 'L' Shaped Lipids: Structure of *N*-,*O*-Diacylethanolamines with Mixed Acyl Chains. (2009) **Chem. Phys. Lipids** 162, 25-33.

5. R. K. Kamlekar[a], **P. K. Tarafdar[a]** & M. J. Swamy*. Synthesis, Calorimetric Studies and Crystal Structures of *N*, *O*-Diacylethanolamines with Matched Chains. (2009) **J. Lipid Res**. (Published online, doi:10.1194/jlr.M900105-JLR200)**.[a]Both authors contributed equally**.

6. **P. K. Tarafdar** & M. J. Swamy*. Exploration of Salt-Induced Bilayer Stabilization in *O*-Stearoylethanolamine: A Combined Calorimetric, Spectroscopic and Crystallographic Study. (2009) **Biochim. Biophys. Acta-Biomembranes** (under revision).

7. M. J. Swamy*, **P. K. Tarafdar** & R. K. Kamlekar. Structure, Phase Behaviour and Membrane Interactions of *N*-Acylethanolamines and *N*-Acylphosphatidylethanolamines. **Chem. Phys. Lipids** (invited review). (2009) (submitted).

Symposium Attended

1. Structure, polymorphism and phase behavior of N, O-diacylethanolamines. Pradip K. Tarafdar, R. K. Kamlekar and Musti J. Swamy – The Interface of Life, An International School on Biomembrane Physics, organized by Indian Institute of Technology Madras, Chennai, India, Jan. 2008 (Oral Presentation).

2. Biophysical Investigations on the Aggregation and Thermal Unfolding of HarpinPss and Identification of Leucine-Zipper-Like Motifs in Harpins. Pradip K. Tarafdar and Musti J. Swamy – 5th Singapore-India Collaborative and Cooperative Chemistry Symposium (SInCCCS-5), organized by University of Hyderabad, Hyderabad, India, Feb. 2009 (Oral Presentation).

3. Novel Synthetic Lipids: Biological Activity and Potential Application. Pradip K. Tarafdar and Musti J. Swamy – 6th Annual In-house Symposium of School of Chemistry, ChemFest 2009, organized by School of Chemistry, University of Hyderabad, Hyderabad, India, Mar. 2009 (Oral Presentation).